NAVAL POSTGRADUATE SCHOOL
Monterey, California

THESIS

OBSERVATIONS OF QUASI-NONRADIATING WAVE SOURCES IN ONE DIMENSION

By

Gregg L. Miller

June 2000

Thesis Advisor: Bruce C. Denardo
Second Reader: Steve R. Baker

Approved for public release; distribution is unlimited.

REPORT DOCUMENTATION PAGE

Form Approved OMB No. 0704-0188

1. AGENCY USE ONLY *(Leave blank)*	2. REPORT DATE	3. REPORT TYPE AND DATES COVERED
	June 2000	Master's Thesis

4. TITLE AND SUBTITLE
Observations of Quasi-Nonradiating Wave Sources in One Dimension

5. FUNDING NUMBERS

6. AUTHOR(S)
Miller, Gregg L.

7. PERFORMING ORGANIZATION NAME(S) AND ADDRESS(ES)
Naval Postgraduate School
Monterey, CA 93943-5000

8. PERFORMING ORGANIZATION REPORT NUMBER

9. SPONSORING / MONITORING AGENCY NAME(S) AND ADDRESS(ES)

10. SPONSORING / MONITORING AGENCY REPORT NUMBER

11. SUPPLEMENTARY NOTES
The views expressed in this thesis are those of the author and do not reflect the official policy or position of the Department of Defense or the U.S. Government.

12a. DISTRIBUTION / AVAILABILITY STATEMENT
Approved for public release; distribution is unlimited.

12b. DISTRIBUTION CODE

13. ABSTRACT *(maximum 200 words)*

A nonradiating wave source is one that drives waves over a region of a medium, where no waves propagate outside the region due to complete destructive interference at the boundary. This thesis describes the first observations of an acoustical source of this type. Physical observations are made with a current-carrying wire that is transversely driven by several types of magnetic field distributions. The wire glows as a result of the current, and the wave pattern can be observed due to the cooling caused by the motion of the wire. The predicted standing wave response in the source region is confirmed. Numerical simulations of a one-dimensional mass-and-spring lattice show that dissipation, nonuniformity, and nonlinearity each cause radiation to escape from the source region. The radiation amplitude relative to the standing wave amplitude is substantially reduced for sources that are distributed over a region rather than lumped over the same region. In addition, it is possible to make adjustments to the drive parameters to substantially minimize the radiation.

14. SUBJECT TERMS	15. NUMBER OF PAGES
Nonradiating Waves, Noise Cancellation	142
	16. PRICE CODE

17. SECURITY CLASSIFICATION OF REPORT	18. SECURITY CLASSIFICATION OF THIS PAGE	19. SECURITY CLASSIFI- CATION OF ABSTRACT	20. LIMITATION OF ABSTRACT
Unclassified	Unclassified	Unclassified	UL

NSN 7540-01-280-5500 (Rev. 2-89)

Standard Form 298

Prescribed by ANSI Std. 239-18

THIS PAGE INTENTIONALLY LEFT BLANK

Approved for public release; distribution is unlimited

OBSERVATIONS OF QUASI-NONRADIATING WAVES SOURCES IN ONE DIMENSION

Gregg L. Miller
Ensign, United States Navy
B.S., Carnegie Mellon University, 1999

Submitted in partial fulfillment of the
requirements for the degree of

MASTER OF SCIENCE IN PHYSICS

from the

NAVAL POSTGRADUATE SCHOOL
June 2000

Author: 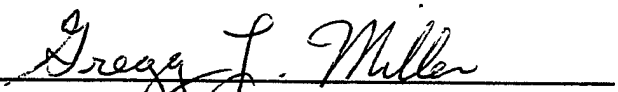
Gregg L. Miller

Approved by: 
Bruce C. Denardo, Thesis Advisor


Steven R. Baker, Second Reader

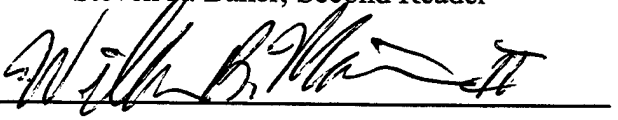
William B. Maier, Chairman
Department of Physics

THIS PAGE INTENTIONALLY LEFT BLANK

ABSTRACT

A nonradiating wave source is one that drives waves over a region of a medium, where no waves propagate outside the region due to complete destructive interference at the boundary. This thesis describes the first observations of an accoustical source of this type. Physical observations are made with a current-carrying wire that is transversely driven by several types of magnetic field distributions. The wire glows as a result of the current, and the wave pattern can be observed due to the cooling caused by the motion of the wire. The predicted standing wave response in the source region is confirmed. Numerical simulations of a one-dimensional mass-and-spring lattice show that dissipation, nonuniformity, and nonlinearity each cause radiation to escape from the source region. The radiation amplitude relative to the standing wave amplitude is substantially reduced for sources that are distributed over a region rather than lumped over the same region. In addition, it is possible to make adjustments to the drive parameters to substantially minimize the radiation.

THIS PAGE INTENTIONALLY LEFT BLANK

TABLE OF CONTENTS

THIS PAGE INTENTIONALLY LEFT BLANK

GLOSSARY OF VARIABLES

A	-	Amplitude of Wave
a, b	-	Limits of the Region of the Force Distribution
c	-	Speed of Wave
d	-	Distance between drive points
F	-	Magnitude of Driving Force
$f(x,t)$	-	Force Distribution
g	-	Width of Wave Packets in Anechoic Tests
h_o	-	Normalization Constant of Response Amplitude
k	-	Wave Number
L	-	Length of Region of Continuous Drive Force
l	-	Translation Constant
M	-	Mass in Anechoic Termination
m	-	Discrete Mass Value of Masses in Lattice of Numerical Simulations
n	-	Integer (Counting) Index
Q	-	Normalization Factor of Force Distribution
$q(x)$	-	Effective Force Density
R	-	Mechanical Resistance of Dashpot
r	-	Spacing of Masses in Lattice of Numerical Simulations
S	-	Spring Constant in Anechoic Termination
s	-	Spring Constants of Springs in Lattice of Numerical Simulations
T	-	Tension of 1-D String
t	-	Time
x	-	Position Along Length of 1-D Medium
y	-	Displacement of a Point on 1-D Medium
Z	-	Impedance
α	-	Constant of Quadratic Nonlinearity
β	-	Constant of Cubic Nonlinearity
γ	-	Transition Scale Factor
δ	-	Dirac Delta Function
ε	-	Scale Factor
λ	-	Wavelength
μ	-	linear mass density for 1-D Medium
ν	-	Damping Parameter of Dissipative Term
ξ	-	Normalization Constant of Response Amplitude
ρ	-	Effective Linear Mass Density of Mass and Spring Lattice
τ	-	Time Translation Factor
τ_0	-	Time Translation Factor
ϕ	-	Scale Factor
ω	-	Frequency of Oscillation
ω_0	-	Natural Frequency of Harmonic Oscillator

THIS PAGE INTENTIONALLY LEFT BLANK

I. INTRODUCTION

A *nonradiating wave source* is one that drives waves over a region of a medium, but where no waves propagate outside the region. This nonradiation is not due to nonuniformity of the medium, but to complete destructive interference of the waves outside the boundaries of the region. Berry et al. (1998) recently considered monofrequency force densities $f(x)e^{i\omega t}$ acting over a finite length of an ideal infinite string, where $f(x)$ is the complex amplitude of the force per unit length and ω is the angular frequency. The authors derived the general mathematical condition for which no radiation occurs outside the driven length, and exhibited the special case of a uniform force density. These authors also comment that nonradiating sources have also been predicted to exist in two and three dimensions.

The result is at first surprising. How can no radiation escape from the driven region? However, a simple physical explanation exists for simple cases of nonradiating sources in one dimension: The radiation cancels in pairs of point sources (Denardo, 1998). The simplest case is a "two-point source" consisting of two point drives with the same frequency, amplitude, and phase, separated by a distance d. Complete destructive interference occurs outside the segment that connects the point sources if there is a half-integral number of wavelengths of the radiation between the point drives: $\lambda/2 = d, d/3, d/5, \ldots$, where the wavelength is $\lambda = 2\pi c/\omega$ and the wave speed is c. The case of a uniform force F = constant over a length L can be considered as an infinite superposition of infinitesimal two-point sources whose separation distance is L/2. Complete destructive interference thus occurs outside the length L if we let $d = L/2$ in the above relationship: $\lambda = L, L/3, L/5, \ldots$. It should be noted that this simple idea extends to dispersive systems (where the wave speed is a function of frequency); for example, waves on a mass-and-spring lattice.

This complete destructive interference in the case of a uniform force density is analogous to that which occurs in the minima of single-slit diffraction in optics. The case of a two-point source is analogous to double-slit interference. It is interesting that these

arguments were naturally considered to have application only in two and three dimensions, but are now seen to be useful for one-dimensional waves.

The existence of nonradiating sources has an important consequence regarding the "inverse" radiation problem, where it is desired to determine a source by knowledge only of its radiation. Due to the existence of nonradiating sources, a source *cannot* be uniquely determined based only upon its radiation. The inverse radiation problem is thus not strictly solvable. On the other hand, if it is desired to reduce wave emissions from a source, such as acoustical emissions from a submarine, it may be possible to modify the source to render it approximately nonradiating.

Although the theoretical existence of nonradiating sources is not questionable, an important issue is the extent to which such sources can arise in actual situations. To our knowledge, there have not been any observations of nonradiating sources. The main purpose of this thesis is to demonstrate the existence of nonradiating sources.

This research was conducted in two parts. The first part of this research involved observing nonradiating sources on a vibrating wire apparatus. The second involved performing numerical simulations using a mass-and-spring lattice. These observations are important because they give an indication of the extent to which nonradiating sources can occur in actual systems.

We utilized a hot-wire in the vibrating wire apparatus for the purpose of visualization. The apparatus is discussed in Chapter III. The construction uses as its medium a nichrome wire, which glows when a current passes through it. Magnetic fields supply the driving force, and the extent of nonradiation is determined by visually observing the color of wire. Regions of greater vibration tend to cool and return to the original color of the wire. Areas of less vibration will tend to remain a glowing orange color from the heating as a result of the current. The pattern of orange and gray seen by the observer gives the pattern of vibration of the wire. This setup can be used to explore a wide variety in the profiles of the driving force but the results are only qualitative.

Using numerical simulations, our objective was to further understand nonradiating wave sources, and observe their behavior in a setting where the experimenter is able to control every environmental parameter that affects propagating waves. Thus, the

behavior as it relates to each of these parameters can be understood. The numerical simulations are presented in Chapter IV. We included the realistic weak effects of dissipation, nonuniformity, and nonlinearity. Because these effects cause a relatively small amount of radiation to emanate from the driven region, we refer to the sources as "quasi-nonradiating" in this case.

THIS PAGE INTENTIONALLY LEFT BLANK

II. THEORY OF NONRADIATING SOURCES IN ONE DIMENSION

In this chapter, the general condition for a nonradiating source in one dimension is derived, and several simple cases are treated and physically explained.

A. GENERAL CONDITIONS FOR NONRADIATION

We consider dispersionless, dissipationless waves in one dimension. An example of this, which we will employ as a physical system, is transverse waves on a uniform string under tension. Our treatment in this section is similar to that of Berry et al. (1998). If the mass per unit length is μ, the tension is T, and the force per unit length is $f(x,t)$, where x and t are the space and time coordinates, respectively, the equation of motion for the displacement $y(x,t)$ is

$$\mu \frac{\partial^2 y}{\partial t^2} - T \frac{\partial^2 y}{\partial x^2} = f(x,t). \tag{2.1}$$

The speed of waves is $c = (T/\mu)^{1/2}$. We consider monofrequency force distributions: $f(x,t) = f(x)\exp(-i\omega t)$, where it is understood that the actual force is the real part of the expression on the right. Equation (2.1) then reduces to the inhomogeneous Helmholtz equation

$$\frac{\partial^2 y}{\partial x^2} + k^2 y = q(x), \tag{2.2}$$

where $k = \omega/c$ is the wavenumber and $q(x) = -f(x)/T$ is the effective force density. The Green's function for the Helmholtz operator $\partial^2/\partial x^2 + k^2$ for outgoing waves in an infinite system is $\exp(ik|x - x'|)/2ik$ (Arfken, 1995). The force per unit length $f(x,t)$ is assumed to be nonzero only for $a \leq x \leq b$. The inhomogeneous solution of Eq. (2.2) is then

$$y(x) = \frac{1}{2ik}\int_a^b q(x')e^{ik|x-x'|}dx' \ . \tag{2.3}$$

The solution to the right ($x > b$) and the left ($x < a$) of the region of the applied force is thus, respectively,

$$\begin{aligned} y(x>b) &= \frac{e^{ikx}}{2ik}\int_a^b q(x')e^{-ikx'}dx' \ , \\ y(x<a) &= \frac{e^{-ikx}}{2ik}\int_a^b q(x')e^{ikx'}dx' \ . \end{aligned} \tag{2.4}$$

Hence, excitations will vanish everywhere outside the driven region $a \leq x \leq b$ if the Fourier transforms of the force density evaluated at the oppositely-traveling wavenumbers $\pm k = \pm\omega/c$ vanish:

$$\int_a^b q(x)e^{\pm ikx}dx = 0 \ , \tag{2.5}$$

where we have dropped the primes on x. This result can thus be stated as follows: *A monofrequency force distribution over a finite interval does not radiate outside the interval if the force distribution has no Fourier component at the wavenumbers corresponding to radiation at the driving frequency.* In the case, the force distribution does not "couple" into radiation outside the driving region.

As a first simple example, we consider the two-point force density

$$q(x) = Q\left[\delta(x + L/2) + \delta(x - L/2)\right]. \tag{2.6}$$

The condition (2.5) reduces to $\cos(kL/2) = 0$, or $kL/2 = (n - 1/2)\pi$, where $n = 1, 2, 3, \ldots$. When this occurs, there is no radiation for $|x| > L/2$. This result is physically explained in the following section. The disturbance for $|x| < L/2$ can be determined by substituting Eq. (2.6) into Eq. (2.3), which yields $y(x) = Qexp(ikL/2)\cos(kx)/ik$. Using the fact that $kL/2 = (n - 1/2)\pi$ for a nonradiating source gives the result

$$y(-L/2 < x < L/2) = \frac{L(-1)^{n-1}Q}{\pi(2n-1)}\cos\left(\frac{(2n-1)\pi x}{L}\right). \tag{2.7}$$

Note that the origin x = 0 is antinode, which must be the case because symmetry dictates that constructive interference occurs there. The force density (2.6) and the corresponding displacement (2.7) are shown in Fig. 2.1 for the cases $n = 1$ and 2.

As a second simple example, we consider the uniform force density

$$q(x) = \begin{cases} Q, & \text{for } |x| < L/2 \\ 0, & \text{for } |x| > L/2 \end{cases} \tag{2.8}$$

Substitution into the condition (2.5) for nonradiation yields $\sin(kL/2) = 0$, or $kL/2 = n\pi$. This result is physically explained in the following section. From Eq. (2.3), the corresponding displacement inside the driving region is

$$y(-L/2 < x < L/2) = \frac{L^2Q}{4n^2\pi^2}\left[1 - (-1)^n\cos\left(\frac{2n\pi x}{L}\right)\right]. \tag{2.9}$$

The force density (2.8) and the corresponding displacement (2.9) are shown in Fig. 2.2 for the cases $n = 1$ and 2.

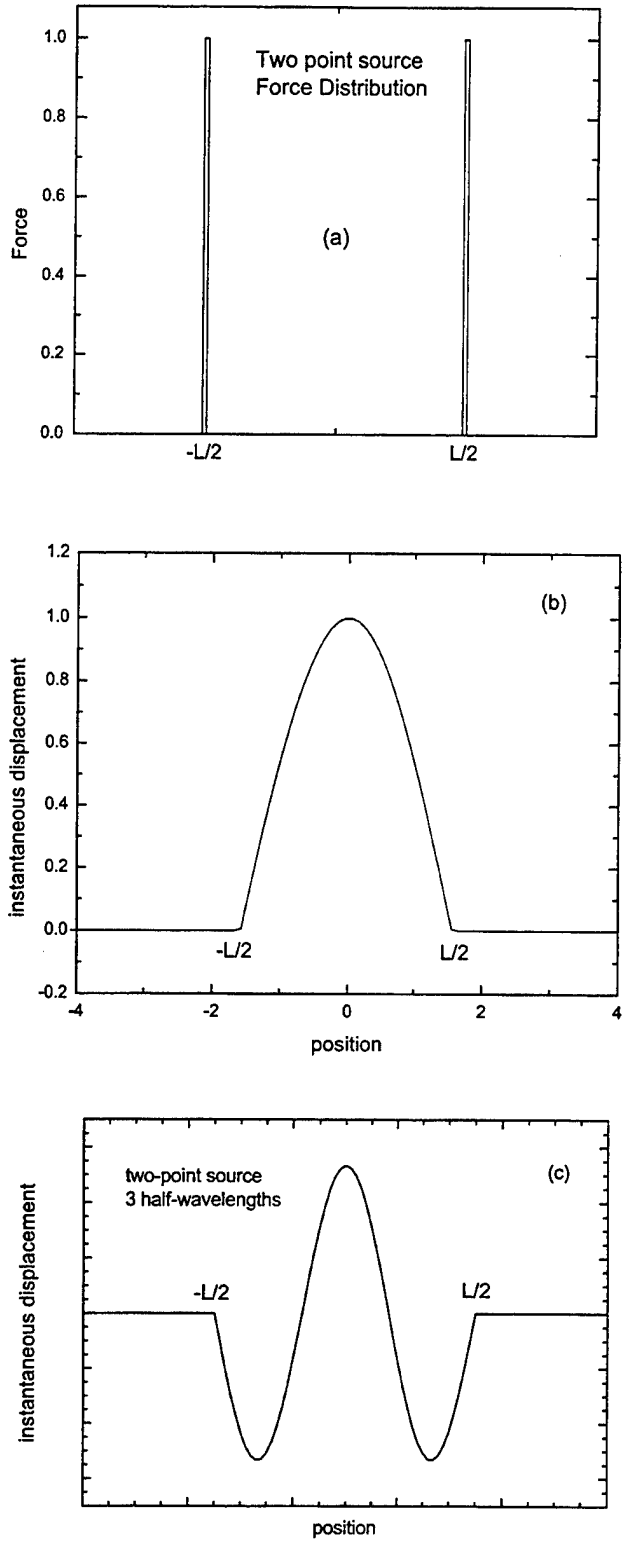

Fig. 2.1 Two-point force: (a) distribution (the lines represent delta functions), and resultant displacement of the string when the condition for nonradiation is met for (b) n = 1 and (c) n = 2.

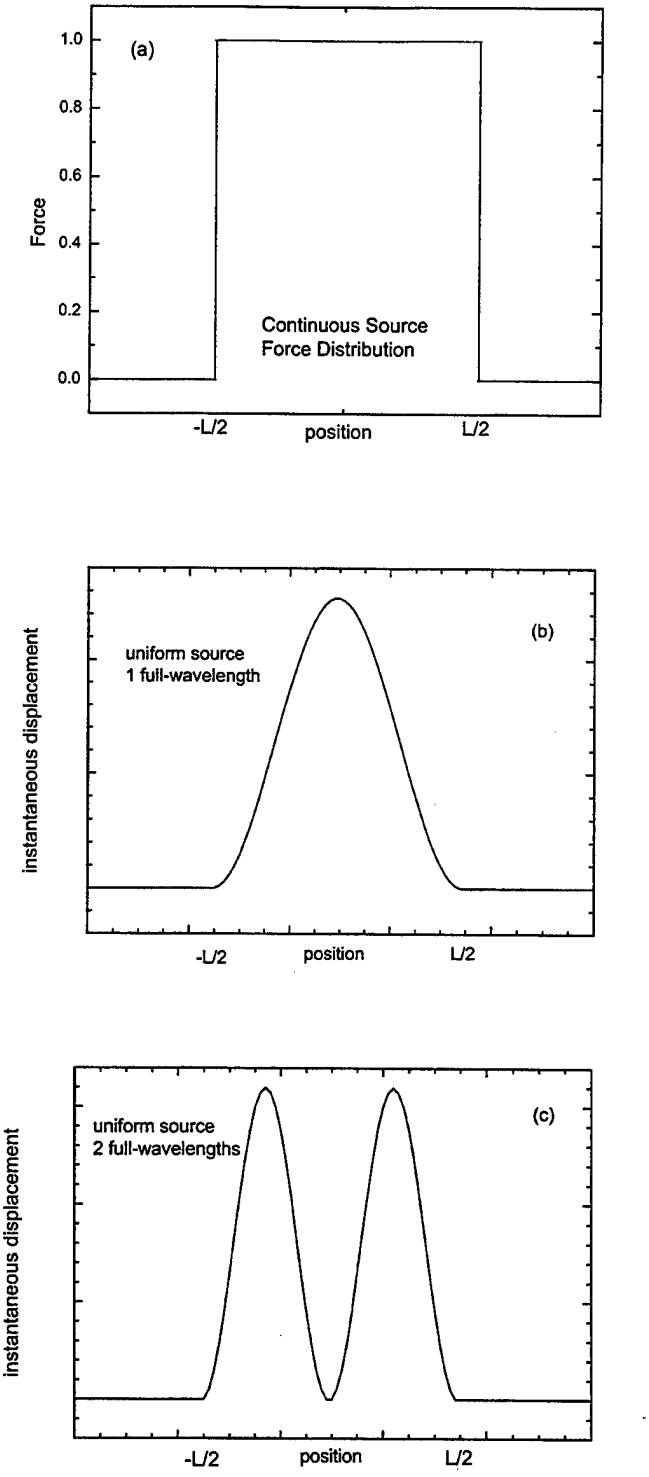

Fig. 2.2 Continuous force: (a) distribution, and resultant displacement of the string when the condition for nonradiation is met for (b) n = 1 and (c) n = 2.

B. PHYSICAL EXPLANATION OF SIMPLE NONRADIATING SOURCES

In the previous section, we examined two simple cases of nonradiating sources. The first consisted of two points separated by a distance L and driven in-phase with angular frequency ω and with the same amplitude. The condition for nonradiation was found to be $kL/2 = (n - 1/2)\pi$, where $k = \omega/c$ is the wavenumber, c is the speed of waves, and n is a positive integer. The second simple case was a force that is uniform over length L and oscillates with angular frequency ω. This was found to be nonradiating when $kL/2 = n\pi$. Our purpose in this section is to give a simple physical explanations of these and related simple cases (Denardo, 1998).

We consider first the elementary extended force composed of two points driven in-phase with the same amplitude. If the drive frequency is chosen such that the distance L between the points equals a half-integral number of wavelengths, then by superposition there is complete destructive interference at all locations outside the interval whose endpoints are the forcing points. The condition for nonradiation is thus $L = (n - 1/2)\lambda$, where n is a positive integer. Because the wavelength is $\lambda = 2\pi/k$, the condition can be expressed as $kL/2 = (n - 1/2)\pi$, which is identical to the condition derived in the previous section.

Now consider the uniform force over the length L. This force distribution can be considered as an infinite superposition of infinitesimal two-point sources of identical amplitude and phase, where each pair of points is a distance $L/2$ apart. There will thus be no radiation outside the driving region when $L/2$ is a half-integral number of wavelengths, or when the length of the driving region is an integral number of wavelengths: $L = n\lambda$. This is equivalent to $kL/2 = n\pi$, which is identical to the condition derived in the previous section. The cancellation is analogous to that which occurs in the minima of single-slit diffraction.

By superposing nonradiating two-point sources, one can construct other situations in which no radiation occurs outside a driving region. Consider two points separated by

the distance λ and driven out-of-phase with the same amplitude. This is the out-of-phase superposition of two contiguous nonradiating two-point sources, and so no radiation will escape. Suppose three points are successively separated by $\lambda/2$, and are driven in-phase with the same amplitude at the endpoints and twice the amplitude at the midpoint. This is the in-phase superposition of two contiguous nonradiating two-point sources, and so no radiation will escape. Four points successively separated by $\lambda/2$ and driven in-phase with the same amplitude is the superposition of two nonradiating two-point sources separated by $\lambda/2$, and so no radiation will escape. Four points successively separated by $\lambda/4$ and driven in-phase with the same amplitude is the superposition of two overlapping nonradiating two-point sources, and so no radiation will escape. As a general continuous example, consider an *arbitrary* amplitude and phase distribution over an interval of a half-integral wavelength, where the distribution is repeated over a contiguous interval. By a similar argument as in the uniform source case above, we find that this combined distribution will be nonradiating.

The physical argument presented above reveals that the simple cases are nonradiating in *any* one-dimensional parity-preserving wave system, and thus suggests that the mathematical theory could be generalized to include such cases, e.g., dispersive waves. The physical argument also raises a question. Due to the wide variety of superpositions of nonradiating two-point sources, can *every* nonradiating force distribution in one dimension be described as a superposition of nonradiating two-point sources? To our knowledge, this question has not been answered.

THIS PAGE INTENTIONALLY LEFT BLANK

III. HOT-WIRE APPARATUS

The hot-wire apparatus was our primary tool to experimentally investigate quasi-nonradiating wave sources since it permitted exploration of both continuous and two point source scenarios. It was also useful since it may be further developed into a classroom demonstration.

A. PHYSICAL SETUP

The hot-wire setup used to investigate the properties of quasi-nonradiating wave sources consisted of common physics laboratory items. A schematic of the setup is shown in Fig. 3.1. We used two kinds of wire, 28 and 30 gauge bare nickel chromium (BNC) wire, similar to that used in everyday toasters. These were obtained from Consolidated Electronic Wire and Cable, through Central Scientific Company (Cenco). The 28 gauge wire has a diameter of 0.0125 inches (0.32 mm) and a linear mass density of 0.66 gm/m. The 30 gauge has a diameter on 0.01 inches (0.26 mm) and a linear mass density of 0.42 gm/m. BNC wire was chosen because it glows when a current is passed through it, a property we intended to exploit. A sufficient length of wire just over two meters was cut, and the left edge was fixed in place with a C-clamp to a vertical bar mounted to the lab table with a table clamp. Approximately 10 cm of wire extended past the clamped portion of the wire. The right edge of the wire was passed over top of a steel pulley, which was mounted to the lab table, and wound around a mass hanger, from which masses would be suspended, controlling the tension of the wire.

An HP33120 function generator was used to generate the sinusoidal voltage used in the experiment. The function generator's output was input to a QSC MX3000a Dual Monaural Amplifier, where the signal was increased to the levels needed to make the wire glow. It is also important to note that the two channels of the amplifier had to be run in bridge mode in order to obtain the necessary Voltage amplitude. From the amplifier the output was connected to each end of the BNC wire by a simple alligator clip. On the

left side of Fig. 3.1, the connection was made to the 10 cm of excess wire outside the clamp, so that the weight of the alligator clip would not interfere with the vibration of the wire. On the right side, the connection was made between the pulley and the hanging mass so that the alligator clip would not interfere with the vibration of the wire. The weight of the clip, adding to the tension of the wire was not significant. The pulley was necessary because hanging masses made precise control of the tension possible. In addition, the pulley was selected, rather than having two fixed ends, to allow the length of vibrating wire to change slightly during operation, since this would aid in keeping the wire from entering into the nonlinear range for vibrations at small amplitudes. The distance between the clamped left edge and the pulley on the right edge was 1.88 m. A FLUKE 83 III hand held Multimeter was inserted in series with the amplifier output, so we could measure the current in the wire.

The magnets used in the setup were Pasco large pole magnets (Model WA-9609A). They rested on adjustable jacks, which were used to raise and lower the magnets and ensure that the wire would be centered in the magnetic field. The magnets were oriented with the field vertical, so that as the apparatus was observed from the side, the observer would look along the plane of vibration. In the case of the continuous magnet source, the multiple magnets were placed end to end and were held together with Quick-Grip bar clamps from American Tool. Figure 3.2 shows a picture of the wire with 10 magnets in the configuration. The alligator clip is clearly visible on the left end and connects the BNC wire to the power amplifier. The pulley is visible on the right, although the weights hanging over it are not. Figure 3.1 shows parts not visible in Fig. 3.2. It is also possible to approximate the two-point source experiment by only using two of the magnets. Because the magnets have a finite width and are not points, the greater the inter-magnet distance relative to the magnet width, the better the system will approximate the ideal two-point scenario.

Pictures of the system were taken using an Olympus Camedia C-2000 Z digital camera. The camera was mounted on a tripod, allowing for maximum stability and clarity of picture.

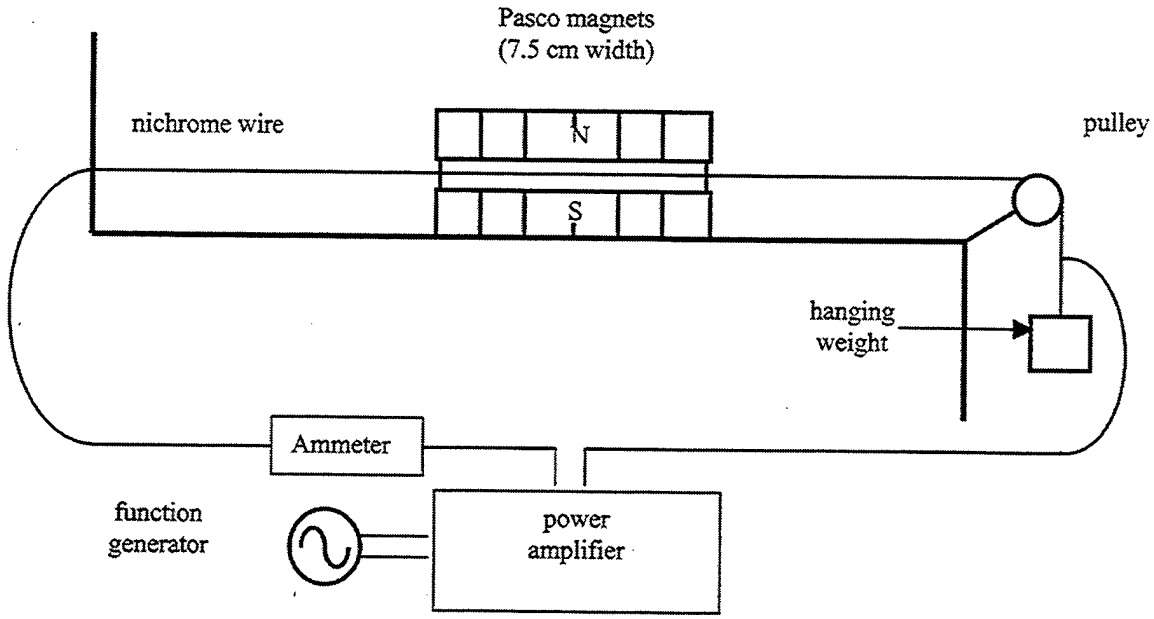

Fig. 3.1 Schematic of hotwire with the six magnet continuous source.

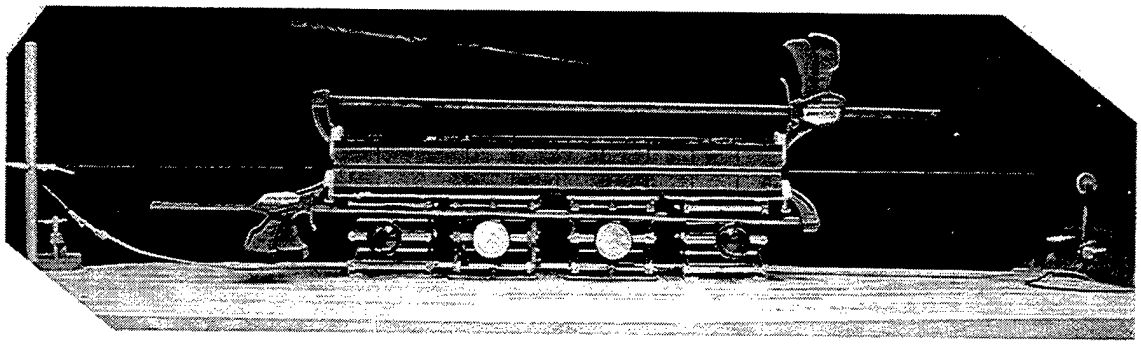

Fig. 3.2 Hotwire setup with 10 magnets

B. PHYSICS BEHIND THE SETUP

In this section, a general picture of the physics behind the hot-wire setup will be given, as well as definitions used in describing the system and explanations as to what behavior was sought and observed.

1. Use of the Hot-wire Setup for Imaging

Using a hot-wire system is a common technique for qualitatively studying vibrations on a wire. A wire is selected that glows bright orange when a current of sufficient magnitude is passed through it.

A magnet is placed near the wire such that the wire passes through the magnetic field, and when the current is run through the wire, a Lorentz force is applied to the moving charges in the wire, and hence to the wire itself. If a sinusoidal alternating current is passed through the wire, the resulting Lorentz force on the wire will also be sinusoidal, and it is this alternating force which is the driving force for the vibrating system. The frequency of the driving force is controlled by simply changing the frequency of the alternating current in the wire.

When extended standing waves exist on the wire, the peaks of the standing waves are the regions on the wire moving with the maximum amplitude of vibration. These regions are moving fast enough to allow the wire to conduct more heat to the surrounding air. Thus, the regions of the peaks cool and return to the original color of the wire. The nodes on the standing wave, which are not moving at all, will retain the heated orange color. There will be a variation in the color of the wire between the nodes and the peaks. The pattern of vibration of the wire can be determined just looking at the color of the wire. Even when viewed from within the plane of vibration, so that no movement can be seen, the color of the wire indicates which regions are moving (peaks) and which are not (nodes).

2. Expected Behavior

For the hot-wire setup, the desired patterns of vibration correspond to Figs. 2.1 and 2.2. We would like to see homogenous orange color outside the magnets (represented on Figs. 2.1(b), 2.1(c), 2.2(b) and 2.2(c) by the region outside $-L/2$ and $L/2$). We want to minimize the amplitude of vibration in this area.

For the first mode of the two-point experiment, the position of the magnet should mark a point on the wire where inside of that point, the color of the wire slowly becomes increasingly gray as one looks toward the other magnet. The point directly between the two magnets should be totally black since the wire will be vibrating with maximum amplitude in this region. If the amplitude is sufficiently large, the wire will be gray along several centimeters of wire next to the center point when the amplitude is near maximum.

For the second mode of the two-point experiment, the length of wire inside the magnets should undergo three changes of color as one looks along the length of the wire toward the other magnet. The point directly in the center of the two magnets will be gray as will a section of wire one third of the way between the magnets and the center point. The area two thirds of the way between the magnets and the center will be a node, and should be orange.

For the continuous magnet source, we placed several magnets next to each other to obtain a magnetic force profile similar to the one represented by Fig. 2.2(a). In the ideal two-point case, one can see from Fig. 2.1(b) that, at the position of the magnet, the slope of the wire is discontinuous. This is not possible for an actual wire, due to both the finite width magnets and because a wire is not perfectly flexible. The slope will be continuous. In the continuous magnetic field case, the slope is also continuous. Thus, the first modes will appear similar in the two-point and continuous magnetic field cases from the point of view of what color the wire will be. They will occur at different frequencies, however, as given in section 2.B.

The second mode in the continuous case will appear much different than for the two-point case. The second mode will appear orange in the center of the magnets, and will be gray halfway between the edge of the magnet array and the center node. Again the second modes of the continuous and two-point cases occur at different frequencies.

Only the first two modes in each case were searched for. We felt that observing the first two modes would be sufficient to convince us that nonradiating sources did exist. As we can demonstrate with the numerical simulations, the system is less nonradiating as nonlinear terms grow stronger, and in a vibrating wire, the nonlinear terms grow with the curvature of the displacement vs. position. As we search for higher modes, we are trying

to fit more peaks and nodes into a predetermined length of wire, thus the curvature of the displacement increases with each mode. Therefore the difficulty of observing a mode should increase as each higher mode is sought for.

3. Effects of Steel Plates

Ideally the magnets would have identical field values at every point. This is not the case, however, and it is important for us to have knowledge of the field strength at points along the driven length of the wire. We refer to this as the magnetic field profile. Not only will the field strength differ at points inside the magnets, but each magnet also has a unique fringe field associated with it. Even when the magnets are pressed up against one another, there is a drop in the field intensity between them. In addition, some of the magnets were purchased longer ago than others, and could have could have undergone some change in their magnetic field profile.

During the course of experimentation on the continuous field source, we discovered that the profile of our magnetic fields substantially deviated from the ideal case given by Fig. 2.2(a). This profile measurement is described in section C.3. In order to eliminate possible sources of error, and to create as uniform a magnetic field as possible, we decided to investigate what effect steel plates placed on the faces of the magnets would have on the quality of the magnetic profile and therefore the nonradiating wave fields. The steel plates were cut to be exactly the same length of the magnet array and to match the width of the magnet faces as well, which is two inches. The results presented in this chapter reflect experimentation done with plates 1/8 inch thick.

The steel would serve two purposes. The first would be to reduce the drop-offs in the magnetic field that appear between two neighboring magnets. Inside the array the steel would become polarized and help to smooth out the fluctuations in magnetic field intensity. The second purpose of the steel would be to help eliminate the fringe fields. The frequencies of nonradiation are calculated using only the distance from one end of the magnet array to the other. If the fringe fields outside this distance are significant, they represent a force on the wire in a position not consistent with the nonradiating

conditions. The value of the fringe fields is determined in part by the distance between the magnet faces. The presence of steel allows us to decrease that distance without raising the intensity of the magnetic fields. The gap in which the wire moves is smaller and therefore the fringe fields are not as important. Since the wire moves in a plane perpendicular to the magnetic field, decreasing the gap between the magnet faces will not affect the motion of the wire, as long as transverse motion is avoided.

Figure 3.3 shows a portion of the magnet array with and without steel plates.

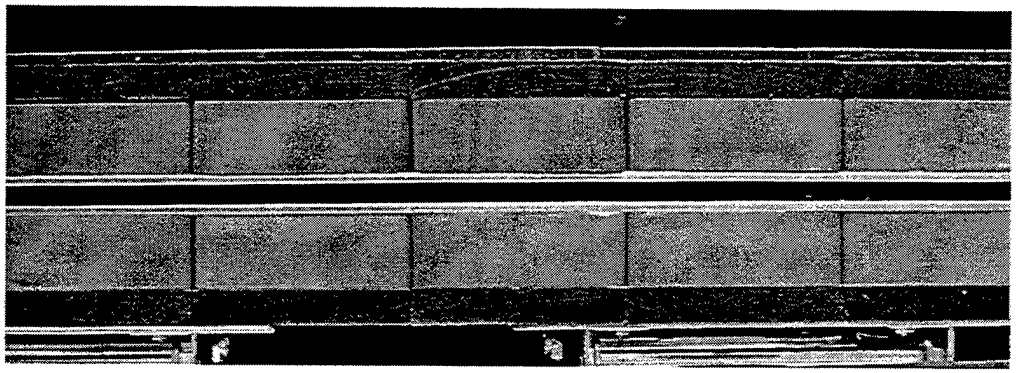

(a)

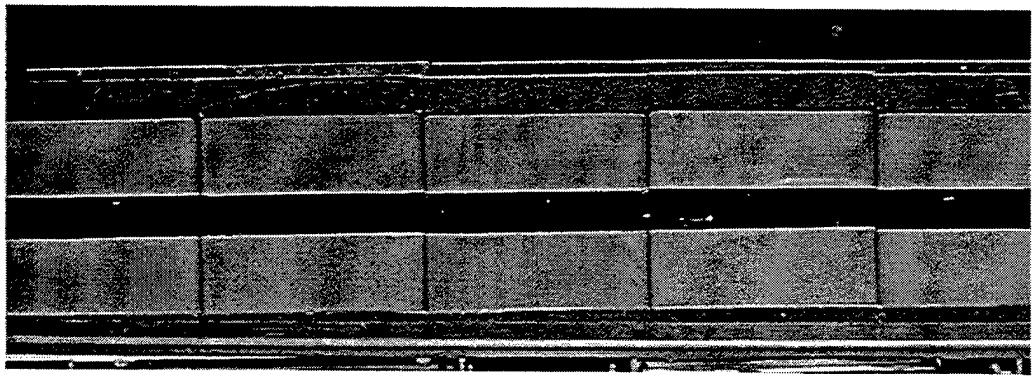

(b)

Fig. 3.3 A blown up picture of what is seen in Fig 3.2. A Section of the array (a) with and (b) without the 1/8 inch steel plates.

4. Definitions Used to Describe the Observations

During the course of research, it became necessary to find a convenient way of qualitatively describing the system in a concise manner that didn't require the use of a verbose description. A definition was agreed upon to describe a system using the words "clean" or "dirty", and it is now necessary to convey the meaning of those words to the reader. When a system is described as clean or dirty, a relative comparison is being made, referring to how close the system approximates and ideal nonradiating wave source. Its usage will be restricted to a comparative term, describing a system that is 'more clean' or 'more dirty' than another system previously described. For the hot-wire, a clean system would describe one in which, outside the range of the magnetic field, there is little or no vibrations. The color of the wire outside the magnets would be a homogenous orange, signifying little vibration. The hot wire does have some variation in the color even when it is not vibrating, due to imperfections in the wire such as slight changes in diameter, and varying air currents. It is necessary to compare the variations in color of the wire outside the magnets while the system is operating, to the variation in color while at rest, to determine the source of the color variation.

A clean system would also have the maximum amount of vibration inside the magnet array. In observing the fundamental nonradiating mode for the continuous source, a clean system would vibrate with a large enough amplitude to be totally black over some range (typically a few centimeters), which is directly in the center of the magnetic field. In observing the 2^{nd} nonradiating mode, a clean system would be totally black over two regions of wire, each of which would halfway between the end of the magnet array and the center. The area of the wire directly in the center of the magnet array would be orange, similar in intensity to the orange outside the magnetic range.

A system becomes dirtier as it deviates from the ideal model. As vibration increases outside the region of the magnetic field, and amplitudes of vibration decrease inside the magnetic field region, the system is said to be increasingly dirty. This is also true when regions of black wire (peaks) inside the magnetic region become orange and orange regions of wire outside the magnets become dimmer from cooling.

5. Avoiding Extended Standing Waves

Through the course of experimentation, we discovered that the nonradiating modes were best obtained if we tried to vibrate the wire at a frequency that was roughly halfway between the frequencies of two consecutive extended standing waves over the entire length of the wire. Unlike the numerical simulations (Chapter 4), the vibrating medium of the experimental setups did not have anechoic (nonreflecting) terminations. The terminations were highly reflective. This would not be problematic if the nonradiating wave sources were perfect, since no radiation would reach the termination, but in our real system, the leakage can reflect and generate extended standing modes of the length of the wire. Extended standing waves of the total length of the wire are stable and desirable states for the wire to exist in.

The pattern of vibration given by nonradiating conditions represents another kind of stable state that the wire can exist in (nonradiating mode), with vibration in between the magnet faces and none outside. This pattern of vibration does not exist at only one specific frequency, but like the extended standing waves, it has a bell shaped tuning response curve around the frequency of nonradiation.

The reason that we wanted to search for our nonradiating modes at frequencies between extended standing modes of the wire was because the extended standing wave modes are more stable states for the wire to exist in than the nonradiating states. If a condition was achieved that was nearly nonradiating, and the frequency was changed only slightly, the system had the tendency to "collapse" into one of the extended standing wave modes. This collapse also exhibited properties of hysteresis. Upon collapse, if the frequency was turned back, the system would not return to the nonradiating mode, but would stay in the extended standing wave mode, until the frequency was turned back sufficiently past the point of collapse. On occasion, we would have to turn the frequency so far back that we would be in danger of collapsing into the neighboring extended standing wave mode. We searched for our nonradiating sources at frequencies between these modes, to try and stay far out on the edge of the tuning curves, where the response

amplitude is small. In this way our system would be less inclined to collapse into an extended mode of the length of the wire.

6. Speed of Waves on a String in Contrast to a Wire

For this experiment, many calculations need to be made with regard to the speed of waves on a wire and the resulting frequencies for the extended modes. For determining the speed of waves we used the relationship

$$c = \sqrt{\frac{T}{\mu}}, \tag{3.1}$$

where c is the speed of the wave, T is the tension in the wire, and μ is the linear mass density of the wire. This equation gives the speed of waves on an ideal string, but the wire we used is not ideal. The value for T typically would be the tension given by the mass hanging over the pulley, but the wire also has a bending stiffness that gives it an effective tension even if there was no hanging mass. This internal tension of the wire can also contribute to nonlinearities in the vibrations. In a real experiment the speed of waves on the wire is larger than given by ideal string theory, and therefore because

$$c = 2\pi\omega / k = \lambda\omega, \tag{3.2}$$

where ω is the frequency and λ is the wavelength, the frequencies of the modes are going to be larger than predicted. As explained in section B.5 it is important to determine the frequencies of the modes are, but since we cannot determine their frequencies exactly by Eq. (3.1), we use this as a starting point and find them experimentally.

C. EXPERIMENTAL PROCEDURES

This section is devoted to explaining the procedures followed in performing the hot-wire experiment.

1. Finding Extended Standing Mode Frequencies

The first step involved in this experiment was finding the frequencies of the extended standing wavemodes. With the wire set up, one magnet was placed around the wire at the center of the wire, and a very small current was passed through the wire. The frequency of the alternating current was a few Hz within what is predicted for the first mode by Eq. (3.1), and the resulting displacement was observed visually. The frequency of the current was slowly adjusted upward and downward until we were convinced we had found the frequency producing the maximum displacement in the wire. This frequency was recorded.

Again using Eq. (3.1) and Eq. (3.2) we tuned the frequency of the current to that predicted for the second mode. Knowing that this has a node at the center, the magnet was moved to the position of the maximum, halfway between the center and the termination point. For all measurements, the magnet was moved to coincide with a region of maximum displacement on the wire. The motion of the wire was observed visually, and the frequency was slowly adjusted upward until maximum amplitude was observed. Again the frequency was recorded.

This process was repeated for each subsequent mode. It is important to note that as higher modes are achieved, the amplitude of vibration will decrease. In order to gain enough displacement by the wire to be noticeable to the eye, we needed to increase the amplitude by increasing the force on the wire. We did this by increasing the current for each measurement of a higher mode. For the first mode, no more than 0.2 A was needed to get a 1-2 cm displacement at the maximum of the wire, but once we reached the 9^{th} or 10^{th} mode, we needed to have greater than 1-1.5 A in the wire. It is possible that the increase in the driving force on our system could cause us to enter a nonlinear regime as

we searched for higher modes. But since we are only interested in a rough estimate of the frequencies of the modes so that we can stay between them (section B.5), the nonlinearity was ignored.

2. Mass, Tension, and Frequency

For the hot-wire experiment, we used 450 grams of hanging mass to provide the tension for both the 28 and 30 gauge BNC wires. If more mass is used, the frequencies are higher, so the moving regions of the wire will cool more rapidly. But the displacements will be smaller, so it will not cool as efficiently. These are competing effects. This value of mass separates the frequencies of the fundamentals by 27 Hz for the 28 gauge wire, and by 22 Hz for the 30 gauge wire. This gives us a reasonably large frequency window to work with, between extended standing modes, without going to close too them. If less mass is used, displacements will be larger, but the frequencies are lower, again competing effects. We decided that once we gained some experience with the system, we could modify this mass at any time to try and achieve the desired results.

3. Measuring the Magnetic Field Profile

The profile of the magnetic fields is especially important in the continuous source experiments. The profile was measured in the following manner. The array of magnets was held together using clamps, and placed next to an optical bench. On the optical bench was a sliding mount with the probe from a M.W. Bell Model 5080 Gauss/Teslameter attached. The setup was arranged so that the probe extended into the area between the magnet faces, and as the mount slid on the optical bench, the probe would travel down the length of the magnet array between the faces. The Gauss/Teslameter gives the value of the magnetic field at the tip of the probe.

Data points were taken every centimeter along the length of the magnet array and for up to several centimeters outside the end of the array, to determine the fringe field.

These data points were recorded by hand and entered into a computer to create magnetic field profile graphs.

The graphs were then analyzed to see if their contour would be consistant with nonradiating conditions. A homogenous field such as that shown in Fig. 2.2(a) may not be possible to acheive, and is not entirely necessary. Since the continuous source setup can be viewed as the sum of many two-point nonradiating sources in sequence, we can achieve nonradiation if the continuous profile varies according to a specific pattern. For example, if with a 10 magnet array, the field begins with a large value on the left most magnet, and decreases slowly over 5 magnets, then jumps back up to an equally large value at magnet 6 before slowly decreasing again, nonradiating conditions will still be met.

Upon analysis of the field profile, we can change the order on the magnets and re-measure, to try and find a profile that is most conducive to nonradiation. This effort was aided by measuring the profile of each magnet individually, in a similar manner, to determine which magnets were the strongest and which were the weakest.

The magnets also have adjustable gaps. We can change the force with which the system is driven without changing the current. Since we need a minimum threshold current to get the wire to glow, the magnet faces can be moved farther apart or closer as needed to change the force on the wire. At minimum separation, the magnet faces have a gap of about 1.3 cm. At maximum separation, the gap is about 2.3 cm. It should be noted that at maximum separation, the drop in field intensity between neighboring magnets becomes more pronounced.

4. Measuring Amplitudes of Vibration

Even though the hot-wire experiment is supposed to be qualitative, for the continuous source setup we wanted to be able and make some kind of rough relative measurement of the amplitudes of vibration inside the magnet array, and of whatever leakage may occur outside the system. Measuring the leakage was not problematic since the wire outside the magnets was easily viewed from any angle. But measuring the

vibration inside the magnets was difficult because the magnets prohibited easy access to the wire. This led us devise a tool that uses a dial rod micrometer to probe the wire and determine its vibrational displacement (Fig. 3.4).

To construct our micrometer, a dowel rod was passed through a piece of pipe that had been fashioned to act as a guide and keep the dowel horizontal. While there is no current in the wire, the dowel rod is pushed through the guide until it touches the wire. A reading is taken on the dowel at the guide to indicate that position. While operating, the wire is vibrating and the process is repeated. The wire can be heard hitting the dowel so we know when contact is made. Again the position of the dowel is marked. The distance between the two marks is the amplitude of vibration of the wire.

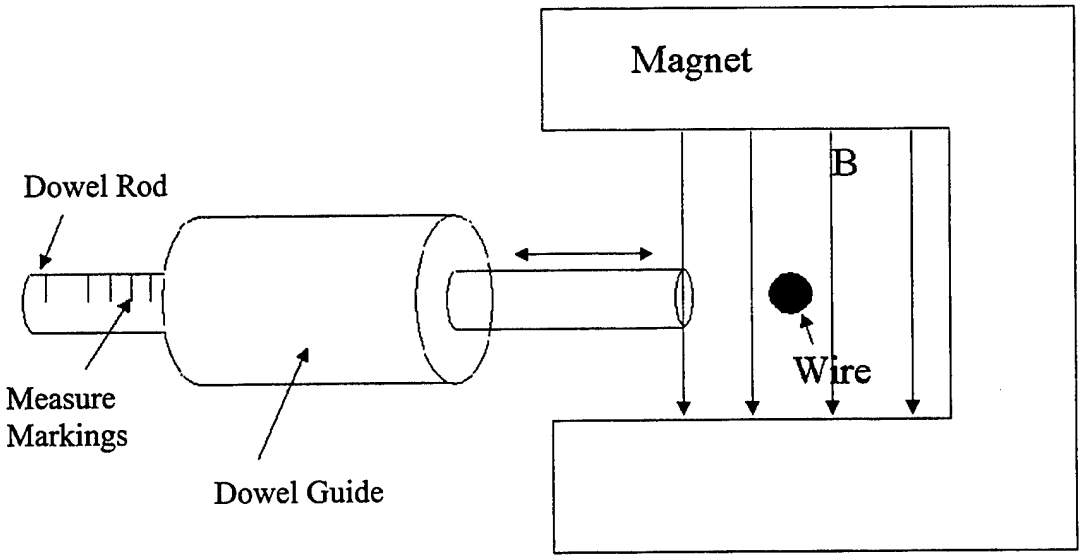

Fig 3.4 A schematic of the dowel rod measuring devise

5. Frequency Sweeping; Listening and Observing

In order to find the frequencies at which our system is nonradiating, we had to be careful in the way we searched through the frequencies. The equations used to find the

frequency at which the system is nonradiating assume an ideal system. We use these equations only to find an approximate value of the frequency. It is our job to tune the frequency to obtain the cleanest possible example of a nonradiating source. To perform this operation, we would rely on two factors. The first is the appearance of the system, and the second is the emitted sound. The procedure employed is as follows.

With the current set to zero, the frequency is set to the value predicted by theory in Chapter II. The current is slowly increased until the vibrations in the system can be heard. When the system is vibrating at one uniform frequency, the emitted sound is a steady tone and is quiet compared to background noise. This is an indication that the system could be oscillating in the nonradiating state. If the system is not in the nonradiating state, the system will be oscillating with multiple harmonics and the sound is typically louder, and not steady. The vibrations that occur could have enough amplitude to cause the wire to collide with the magnet faces. This can easily be heard. In addition to this, when the system is not in the nonradiating state, the sound produced can have a quasi-periodicity (low frequency modulation) which can also be heard.

If the sound continues to indicate one frequency (the nonradiating frequency), then the current is increased to the threshold at which the wire glows. If the sound indicates multiple frequencies, the current is kept steady as the frequency is tuned to obtain one single frequency, and then the current is increased.

Once the wire is glowing, the state of the system is more easily seen. If the system is in a nonradiating state, a picture is taken, otherwise the frequency is tuned. Changes in the frequency were made slowly, in small increments, to allow for transient motion to die out. Changes were made in increments no larger than 0.5 Hz, and the system was allowed to settle for several seconds before another change was made. This was also true for changes made in the frequency while the current was still being increased. Pictures were only taken when the system was in a stable state, after the transient motion ceased. It did occur that a system would exhibit a quasi-periodic behavior, and appear alternatingly more and less clean. In these cases, the picture was taken when the system appeared the cleanest, but the quasi-periodicity was noted.

D. RESULTS AND OBSERVATIONS

This portion of the chapter gives the results of the experimentation. It includes pictures as well as quantitative data taken during the course of the hot-wire experiment. The results will be given in a format that includes a description of the specific setup, giving the number of magnets, the position of the magnets, the frequency at which the observation was made, and the pictures taken. Included in this will be the profiles of the magnetic field in the cases of the continuous sources. The pictures will be followed by any commentary about that specific scenario.

Section D.1 gives tables showing the results of the extended standing wave modes of the wire. The results in sections D.2, D.3, D.4 and D.5 are that of the system during operation in attempts to observe nonradiating sources. During the course of research, there were slight changes in the methodology used in making the measurements and in the setup itself, and additions to the equipment used. These are noted as they occured. All experimentation performed on the 28 BNC wire was completed before experimentation on the 30 BNC wire began. We did not go back and make modifications to the experiment on the 28 BNC wire that were made in the setup during the experimentation on the 30 BNC wire.

1. Frequencies of Extended Standing Wave Modes

We first begin with the frequencies of the extended standing wave modes for the two different BNC wires. Figure 3.5 shows the values of the theoretical frequencies as well as the experimental values for each mode n of the 28 BNC wire. Figure 3.6 shows the same for the 30 gauge BNC wire. Tables 3.1 and 3.2 show the numerical values of the data contained in Figs. 3.5 and 3.6 respectively.

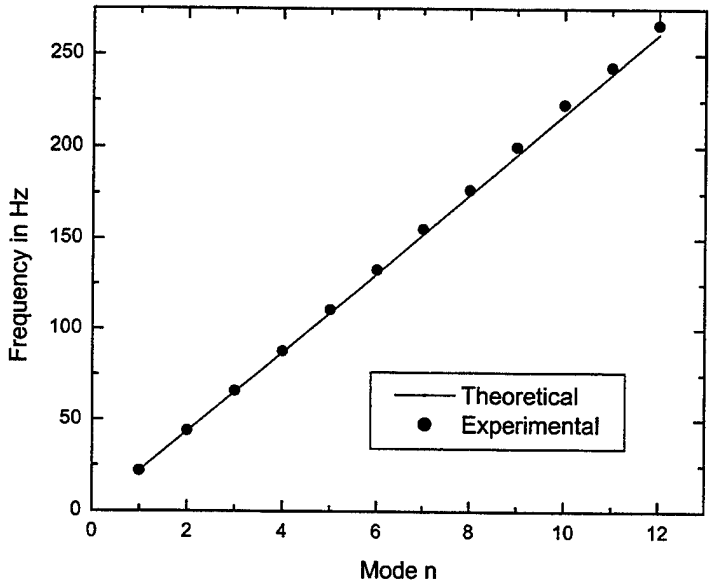

Fig. 3.5 A plot of the frequencies of modes of a 28 gauge BNC wire, 1.88 m in length, is shown. The line representing theoretical values is also shown.

Mode	Predicted Frequency (Hz)	Experimental Frequency (Hz)
1	21.75	22
2	43.5	44
3	65.25	66
4	87	87.9
5	108.75	110.7
6	130.5	133
7	152.25	155.4
8	174	176.8
9	195.75	200.3
10	217.5	222.9
11	239.25	243.2
12	261	266.1

Table 3.1 Data plotted in Fig 3.5.

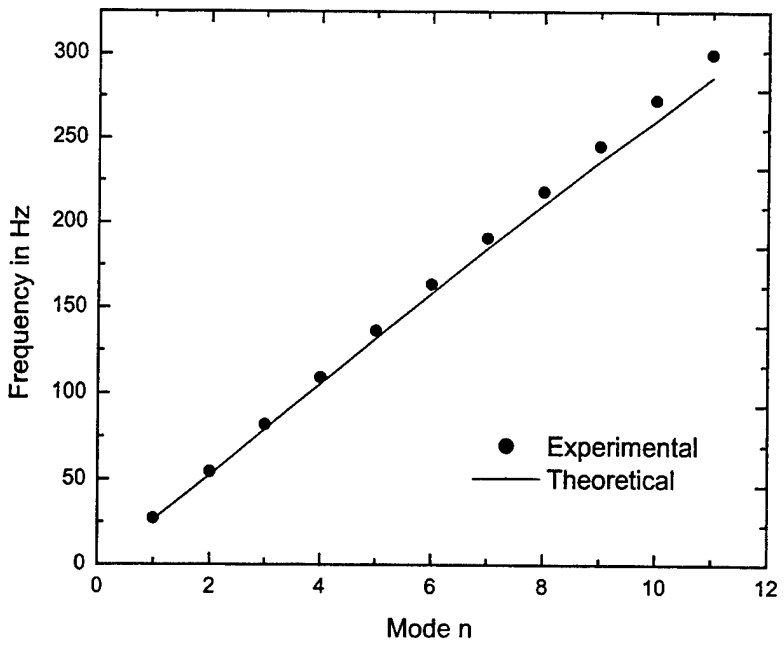

Fig. 3.6 A plot of the frequencies of modes of a 30 gauge BNC wire, 1.88 m in length, is shown. The line representing theoretical values is also shown

Mode	Predicted Frequency (Hz)	Experimental Frequency (Hz)
1	27.26	28.3
2	54.53	56.5
3	81.8	85.1
4	109.1	113.3
5	136.31	141.7
6	163.57	170.1
7	190.83	198.7
8	218.09	226.5
9	245.35	254.4
10	272.61	280.4
11	299.87	308.2

Table 3.2 Data plotted in Fig 3.6.

2. Two-Point Source

The first case we considered was a two-point source. Using the 30 BNC wire, magnets 7 and 8 (see Appendix D) were placed with a distance of 51.9 cm between the centers. For the first nonradiating mode, this distance corresponds to a one-half wavelength or frequency of 98.6 Hz, which is between extended standing modes 3 and 4 of the overall wire, according to Fig. 3.6.

Figure 3.7(a) shows the setup with the laboratory lights on, and the two magnets can be seen. Figure 3.7(b) shows the system as it appeared in operation in the dark, with a current of 1.93 A in the wire, and frequency 99.2 Hz, which that produced the cleanest looking nonradiating source. The frequency producing the cleanest nonradiating mode was difficult to determine since the source looked very clean over a range of frequencies. The region of wire between the two magnets is distinctly darker than the surrounding wire, signifying significantly greater vibration. A measurement of the relative radiation amplitude (Section III.C) with the micrometer was not made in this case, but experience tells us that amplitudes of vibration on the order of 0.5 cm or greater are needed to cool the wire to its original color.

The second mode could not be observed in this configuration. When driven at the predicted frequency (295 Hz), we could not obtain a pattern of vibration consistent with the second nonradiating source. While tuning the frequency, the observed pattern of the wire would collapse into the 10^{th} extended standing wave mode of the wire as the frequency was lowered to near 280 Hz, and the wire would also collapse into the 11^{th} extended standing wave mode when the frequency approached 308 Hz. In between, the wire was a homogenous orange color and little vibration could be seen. Vibration could be heard, and the wire emitted sound of very unusual harmonics, signifying a superimposition of different wave states.

We then increased the separation of the magnets to a distance of 75.2 cm, which corresponds to a frequency of 68.2 Hz for the first nonradiating mode. This frequency is between those of the 2^{nd} and 3^{rd} standing modes of the wire. The results are shown in Fig. 3.8, for a current of 1.945 A in the wire.

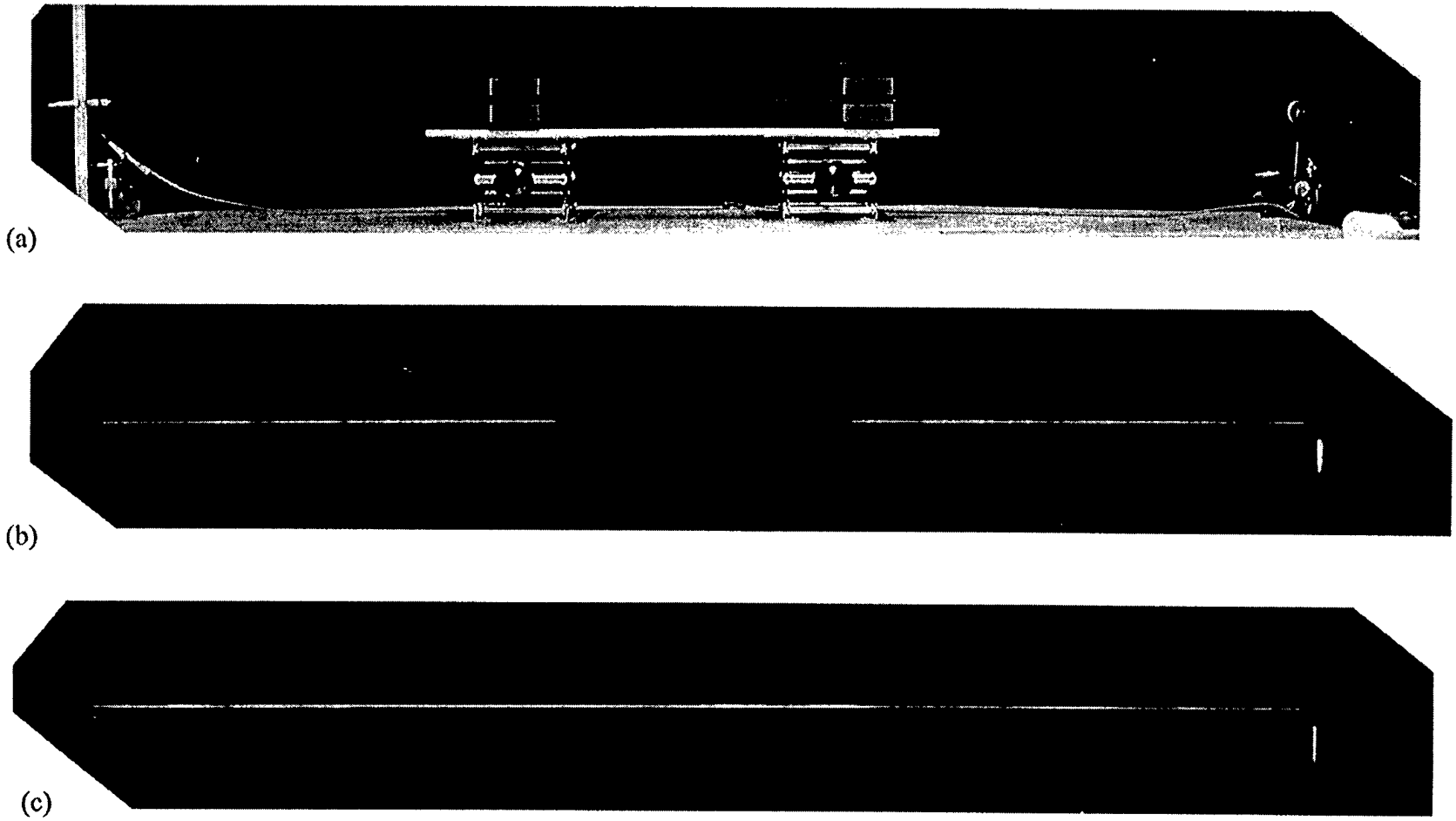

Fig. 3.7 The two point nonradiation experiment for a separation of 51.9 cm. (a) Setup and (b) system in operation. The pictures are lined up so that it can easily be see which positions on the glowing wire are cooling relative to the position of the magnets. For comparison, (c) shows the wire with the current but no magnets and therefore no motion, so the inhomogeneous regions of the wire can be noted.

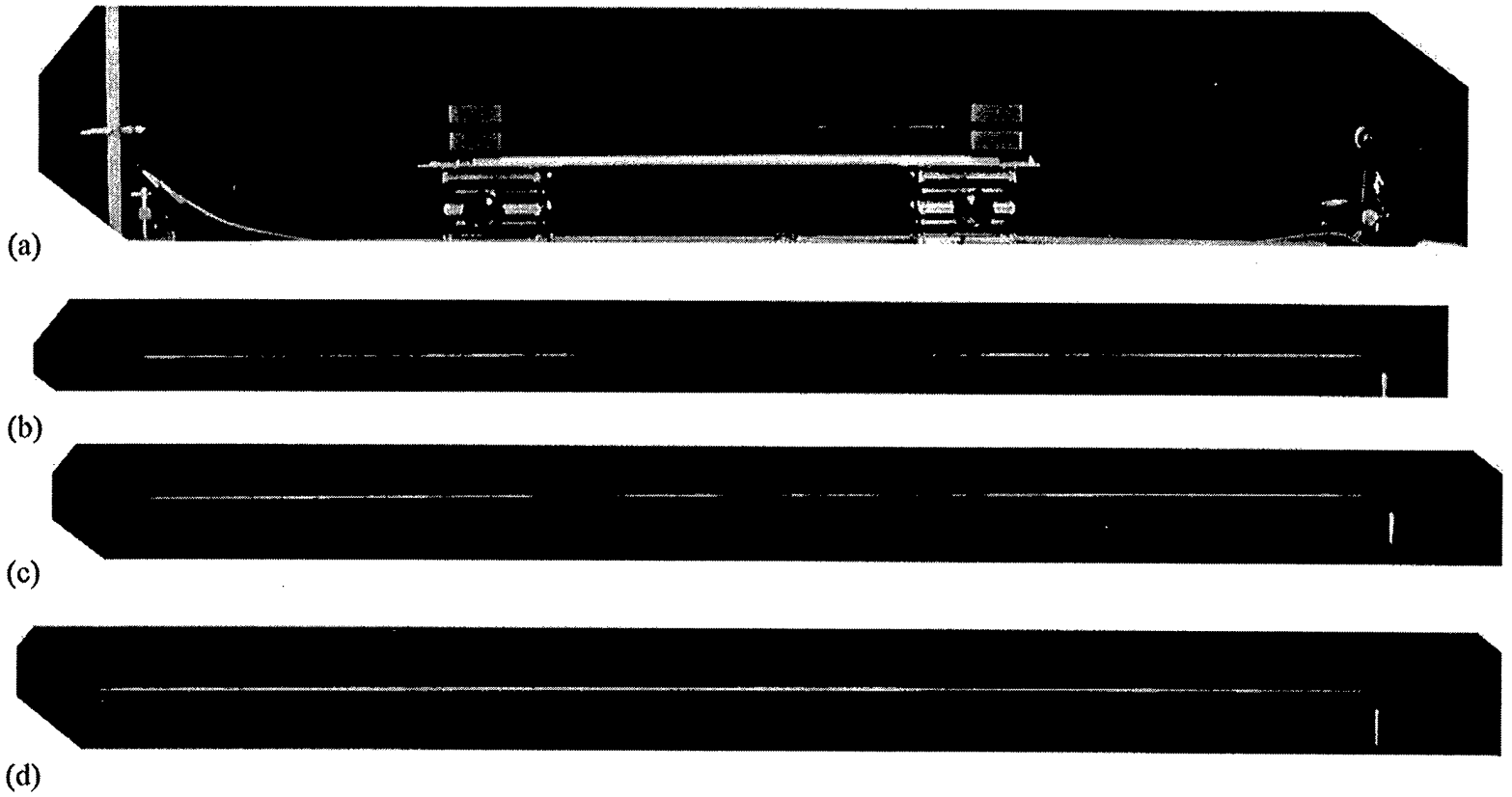

Fig. 3.8 The two-point experiment with 75.2 cm between the magnets. (a) setup, the (b) first and (c) second nonradiating modes. We have also included the reference picture of the still wire (d). All the pictures the rest of the chapter are lined up in the same manner as Fig 3.7.

As in Fig. 3.7, the first picture 3.8(a) is with the laboratory lights on. The second picture 3.8(b) is the first nonradiating mode. This picture was taken while the driving frequency was 70.0 Hz, but the system was clean over a range of frequencies. The third picture, Fig. 3.8(c), is the second nonradiating mode and was taken at 204.6 Hz. The second mode was very difficult to obtain and it can be seen that this nonradiating mode is not very clean. It can be seen that there are three regions of the wire in between the magnets that are darker than the rest of the wire. The areas of maximum vibration are not totally dark, but the picture is good enough to see that the nonradiating mode does exist.

The two-point source experiments for the 28 BNC wire were not highly successful. We believe that in order to convince ourselves that nonradiating sources exist for a given system, it should be possible to demonstrate at least the first two nonradiating modes. This was not the case for the 28 BNC wire. Although a response similar to that expected for the first nonradiating mode was possible, it was never as clean as with the 30 BNC wire. The second nonradiating mode was never successfully observed, not even a very dirty one.

We did start off the experimentation by looking for the modes of the two-point source 28 BNC system, but we abandoned it because of our lack of success, and went to the continuous source for the 28 BNC wire setup. The continuous source setup occupied the majority of the experimentation time, and it was only after greater success with the 30 BNC wire over the 28 BNC wire, did we go back and try the two-point source experiments with the 30 BNC.

3. Continuous Source with 10 Magnets

The continuous source nonradiating experiment with 10 magnets was the most extensively studied system. We attempted to obtain examples of nonradiation for a number of different magnet configurations, both with and without the steel plates installed. We first consider the case without steel plates.

Without steel plates, the continuous source nonradiating experiments began first with measurement of the magnetic field. The magnets were numbered 1 through 10 based

on their initial order. After an initial measurement, it was decided to rearrange the magnets, based on the individual magnet strengths. The intensity of the magnetic field for a point inside the gap for a magnet in the array differs greatly from that of an individual magnet. The relative field intensities inside the magnet gaps did not stay the same when they act in concert. The order of 6 3 7 5 8 4 9 2 10 1 was used. Figure 3.9 shows the results of the measurement of the field in this configuration and with minimum separation between the magnet faces. The position 0 marks the left edge of the magnet array and 76 marks the right edge. Points outside of this signify fringe fields.

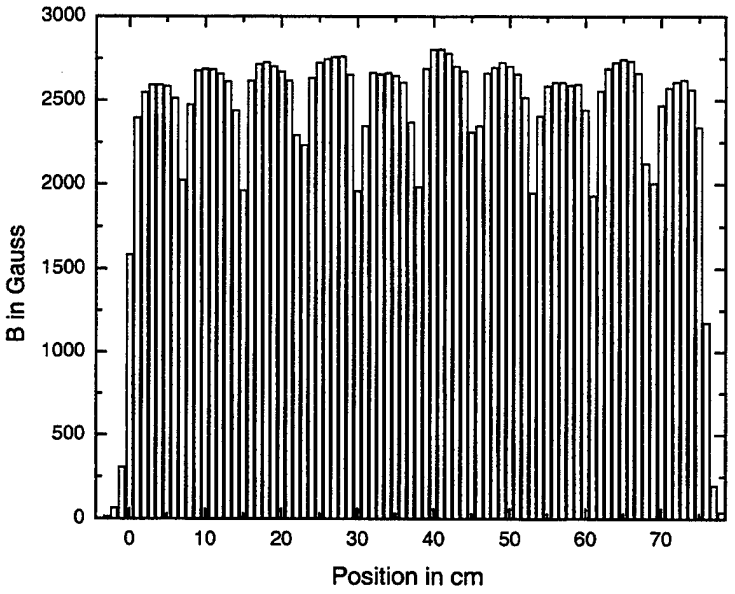

Fig. 3.9 The magnetic field profile of the 10 magnets in the order used in much of the experimentation.

Figure 3.10 shows the results of this setup for operation with the 28 gauge BNC wire, which required a current of 2.7 A to begin glowing, and needed about 2.9 A to glow bright enough for a clear picture. We did not use more than 3 A in the wire. Early on, several wires were broken when a higher current than this was passed through the wire. Figure 3.10(b) was taken at a frequency of 108 Hz and Fig. 3.10(c) was taken at 233.1 Hz. This is notably higher than what is predicted. According to Fig. 3.5, the first

nonradiating mode occurred at a frequency very close to an extended standing mode of the wire, but this did not seem to dramatically impact the search for the first nonraditing mode. The second nonradiating mode is between two extended standing wave modes.

In the attempt to find the second mode, some very interesting behavior was observed. For the 76 cm length of the magnet array, the frequency at which the 2^{nd} nonradiating mode should have been observed is 215 Hz. This is based on the theory for the speed of waves on a string, which predicts frequencies that are typically low compared to observation. The frequency was set at this value and then slowly increased.

Starting at a frequency of about 230 Hz, the system began to exhibit properties of a nonradiating source. Peak amplitudes of vibration inside the magnets tended to be on the order of 0.5 cm, while the amplitudes outside tended to be less than a 0.5 mm. Even though a frequency of 230 Hz is close to the 10^{th} standing wave mode of the wire, the nonradiating setup produced its own standing wave patterns that were much different. It was possible to observe 6 distinct peaks along the length of the wire. Our belief that this is the second nonradiating mode is due to the relative brightness of the 2 interior peaks compared to the 4 exterior ones. There were the two large peaks inside the magnetic field, and there were two smaller peaks between the edge of the magnets and the ends of the wire on either side. These vibrations were noticeable in the color of the wire. Two distinctly dark regions were seen inside the magnetic field where the amplitude was large enough to permit significant cooling of the wire. Where leakage occurred, the smaller vibrations outside the magnets were enough to cool the wire to a slightly less bright orange, but not enough to cool it back to its original black. It is also important to mention that the 6 peaks observed in the second nonradiating mode were not uniformly spaced. The two peaks inside the magnetic field were separated by a greater distance than the four peaks outside the field. The edge of the magnets nearly matched two of the nodes on the wire so that the interior peaks were separated by 76/2 = 38 cm, and the exterior peaks were separated by about 30 cm. Figure 3.11 schematically shows the wire displacement.

Other interesting behavior observed was the tendency of the system to start off clean, but deteriorate as time passed. After a time of about two seconds (decay time), the amplitude of vibration in the center of the magnets decreased somewhat, and

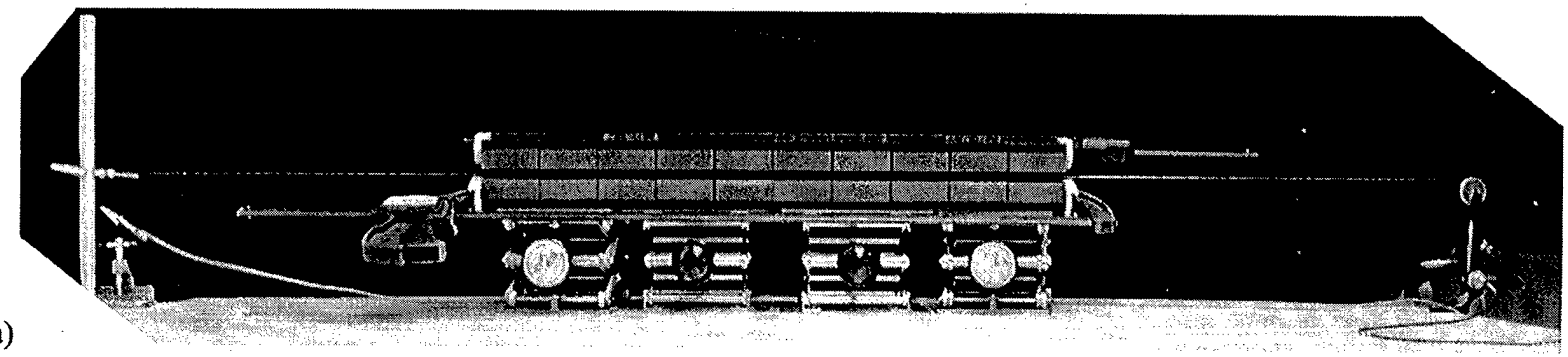

(a)

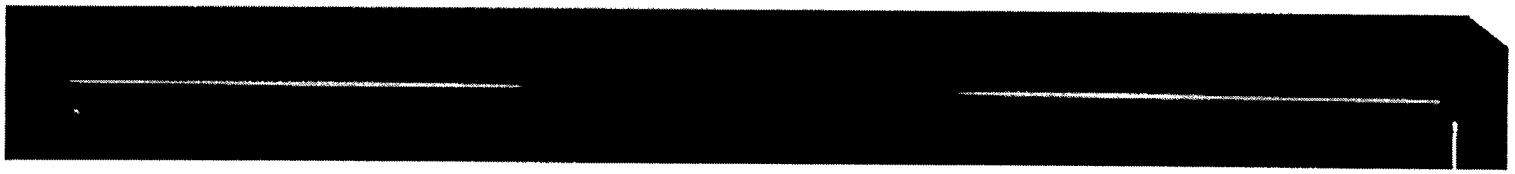

(b)

(c)

Fig. 3.10 Continuous source with 28 gauge BNC wire: (a) setup, (b) first and (c) second nonradiating modes.

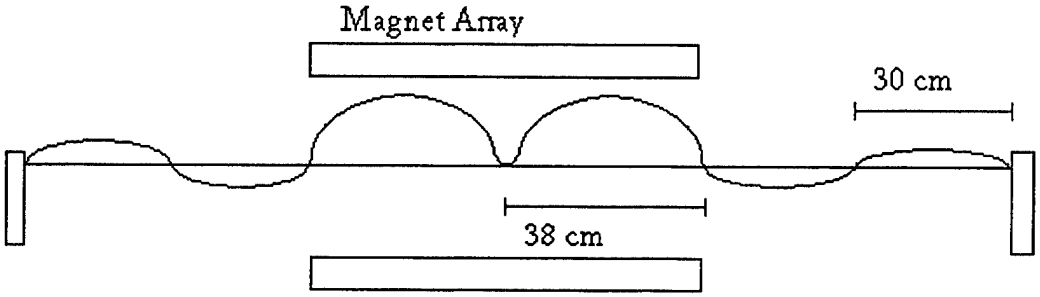

Fig. 3.11 The displacement of the wire described above, showing the position of the peaks

the wire began to heat up and change from black to a dim orange. Although it was not possible to determine with precision how much the amplitude changed, it was enough to change color. The color of the wire outside the magnets grew slightly dimmer and the amplitude of vibration increased slightly to 0.75 mm. Although the relative colors along the length of the wire still made it possible to discern where the peaks and troughs were, the system was much dirtier.

If the frequency was slightly increased, the system would reacquire the cleaner nonradiating source look. The two central dark regions would become black again, and the outer four peaks would decrease in amplitude and become more orange. However, this effect was temporary. After another few seconds the system would decay into a more dirty state again, similar to the one described above. If the frequency was increased again, this process would be repeated. At greater frequencies, the length of time required for this cycle to occur would lengthen. The two second decay time stretched to about five seconds by the time 234 Hz was reached. Above 234 Hz, the decay time decreased again until 235 Hz. Upon reaching 235 Hz, the system was rapidly disrupted and collapsed into a wildly oscillating state that somewhat resembled an extended mode. There appeared to be 10 equally spaced peaks and nodes along the length of the wire.

The amplitudes of the peaks was such that the wire was colliding with the magnets and the whole system was making very loud sounds. This frequency is very near to what experience has determined the 10^{th} standing wave mode would be (somewhat higher than what theory predicted) and we believe that the wire collapsed into the 10^{th} mode. The system was not permitted to remain in this state for very long for fear of damaging the magnets.

Another interesting behavior that the system exhibited was hysteresis. At constant current, the approximate nonradiating source could only be maintained if the frequency was stepped up from below, as described in the preceding paragraph. If the frequency was ever stepped down, the system would become increasingly dirty. When the system collapsed into the wild state previously described, turning the frequency down to below 235 Hz did not return the system to a nonradiating system of any sort. The system would not return to an approximate nonradiating source unless the frequency was lowered to below 230 Hz. Then the process of slowly increasing the frequency could then begin again.

Using the 30 BNC wire, the experiment was repeated. The order of the magnets stayed the same, so the magnetic field profile was the same as well. Under the same tension, theory predicts the first two standing wave modes of the 30 BNC wire will occur at a frequency of 134.8 Hz and 269.6 Hz respectively. The 30 BNC wire glows at a current of about 1.7 Amps. Figure 3.12 shows nonradiating states. Figure 3.12(b) was taken at a frequency of 134.4 Hz and with a current of 1.95 A. Figure 3.12(c) was taken at a frequency of 299.8 Hz and 1.95 A.

For the 30 BNC wire, we began using the dowel rod micrometer to measure the amplitudes of vibration in the hot-wire system. For the first nonradiating mode, the vibration amplitude inside the magnets was about 6 mm. The leakage outside the magnets was only vibrating with an amplitude less than 0.5 mm. This gives a relative radiation amplitude of about 0.083. For the second nonradiating mode, the inside vibration was about 3 mm and the leakage was less than 0.5 mm. This gives a relative radiation amplitude of 0.167.

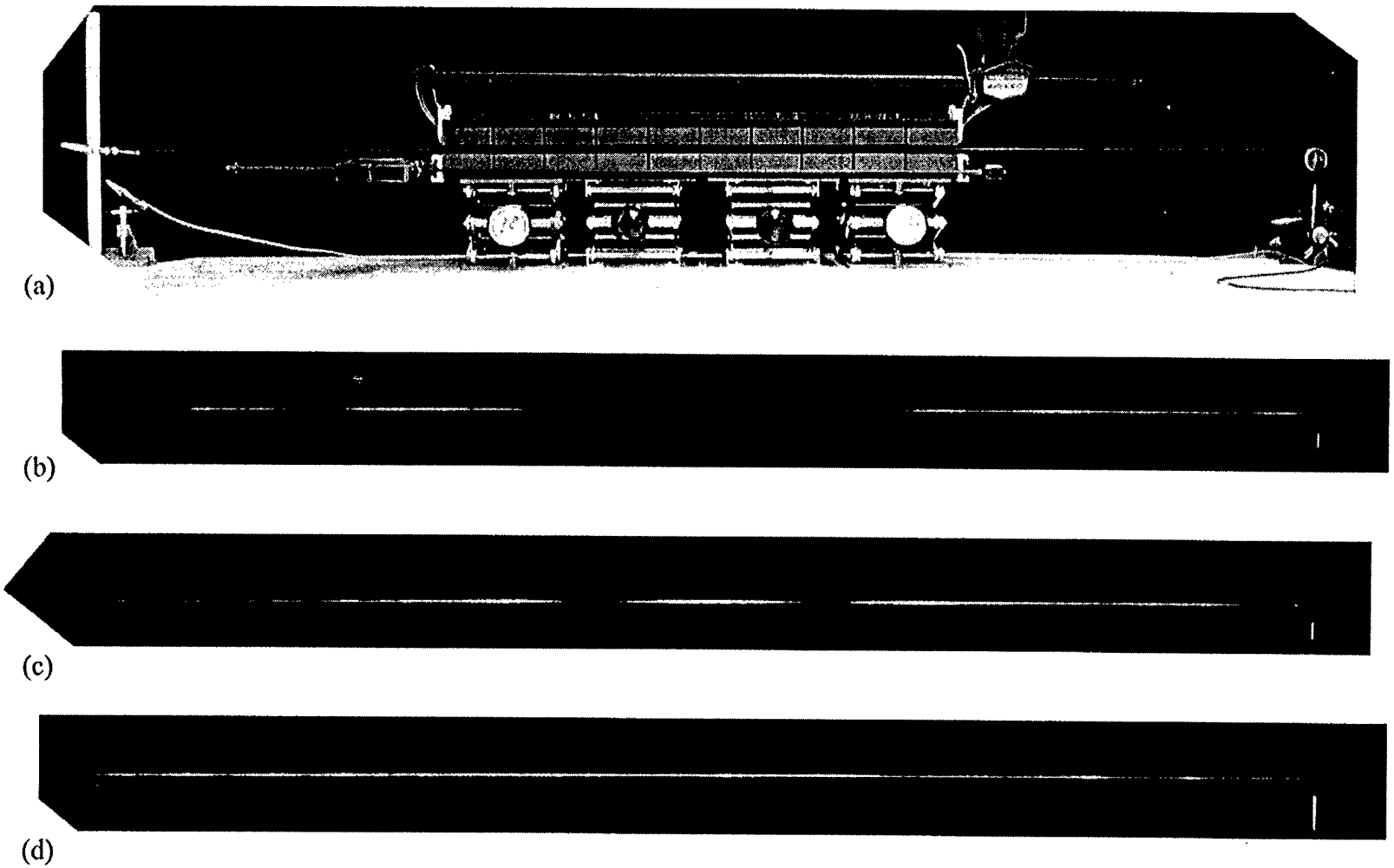

Fig. 3.12 The setup (a) for the 30 BNC wire, the first nonradiating mode (b), the second nonradiating mode (c) and the reference still wire (d).

We also performed the experiment with the magnet faces at maximum separation. (2.3 cm) Figure 3.13 shows this magnetic field profile, with the magnets in the same order as above. We thought that perhaps a reduced magnetic field and smaller driving force might improve the results.

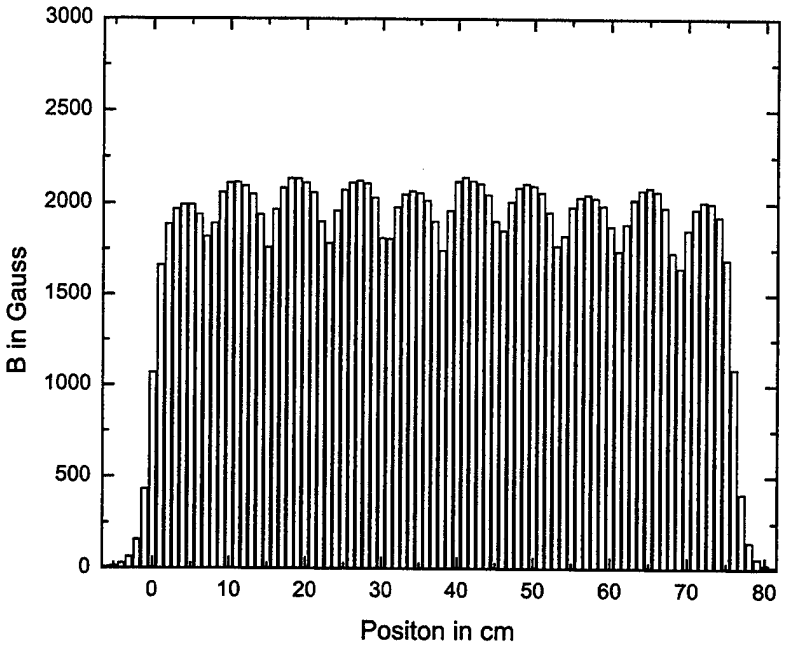

Fig. 3.13 Magnetic Field profile of magnets with maximum face separation. Notice that the fringe field extends a greater distance than that of fig 3.5

This setup did not produce satisfactory results for either the first or second nonradiating modes. We believe that this is due to the fringe fields. They extend well outside the magnet array and act as a force on the wire in a position not consistent with nonradiating conditions.

To attempt to improve the quality of the nonradiating source, we decided to add the steel plates as described in section B.3, and observe if a more homogenous B field would affect the experiment. Figure 3.14 below shows the magnetic field of the array

with the magnet faces at minimum separation (1.3 cm) and 1/8 inch thick steel plates inserted into the array. The resulting gap width was about 0.6 cm.

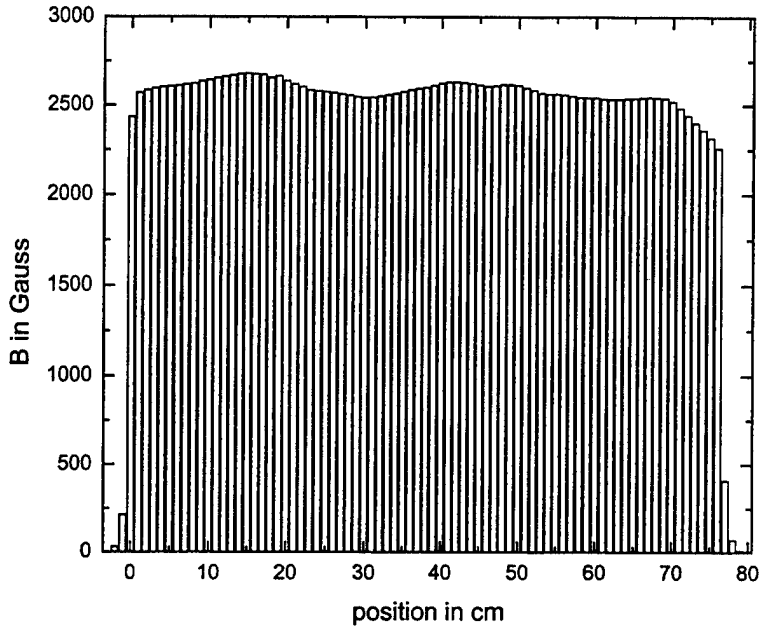

Fig. 3.14 The profile of the magnets with 1/8 inch steel plates inserted between the plate faces. The order of magnets is still 6 3 7 5 8 4 9 2 10 1

This did not give us the uniform field we were looking for. Because the gap between faces is not *exactly* 1.3 cm for all the magnets, when each magnet is adjusted to its minimum, the steel plates did not come in contact with the face of each magnet. A lack of contact between the magnet face and steel plates in several points gave rise to the nonuniform field above. Would it be good enough to produce a nonradiating source?

Figure 3.15 shows the experiment with 28 gauge BNC wire. The pictures were taken with 2.9 Amps in the wire. For comparison, we have included the second nonradiating mode for the case of no steel, Fig. 3.15(d). The case with the steel has a slightly longer length of wire that is black. This signifies a larger amplitude and a cleaner nonradiating wave source.

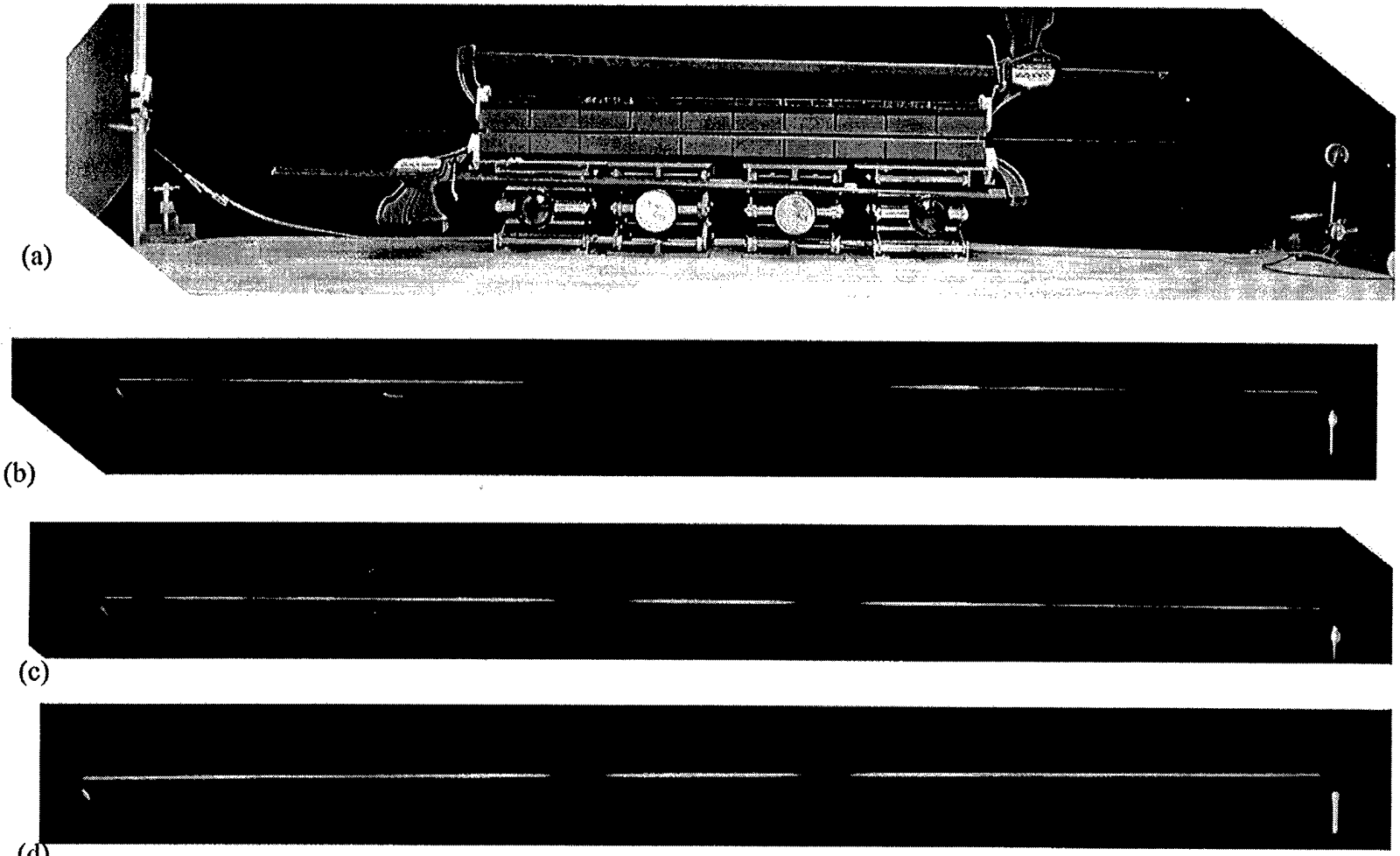

Fig. 3.15 The first two nonradiating modes (b) and (c) in the case with steel for the 28 BNC. For comparison (d) is the second mode from the previous section with no steel.

The procedure was repeated for the 30 gauge BNC wire. Figure 3.16 shows the observed nonradiating modes. For the first mode, Fig. 3.16(b), the picture was taken at a frequency of 134.4 Hz and with a current of 1.97 Amps. Using the dowel rod micrometer, we found the displacement inside the magnet array to be about 5 mm, and the displacement outside to be less than 0.5 mm, for a relative radiation amplitude of less than 0.1.

For the second nonradiating mode, Fig. 3.16(c), the picture was taken at a frequency of 301.0 Hz and a current of 1.91 A. The interior displacement was about 4.5 mm, and the exterior displacement was less than 0.5 mm. The relative radiation amplitude is smaller than 0.11.

It can be seen in the pictures for the continuous source experiment that, at the point where the wire exits the magnet array, there is a decrease in the brightness. This is especially noticeable in Fig. 3.15(c). However, at this point there is not a rapid change in the pattern of vibration. It was proposed that this color change was the result of the wire inside the magnets being confined to vibrate inside a very small area. As the wire heated the air around it, the air was trapped, and this kept that region of wire warmer, and more orange compared to the wire outside the magnets, regardless of the pattern of vibration.

To test this theory, we decided to erect planks of wood around the wire. This would subject the entire wire to this confining effect, rather than have a different cooling effect for the wire inside the array than outside of it. We only put wood above the wire since heat rises, and we felt that this was the direction in which it was most important to confine the heat. Figure 3.17 shows the position of the wood relative to the rest of the setup, and Fig. 3.18 shows the effect that the wood has on the appearance of the setup. Figure 3.18(a) and Fig. 3.18(b) compare the first nonradiating mode of the 30 BNC wire with the steel, one with the wood and one without. Figure 3.18(c) and Fig. 3.18(d) do the same for the second nonradiating mode. Notice that in Fig. 3.18(b) there is not the extreme drop in brightness that Fig. 3.18(a) has just outside the black region. Comparing Fig. 3.18(c) and Fig. 3.18(d), we observe that the effect of the wood is more noticeable at the terminations of the wire.

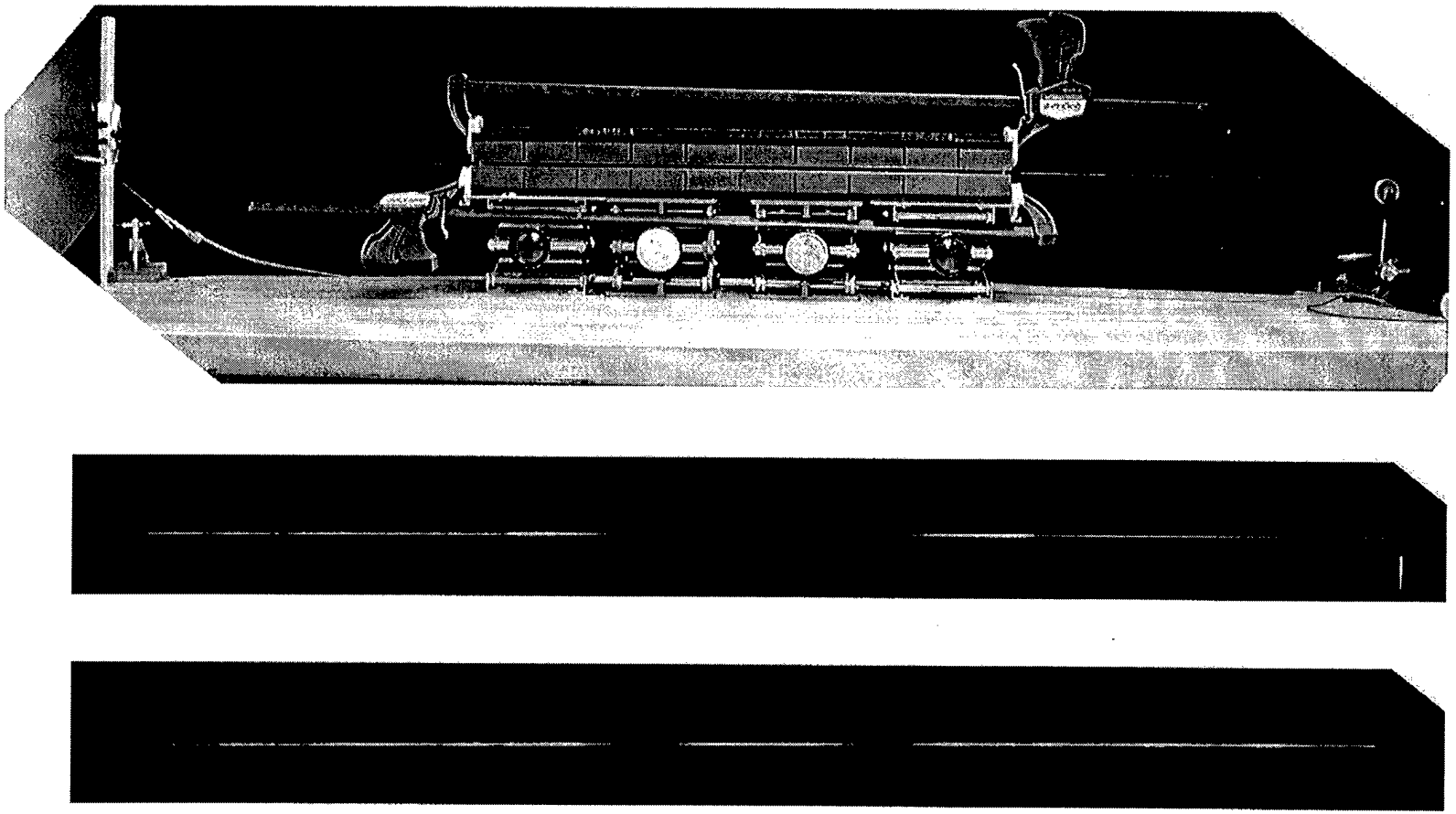

Fig. 3.16 The setup (a) for 30 gauge BNC with 1/8 inch thick steel plates. The first nonradiating mode is shown in (b) and the second mode in (c)

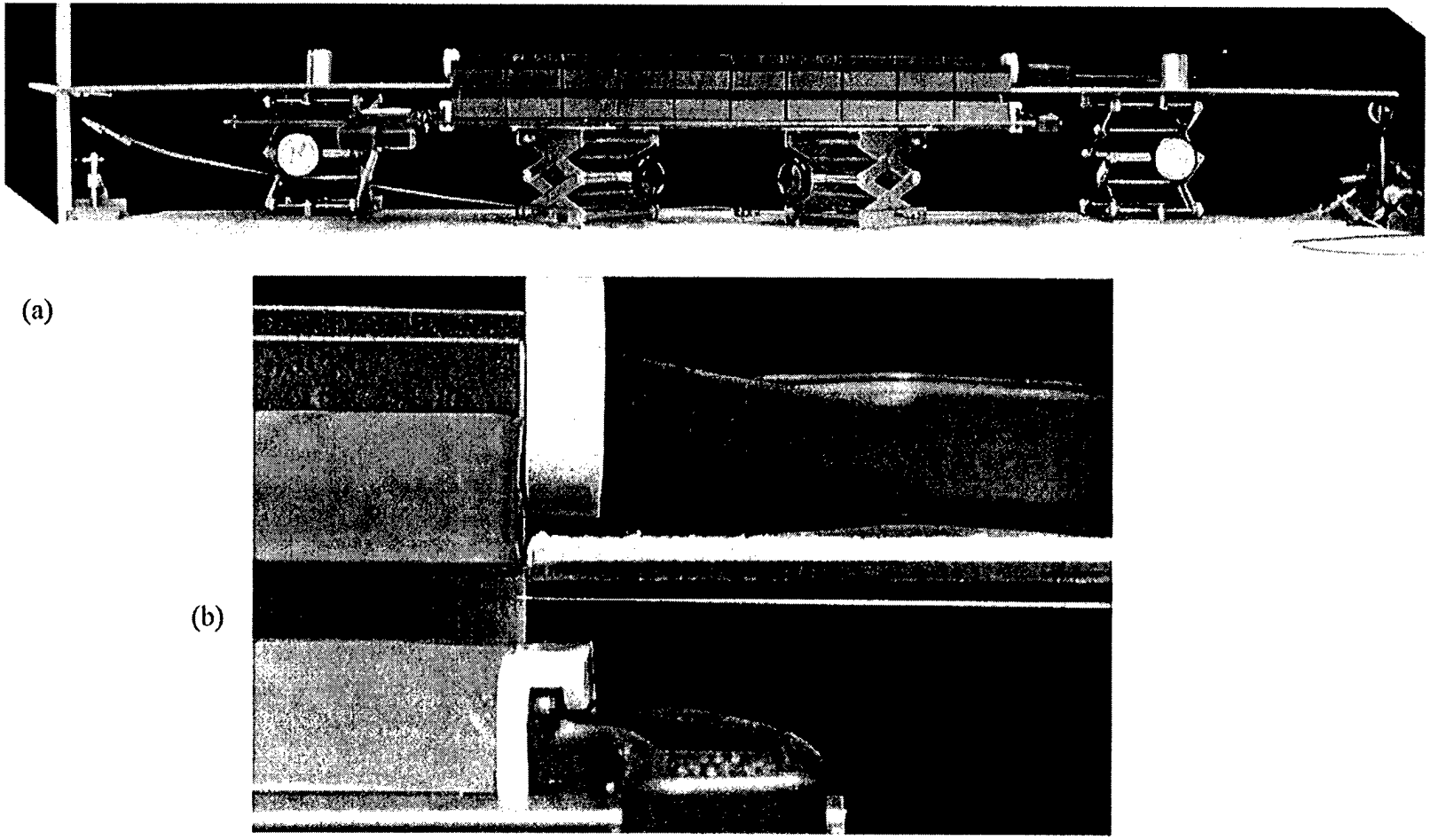

Fig. 3.17 (a) Setup with wood in place outside magnet array, and (b) zoomed-in view of the right edge showing the wood above the wire.

Fig. 3.18 The 10 magnet array for 30 BNC wire. The first mode (a) with and (b) without wood, and the second mode (c) with and (d) without the wood erected around the wire.

4. Continuous Source with 8 Magnets

A large factor affecting the quality of the nonradiating source in our experiment is nonlinearity. In a vibrating wire system, the degree of nonlinearity is related to the curvature of the wire while vibrating. Since we need motion in order to cool the wire to its original color, the longer the range over which force is applied, the easier it is to achieve this without a lot of curvature in the wire. We would like to see how small a range the system can be driven over, and still be nonradiating. We removed two of the magnets and repeated the experiment with only 8 while using the 30 gauge wire. The length of the array is reduced to 61.1 cm, which means that we predict the first two modes of nonradiation to occur at 167.75 Hz and 335.5 Hz respectively.

For the case without steel plates, we selected the magnet order 7 3 2 8 10 5 4 1 with the magnet faces at minimum separation (1.3 cm). Figure 3.19 shows the profile of the magnetic field for this configuration. The left edge of the array is marked by position 0, the right edge is marked by position 60.

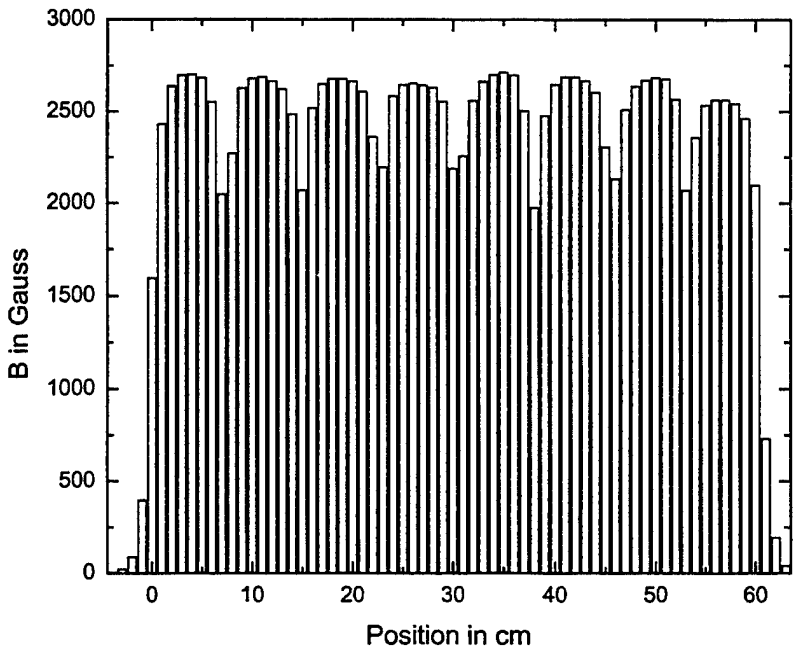

Fig. 3.19 Magnetic field profile of 8 magnet array. In this configuration there were no steel plates inserted into the array.

Figure 3.20 shows the observed nonradiating states for this configuration. The picture of the first nonradiating mode Fig. 3.20(b) was taken at a frequency of 166.2 Hz with a current of 1.949 A, where the wood heat shield was once again employed. The amplitude of vibration inside the magnet array was about 3.5 mm, and outside was less than 0.5 mm, giving a relative radiation amplitude of 0.14.

Figure 3.20(c) shows the second nonradiating mode. This picture was taken at a frequency of 361.6 Hz and a current of 1.96 A. The amplitude of vibration at a peak inside the magnet array was near 2 mm. Outside the array, vibrations were difficult to measure. There was vibration, but it was only on the same order as the diameter of the wire. In Fig. 3.20(c), the regions of blackness are not as black as in the cases with 10 magnets. This is reasonable because the amplitude of vibration is smaller, and the relative radiation amplitude is larger, making this not quite as good a nonradiating source.

We again inserted 1/8 inch steel plates into the magnet array, with the magnets left in the same order. Figure 3.21 shows the magnetic field profile for this configuration The modes are predicted to occur at the same frequencies as they would without steel plates. Figure 3.22 shows the nonradiating modes for the 8 magnet setup with 1/8 inch steel plates. The first mode, Fig. 3.22(b), was found at 164.5 Hz and using 1.964 A. The relative radiation amplitude was 0.14 with the interior displacement at 3.5 mm and the exterior at less than 0.5 mm. The second mode, Fig. 3.22(c) was found at 363.9 Hz using 1.969 Amps. The relative radiation amplitude was less than 0.25, with the amplitude of vibration inside the array being 2 mm, and outside less that 0.5 mm.

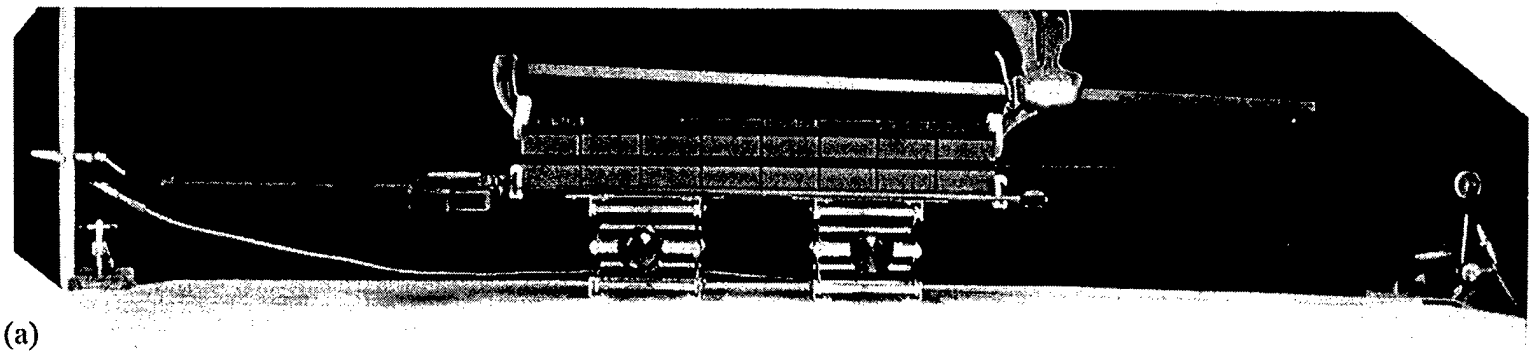

(a)

(b)

(c)

Fig. 3.20 Source with 8 magnets. In (a) the setup is shown without wood since this tends to obscure the picture, but the wood was included during the taking of (b) the first nonradiating mode, and (c) the second nonradiating mode.

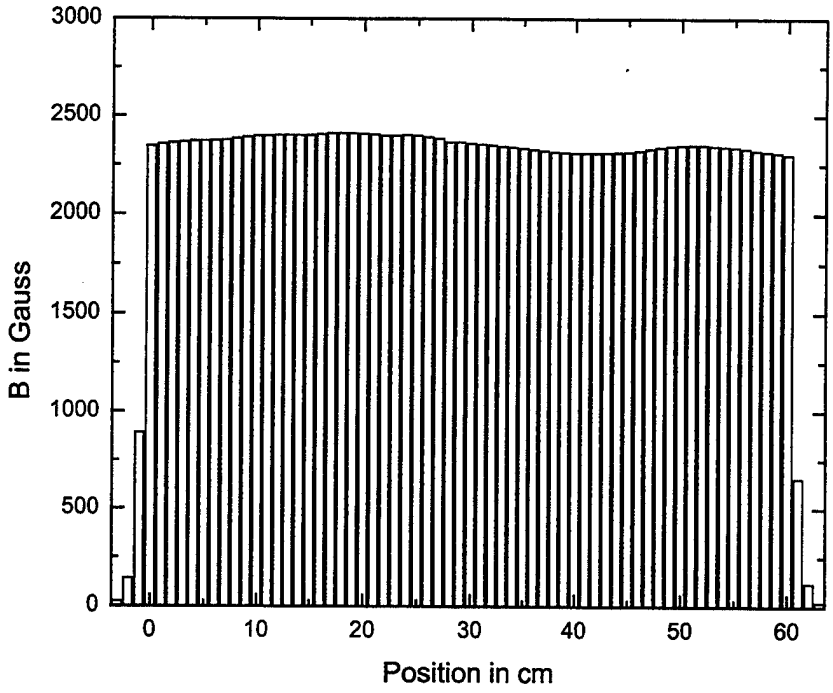

Fig. 3.21 The profile of 8 magnets with 1/8 inch steel plates and the magnets at minimum separation. With the peaks smoothed out, as compared to Fig. 3.19, the magnetic field above is approximately the average of the field given in Fig. 3.19.

Relative radiation amplitudes for the 8 magnet array are greater than those found for the 10 magnet array. This can be seen in the pictures, particularly for the second nonradiating modes. In Fig 3.20(c) there is a thin line visible where the amplitude is at its maximum, signifying that the wire in those regions is still glowing a little bit. In addition to this, there is more variation in the color of the wire outside the array, signifying greater leakage. For the 10 magnet array, the second nonradiating mode, the wire was able to cool down and turn completely black, while still maintaining a homogenous orange outside the array.

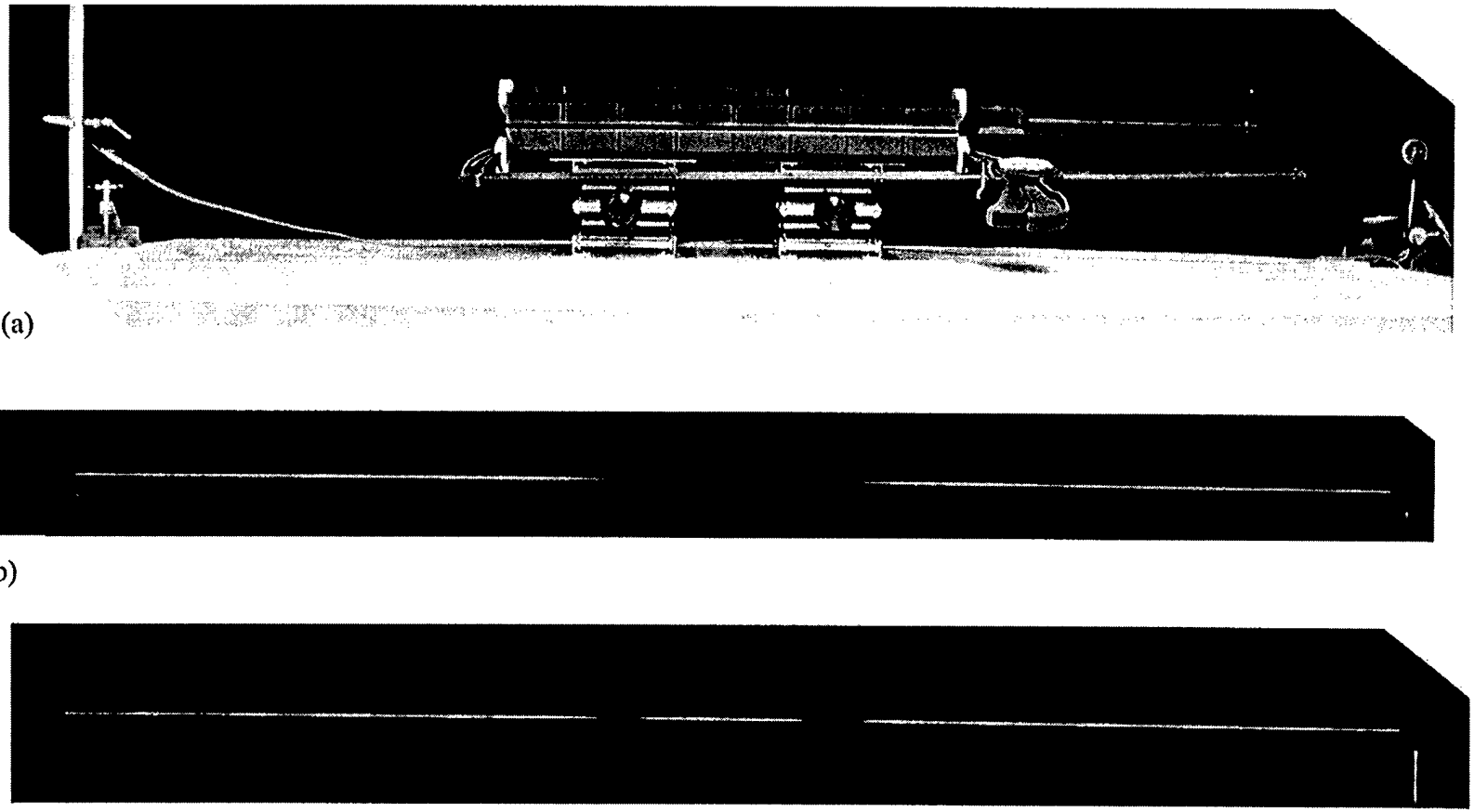

Fig. 3.22 Source with 8 magnets and steel plates. The setup (a) is shown here with the steel, but without the wood for clarity. The wood was used for the first mode (b) and the second mode (c).

5. Continuous Source 6 Magnets

We experimented with a 6 magnet array for the same reason as the 8 magnet array. In this case, the magnet array is getting short enough that the curvature of the wire is quite large when enough displacement is achieved to cool the wire. This is not a substantial problem for the first nonradiating mode, but it is more so for the second. As shown below, the systems here are dirtier compared with the ones in the previous two sections. Since the presence of the steel produces a cleaner nonradiating system, this setup only is presented here. Figure 3.23 shows the magnetic field profile of magnets 3 5 2 4 8 1. The 6 magnet array is 45.7 cm long, which means our predicted frequencies of nonradiation are 224.3 Hz for the first nonradiating mode and 448.6 Hz for the second nonradiating mode.

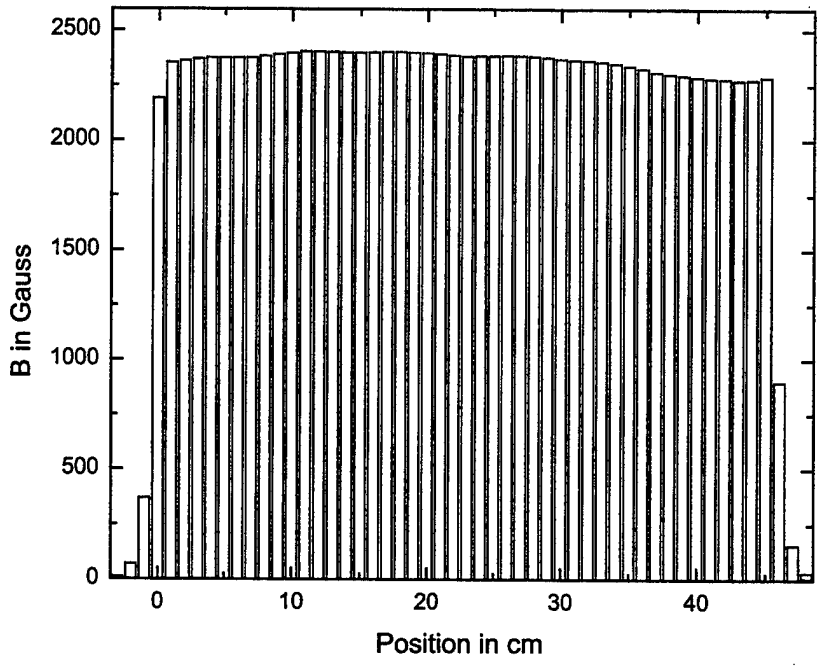

Fig. 3.23 The magnetic field profile of the 66 Magnet array.

Using a current of 1.935 A, the first mode was found at 247 Hz. The relative radiation amplitude was less than 0.16 with the amplitude of the peak inside the array at 3 mm, and vibrations outside the array occuring at an amplitude smaller than 0.5 mm. Using a current of 1.953 Amps the second nonradiating mode was found at a frequency of 489 Hz. The relative radiation amplitude here was about 0.25, with an interior peak amplitude of 2 mm, and leakage vibrations of 0.5 mm amplitude. These relative radiation amplitudes are not that different from those found for the 8 magnet array, but we believe that error in the use of the dowel rod micrometer accounts for this. As can be seen below, the quality of the nonradiating state was not as good for the 6 magnets as for the 8. Figure 3.24 shows the modes. The second nonradiating mode here is very dirty compared to the 8 and 10 magnet array. The regions of maximum amplitude are not nearly as dark.

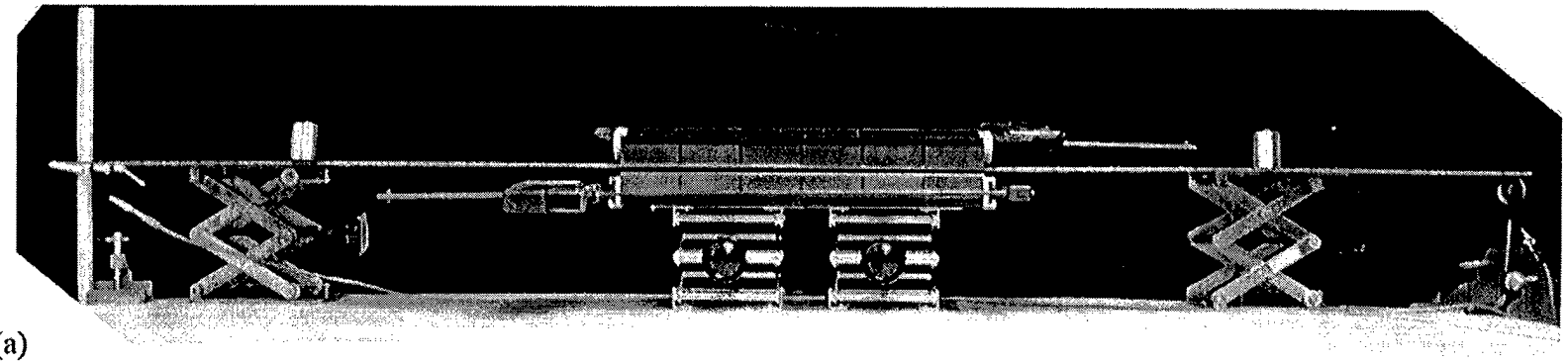

(a)

(b)

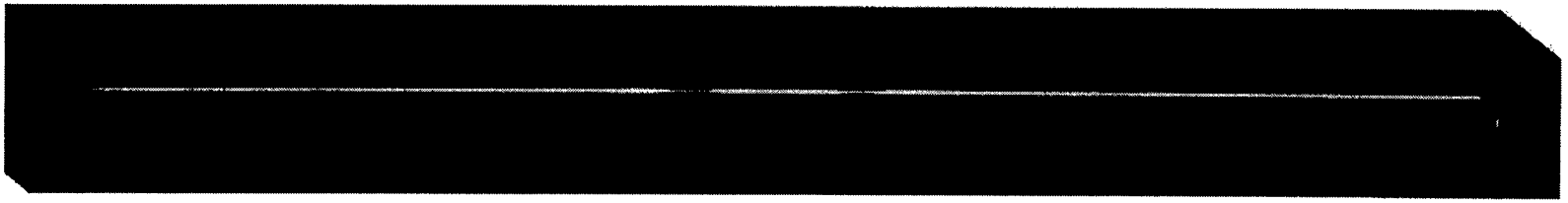

(c)

Fig. 3.24 Source with 6 magnets and steel plates. The setup (a) is shown here with the wood included. The first mode is shown in (b), and the second mode in (c). Notice that the second mode does not result in black spots in the regions of maximum amplitude.

E. CONCLUDING REMARKS

Much experimentation was conducted that is not included in this thesis. Most of it involved our search for the second nonradiating mode with the continuous source for the 28 BNC wire. We initially began with the 28 gauge BNC wire and 4 magnets. When success eluded us, we added two magnets, then two magnets, then two more magnets. With 10 magnets in the array and the second mode still difficult to find, it was believed the source of our difficulty was the variations in the magnetic field. Many different magnet orders were tried with and without steel to achieve a smoother profile. We experimented with changing the magnet face separation to change the strength of the magnetic field. We also used steel that was ¼ inch thick in the assumption that thicker steel would help smooth out imperfections in the field even more, and eliminate the extended fringe fields that went along with greater magnet face separation. The majority of these combinations met with little success, the most common trait among the failures being that of quasi-periodicity. Several attempted setups resulted in a situation where regions of black wire were seen in the appropriate places, and the wire outside the array was a smooth orange, but this state was not stable. Over the course of several seconds, this appearance would become dirtier and cleaner in a rhythmic pattern. We were not happy with this result, and would only be convinced of the existence of nonradiating sources if it could be observed in a real system as a stable state. But still I was convinced that the problem was a nonuniform driving force, and never questioned that my selection of wire needed changing.

Only after several weeks, and with reluctance, did I decide to change to the 30 gauge BNC wire. On my first try, with no steel plates and with minimum face separation for the magnets, I observed a stable nonradiating wave source. It had no quasi-periodicity, and had the expected pattern of darkness and lightness as dictated by nonradiating wave theory. From that point on, I conducted all the experiments with the 30 gauge BNC.

With the 30 gauge BNC wire, I am convinced that we have demonstrated the first two nonradiating modes of a one dimensional vibrating wire system.

IV. NUMERICAL SIMULATIONS

Numerical simulations of a one-dimensional mass-and-spring lattice are examined in this chapter. There are several motivations for these investigations. One is that we can test the nonradiation theory by the behavior of the lattice in the continuum limit. Another is that we can extend the results beyond the simple wave equation for which the theory was derived. Still another, which is most important, is that we can include damping, dissipation, and nonlinear terms, and observe the effect these have.

The program simulates a mass-and-spring lattice with a theoretically anechoic termination. This nonreflective termination consists of a frequency-dependent dashpot and a mass of value ½ the lattice mass. Further detail of the anechoic terminations is found in Appendix A. The Euler-Cromer method (Giordano, 1988) is employed. The code was written in C++ and can be found in Appendix B. The lattice spacings (r), masses (m), and spring constants (s) are all chosen to be unity. Because of this selection, the quantities described in the simulations, including the time step intervals, and both the natural frequencies (ω_o) and frequencies of oscillation (ω), are dimensionless. The time steps correspond to about 1/120 of a cycle of the cutoff frequency ($2\omega_o$), and the frequencies we considered were small compared this. We had on the order of 1000 time steps per period of response.

A. MASS-AND-SPRING LATTICE

We consider longitudinal oscillations of the uniform mass-and-spring lattice shown in Fig 4.1. If the displacement of the n^{th} particle is $y_n(t)$, the equation of motion is

$$\frac{\partial^2 y_n}{\partial t^2} = \omega_o^2 \left(y_{n-1} - 2y_n + y_{n+1} \right), \tag{4.1}$$

where $\omega_o^2 = s/m$. In the continuum limit, where the spatial variation of y_n is infinitesimal over the distance of the lattice spacing r, Eq. (4.1) becomes the standard wave equation

$$\frac{\partial^2 y}{\partial t^2} - c^2 \frac{\partial^2 y}{\partial x^2} = 0 , \tag{4.2}$$

where $x = na$, $y(x,t) = y_n(t)$, and the wave speed is

$$c = \omega_o r = r\sqrt{\frac{s}{m}} . \tag{4.3}$$

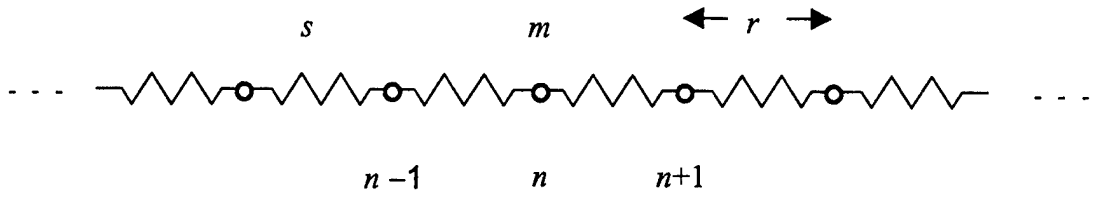

Fig. 4.1 Section of a uniform mass-and-spring lattice, where m is the particle mass, s is the spring constant, and a is the equilibrium lattice spacing.

It should be noted that the quantity c is defined whether or not the system is behaving in the continuum limit.

The dispersion law corresponding to Eq. (4.1) is determined by substituting the traveling wave expression $y_n = A\exp(i\omega t \pm iknr)$, where k > 0, and demanding that this expression satisfy the equation. The result is

$$\omega = 2\omega_o \sin\left(\frac{kr}{2}\right) . \tag{4.4}$$

Waves on the mass-and-spring lattice are dispersive; that is, the phase velocity ω/k depends upon the frequency. In the continuum limit ($kr \to 0$), the waves are nondispersive; the dispersion law reduces to $\omega = ck$. It should also be noted that the limiting minimum value of ω is 0, corresponding to the limiting case of waves of infinite wavelength, and the maximum value is $2\omega_o$, corresponding to the upper cutoff mode which has wavelength $2r$.

B. NONRADIATING SOURCES

To numerically investigate nonradiating sources, we first consider the simplest case of a "two-point" source, which consists of two points of a medium being driven in phase with the same amplitude. This is a nonradiating source if the points are separated by an odd number of half-wavelengths. That is, complete destructive interference occurs at all points outside and including the driven points.

If we choose the points to be separated by 4 lattice spacings, nonradiation should then occur if the frequency corresponds to the dimensionless wavelength $\lambda = 8$ or wavenumber $k = \pi/4$. By the dispersion law (4.4), the frequency corresponding to this wavenumber is $\omega = 2\sin(\pi/8)$. If we consider a 501-site lattice (sites 0 through 500) that is initially at rest in equilibrium, and drive sites 248 and 252 with the force $F\sin(\omega t)$ for t ≥ 0, where $F = 1$, Fig. 4.2(a) shows the displacements at the dimensionless time $t =$ 227.83, which is before the disturbances strike the ends of the lattice, and which corresponds to maximum displacements of the sites 249, 250, and 251. The data show much radiation, in addition to an overall constant displacement of the sites. How can this situation represent a nonradiating source? It is natural to suspect that the problem is due to the "flat-top" drive, a monofrequency drive whose amplitude is zero for $t < 0$ and a nonzero constant for $t \geq 0$. The abruptness of this drive may produce the overall displacement and also give rise to frequencies in a band about ω which thus cannot destructively interfere. It should be noted that nonradiation does indeed appear to have occurred near the sources, although some "ringing" is apparent.

To test the hypothesis that the behavior in Fig. 4.2(a) represents transients due to the abruptness of the drive, we consider a drive whose amplitude smoothly rises from zero to a constant value. We consider the force $A(t)\sin(\omega t)$, where the amplitude is

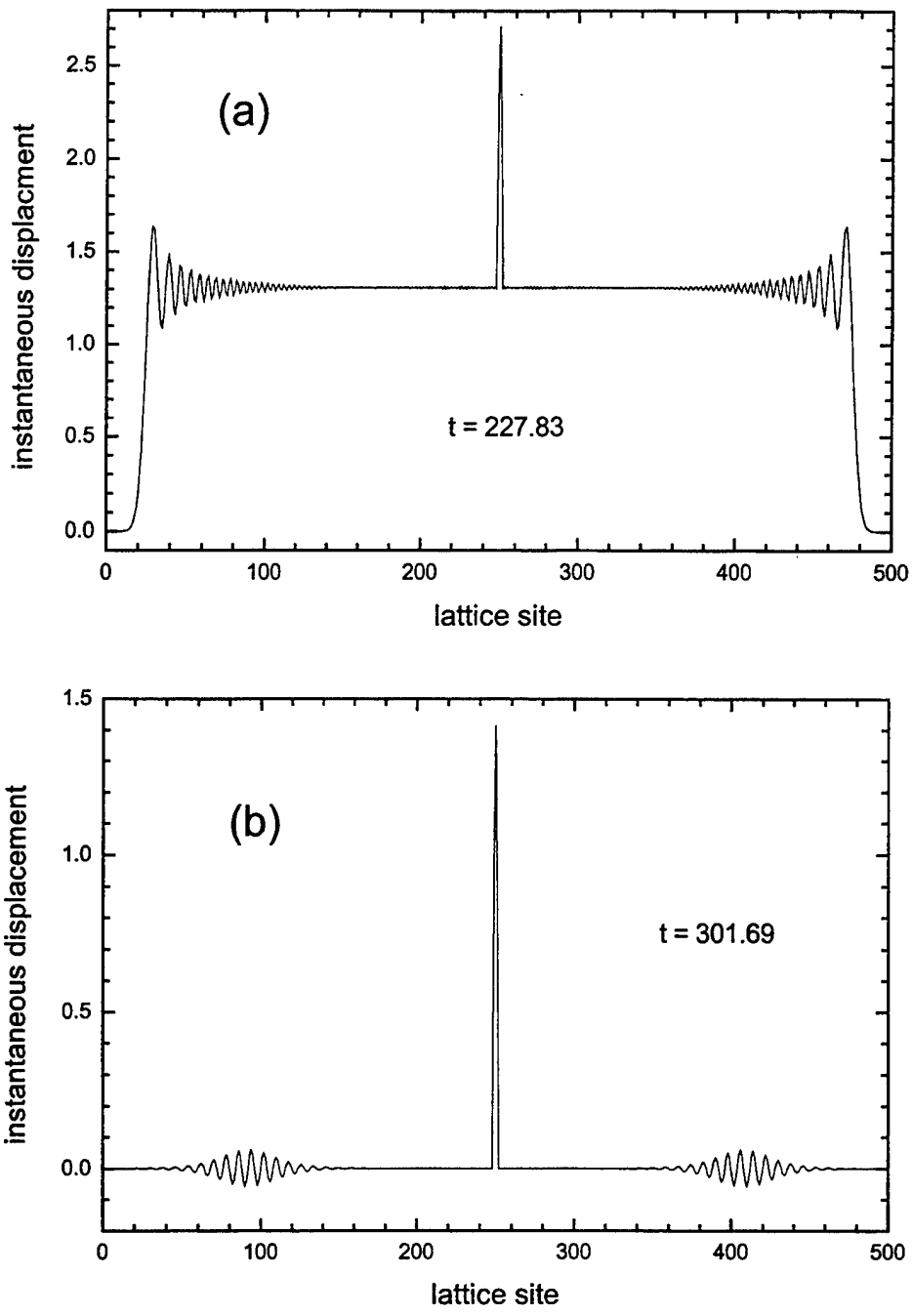

Fig. 4.2 (a) Response of the lattice to a two-point flat-top drive at sites 248 and 252. The spike is due to responses at sites 249, 250, and 251. The time $t = 227.83$ corresponds to a maximum of the displacements of these sites. (b) Response of the lattice to a drive that is smoothly modulated from zero to the constant value in (a). The time $t = 301.69$ corresponds to maximum displacements of the sites 249, 250, and 251.

$$A(t) = F\,\frac{1+\tanh\left[(\omega t-\tau)/\gamma\right]}{2}, \tag{4.5}$$

where the simulations are begun at $t = 0$, and where $\tau > 0$. The factor of the constant F is approximately zero for $\omega t < \tau - \gamma$ and unity for $\omega t > \tau + \gamma$, with a smooth exponential transition between. Hence, for appropriate values of the parameters, Eq. (4.5) offers a means of smoothly turning on the force to values that approximately equal the constant F.

For $\omega = 2\sin(\pi/8)$, $F = 1$, $\tau = 100$, and $\gamma = 20$ in Eq. (4.5), Fig. 4.2(b) shows the displacements of the lattice sites at time $t = 301.69$, which corresponds to maximum displacements of the sites 249, 250, and 251. Each wave packet is moving toward the nearer termination. The smooth turning on of the force has dramatically improved the response compared to Fig. 4.2(a). Specifically, the wave packets now bear a very strong resemblance to the drive due to the near-monofrequency of the. There is also no overall constant displacement. When the rise time is decreased, we find that the waveform approaches that in Fig. 4.2(a).

The displacements in Fig. 4.2(b) near the center of the lattice are shown in Fig. 4.3(a). The curve is a sinusoid, which fits the data extremely well. To exhibit the next nonradiating excitation, we can either increase the frequency to the value corresponding to three half-wavelengths over the same region, or we can use the same frequency and triple the length of the region. We choose the second case here. The results are shown in Fig. 4.3(b). Again, the sinusoid fits the data extremely well.

Figure 4.4 shows the results of simulations with a two-point source drive at sites 225 and 275 (50 lattice spacings apart). Figure 4.4(a) shows the fundamental nonradiating state. The drive frequency corresponds to one half-wavelength between the driven sites according to the dispersion law (4.4). Figure 4.4(b) corresponds to the nonradiating source with three half-wavelengths. In both cases, the theoretical displacement inside the source is a sinusoid, which is found to fit the data extremely well.

We now consider the case of a medium that is being driven over a continuous range. Figure 4.5 shows the results of simulations with a uniform oscillatory force acting over sites 225 through 274 (50 lattice sites). It is important to note that the uniform

source occupies an *even* number of sites, so that the radiation cancels due to individual two-point sources. We observe substantial radiation for an odd number of sites. The radiation will vanish in the continuum limit, but approximating this with numerical simulations of a lattice is not practical.

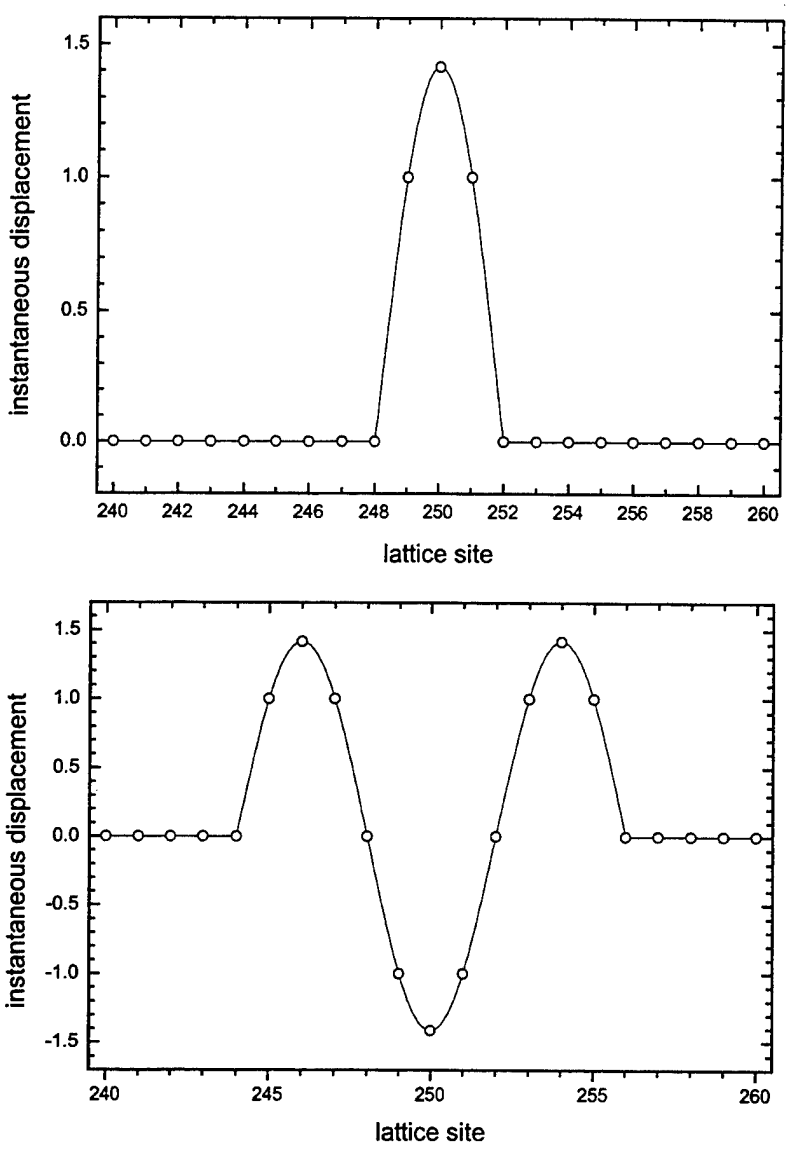

Fig. 4.3 (a) Expansion of the data in Fig. 4.2.(b), for a two-point drive at sites 248 and 252 (4 lattice spacings apart). (b) Response of the lattice to a two-point drive at sites 250 and 259 (12 lattice spacings apart) with the same drive frequency.

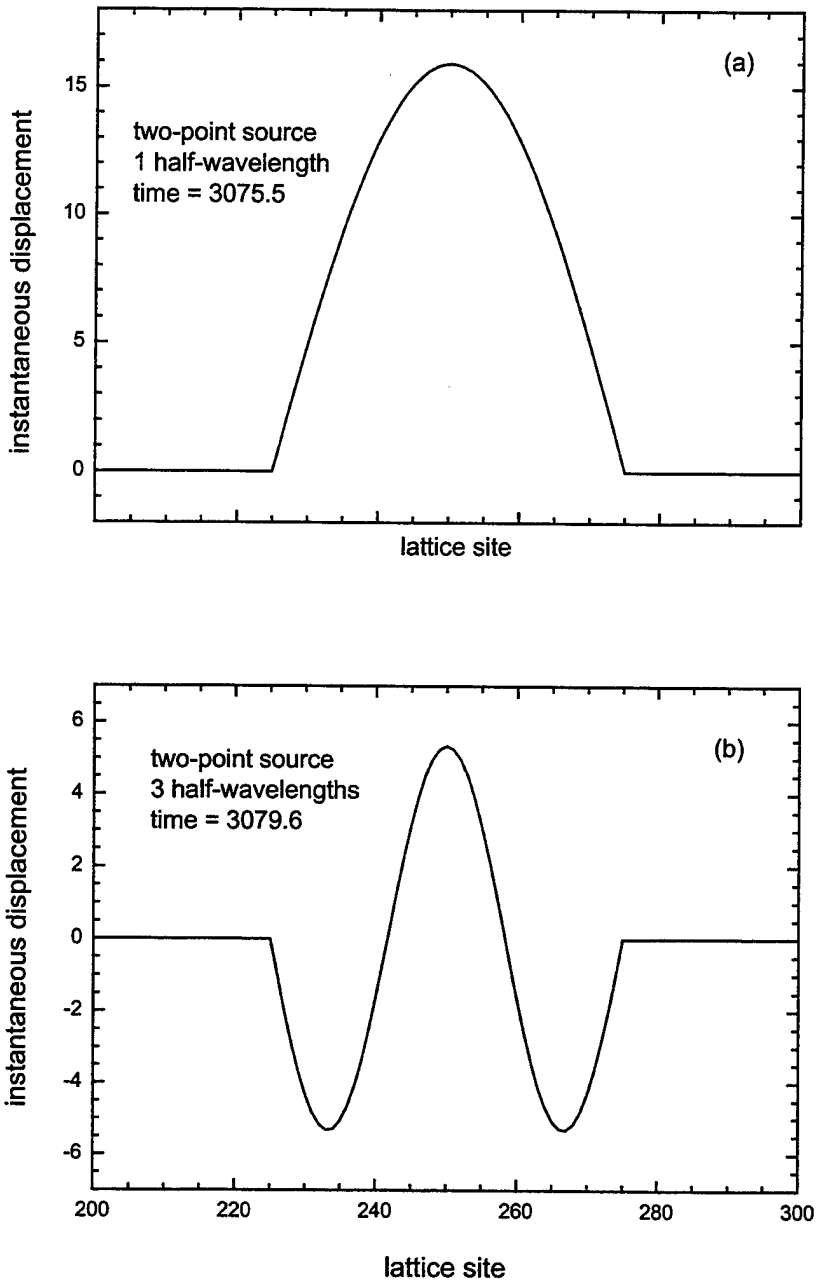

Fig. 4.4 Response of a lattice to a two-point nonradiating source, with drives at sites 225 and 275. The fundamental state, which corresponds to one half-wavelength between the driven sites, is shown in (a). The state with three half-wavelengths is shown in (b). These graphs were at times sufficiently long enough so that the anechoic terminations have absorbed all the waves that arise with the smoothly modulated drive force is initiated.

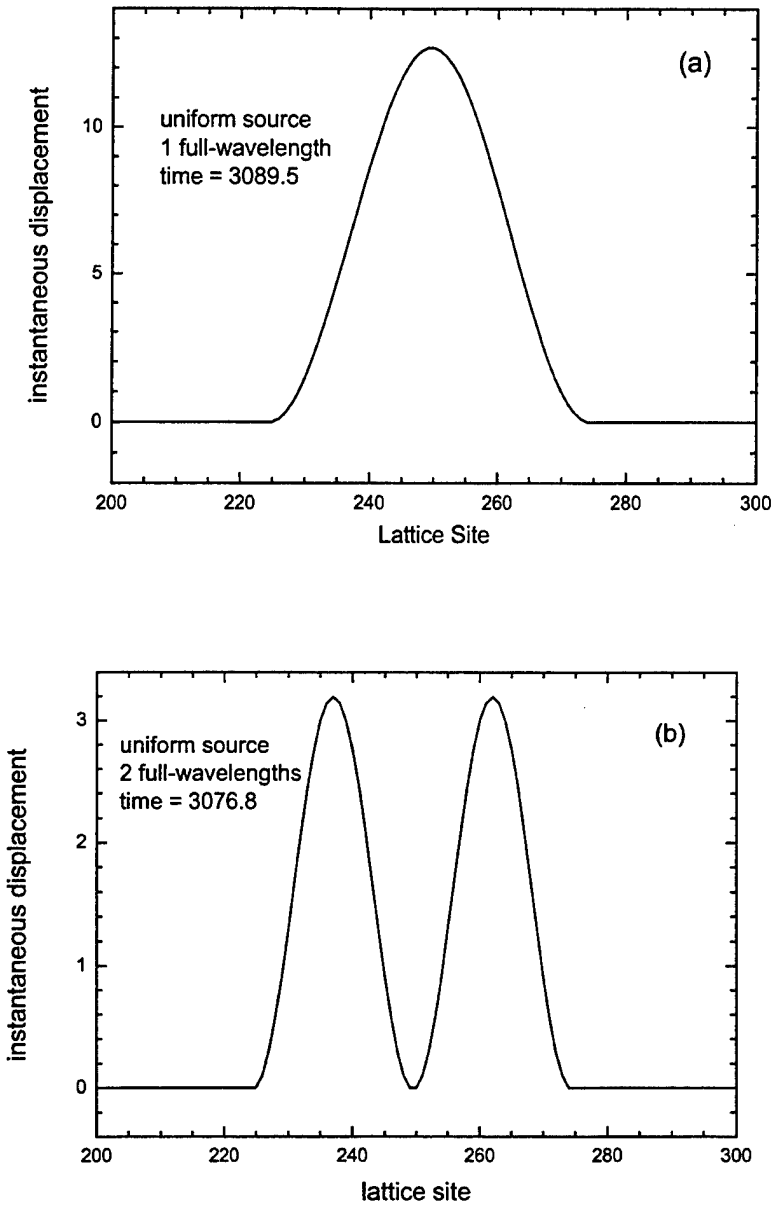

Fig. 4.5 Response of a lattice to a uniform nonradiating source, with drives at sites 225 through 274. The fundamental state, which corresponds to a wavelength of 50 lattice spacings, is shown in (a). The state corresponding to a wavelength of 25 lattice spacings is shown in (b).

The theoretical expression for the response in the continuum limit is the square of a sinusoid (Berry, 1998), that can be fit to the data very well. Slight deviations at the ends of the source are observed. Indeed, Berry et al. show for a continuum that any nonradiating source yields a response whose amplitude and slope both vanish at the endpoints. The lack of an exactly zero slope in our case is a result of the discreteness of the lattice.

When the distance between two driven points is an integral (rather than half-integral) number of wavelengths, nonradiation can be achieved if the drives are adjusted to be in antiphase. In the following sections, we utilize this to compare the relative radiation from two-point and uniform quasi-nonradiating sources. When the distance between the two points is neither a half-integral nor integral number of wavelengths, one might think that nonradiation can be achieved by adjusting the relative phase of the driven points. This is not the case, however. Adjusting the relative phase can result in the absence of radiation in one direction, but not simultaneously in the other direction. The destructive interference in this case is commonly referred to as *noise cancellation*. The nonradiation problem is more stringent in that both directions are involved.

C. INCLUSION OF DISSIPATION

We include linear dissipation in the lattice by adding the term $-\nu dy_n/dt$ to the right side of the equation of motion (4.1), where ν is the damping parameter. Figure 4.6 shows the results of a simulation for a two-point source with in-phase drives of amplitude $F =$ 1.0 at sites 225 and 275, and with damping parameter $\nu = 0.01$. In the absence of dissipation, no radiation occurs outside the source and there is a single antinode inside. The time (3074.3) is such that the approximate standing wave response between the sites is maximal. Radiation occurs because the amplitudes of the individual waves from the drives decrease with distance from the drives. The two waves traveling in each direction outside of the two-point source are still in antiphase to a very good approximation, but the imbalance in amplitude destroys the perfect destructive interference. It is readily shown that, for a fixed frequency, the speed of propagation decreases due to the

dissipation, so the wavelength of a wave decreases. However, the effect is quadratic in the dimensionless damping parameter ν/ω, and so is very small for our case of weak damping.

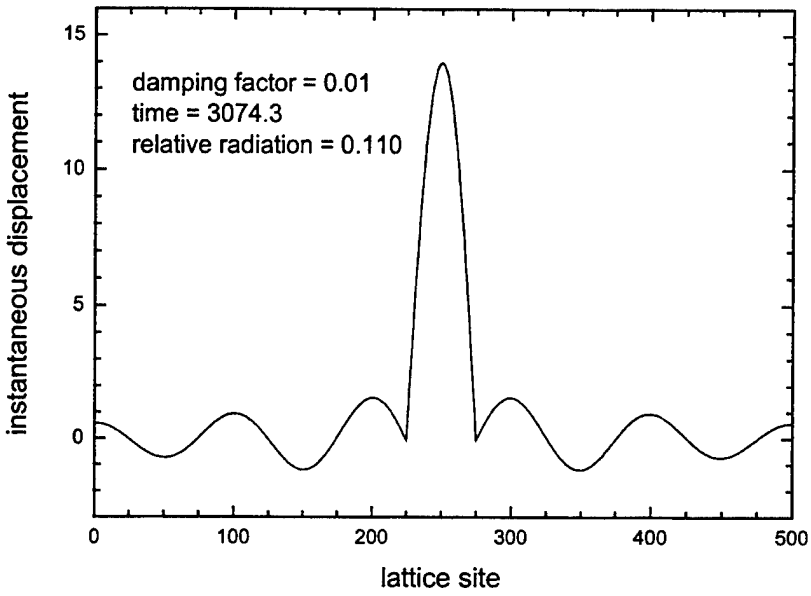

Fig. 4.6 Damped lattice driven with a two-point source at sites 225 and 275, where the frequency corresponds to a single half-wavelength. The response between the drives is an approximate standing wave. The responses outside the drives are outward traveling waves.

To quantify the radiation, we define the *relative radiation amplitude* as the amplitude of the radiation just outside a source divided by the peak amplitude of the approximate standing wave inside the source. We will conveniently approximate this value from graphs such as Fig. 4.6 by measuring the amplitude of the first peak of the radiation outside the source. The value of the relative radiation amplitude in Fig. 4.6 is approximately 0.11.

It would appear impossible to reduce the relative radiation amplitude by perturbatively adjusting the drive parameters, and simulations indeed confirm this. However, this is not to say that the peak amplitude of the standing wave between the two

drives does not increase. The peak amplitude increases as the frequency is reduced (the input impedance decreases). However, the relative radiation amplitude increases because the amplitude of the radiation increases by a greater relative amount due to individual waves no longer being in antiphase.

For the two sites driven in phase, the next quasi-nonradiating mode occurs for three half-wavelengths between the drives at sites 225 and 275, or a dimensionless wavenumber of $kr = 2\pi/\lambda = 6\pi/50$, which corresponds in the dispersion law Eq. (4.4) to nearly three times the frequency of the fundamental mode because our case is near the continuum limit. We expected a substantially greater value of the relative radiation amplitude, because the attenuation distance was expected to scale with wavelength. However, we found the approximate value 0.12, which is suspiciously near the value of 0.11 for the fundamental mode. Comparison of the damped waves from a single driven site at the fundamental and second frequencies reveals that each wave exhibits the same relative attenuation. Indeed, it is readily shown that the exponential attenuation factor is a constant (independent of ω) in the continuum limit and for weak damping ($\nu << \omega$). This is in contrast to other models of damping, for example, sound in bulk fluids where the damping parameter for a monofrequency wave is proportional to the square of the frequency (Landau, 1959), and thus where higher frequencies decay more rapidly with distance.

For the case of a uniform source, we drove the lattice from sites 225 through 274 at the frequency corresponding to a wavelength of 50 lattice spacings. In the absence of dissipation, no radiation occurs outside the source and there is a single antinode inside. For the same damping factor $\nu = 0.01$ as above, Fig. 4.7(a) shows that the radiation and approximate standing wave inside the source have roughly the same appearance as the two-point case in Fig. 4.6. To properly compare the relative amounts of radiation of a two-point source to the uniform source in Fig. 4.7(a), we consider a two-point source at the same frequency as the uniform case, which can be achieved by reversing the polarity of one of the drive forces. Such a two-point source is nonradiating in the absence of dissipation. For the damping factor $\nu = 0.01$, Fig. 4.7(b) shows the result of a simulation of the two-point source with a force amplitude $F = 1.0$ at each site. We then chose the

force amplitude of the uniform source in Fig. 4.7(a) to be the total force of 2.0 distributed over each of the 50 driven sites, or an individual force of $F = 0.04$. Due to tendency of waves from the many sources to destructively interfere, the uniform source yields a smaller standing wave amplitude inside the source and a smaller amplitude of the radiation outside the source. What is interesting, however, is that the relative radiation amplitude for the uniform source is approximately 0.062, which is roughly *half* the value of 0.12 for the two-point source. We conclude that, compared to lumped point sources, uniform sources tend to yield greater relative destructive interference outside the driven region.

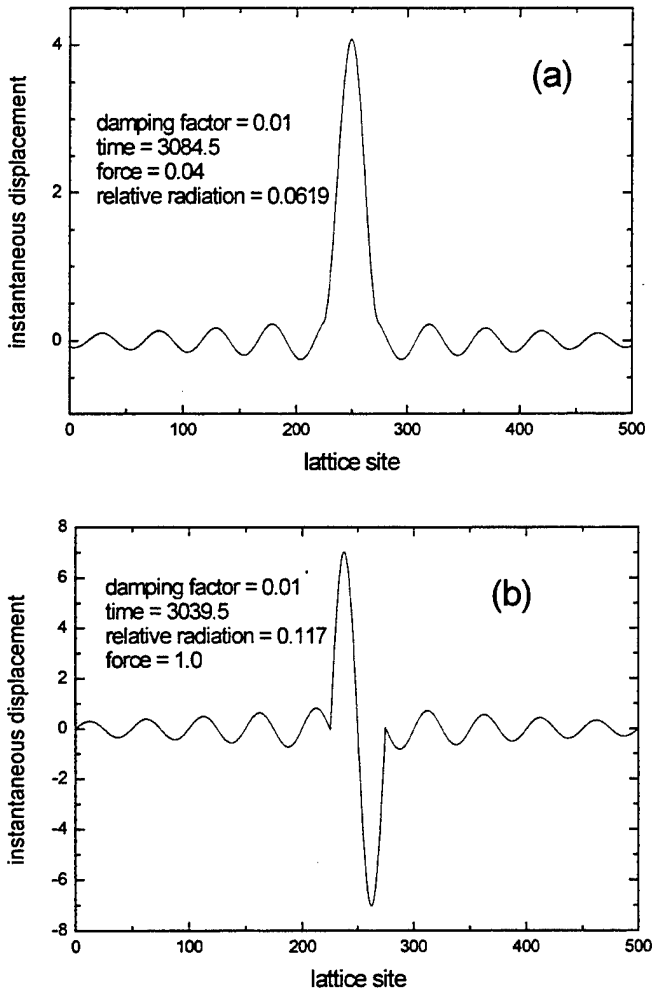

Fig. 4.7 Damped lattice driven with (a) a uniform drive from sites 225 to 274 with frequency corresponding to one wavelength, and (b) a two point out of phase source at sites 225 and 274 with a frequency corresponding to two wavelangths

D. INCLUSION OF NONLINEARITY

Interesting results of our numerical simulations occurred when nonlinearity was added to the mass-and-spring lattice. We consider the case in which the springs are unstretched when the lattice is in equilibrium, and where the springs have either a cubic or quadratic nonlinearity in the displacement from equilibrium. Specifically, we add either $\beta[(y_{n+1}-y_n)^3 - (y_n-y_{n-1})^3]$ or $\alpha[(y_{n+1}-y_n)^2 - (y_n-y_{n-1})^2]$ to the right side of Eq. (4.1). The cubic nonlinearity corresponds to hardening and softening deviations from Hooke's law for $\beta > 1$ and $\beta < -1$, respectively. The quadratic nonlinearity for $\alpha > 0$ corresponds to springs that harden when stretched and soften when compressed, and the opposite for $\alpha < 0$.

1. Cubic Nonlinearity

Figure 4.8(a) shows results for a two-point source occupying 50 lattice spacings for a drive amplitude of 0.3 and a softening *cubic* nonlinearity ($\alpha = 0$ and $\beta = -1$). The drive frequency corresponds to one half-wavelength between the driven points according to the linear dispersion law Eq. (4.4). The time corresponds to a maximum response of the approximate standing wave between the two drive points. A natural hypothesis is that the radiation occurs because the nonlinearity has caused harmonic generation by the time a point on the wave from one source reaches the other. These harmonics cannot be cancelled. Furthermore, the production of the harmonics comes at the expense of a loss of energy of the fundamental, so the fundamentals from the two sources do not cancel. The presence of higher harmonics is evidenced by the clearly visible distortion of the radiated waveform. Tests with the anechoic termination showed that the effect of harmonics not being completely absorbed by it are negligible on the scale of Fig. 4.8(a).

Although this hypothesis is reasonable, another effect dominates the behavior. Nonlinearity can cause different points of a wave to travel with different speeds. The softening cubic nonlinearity in our lattice causes a lessening of the stiffness for both compressions and rarefactions, which causes these points of a wave to move more slowly

than others. Hence, the average wavelength is decreased, which reduces the destructive interference outside each of the driving points. It thus occurred to us to decrease the drive frequency in order to observe if the destructive interference in Fig. 4.8(a) could be improved. The results are shown in Fig. 4.8(b) for the drive frequency in the linear dispersion law (4.4) corresponding to the half-wavelength being increased from 50.0 lattice spacings to 51.6 lattice spacings. The increase in the wavelength was adjusted through trial and error to minimize the radiation, which is dramatically reduced by an order of magnitude. Note how the fundamental is nearly completely cancelled; the predominant wave is the third harmonic, which has one-third the wavelength of the fundamental. We were initially puzzled by the near absence of the fundamental in the radiation, because the absence of a fundamental would violate the energy conservation as stated above. The resolution is due to the fact that the energy of a wave is proportional to the *square* of the amplitude. Hence, the weak production of higher harmonics causes the amplitude of the fundamental to decrease by a very small amount.

The substantial improvement in the destructive interference at the fundamental frequency from Fig. 4.8(a) to Fig. 4.8(b) by only shifting the drive frequency is surprising. In the continuum limit, the equation of motion for our lattice with the cubic nonlinearity is $\partial^2 y/\partial t^2 - c^2\partial^2 y/\partial x^2 = \beta(\partial y/\partial x)^2\partial^2 y/\partial x^2$. If we consider the linear wave $y = A\cos(kx-\omega t)$ as an approximate solution, we find $\omega^2 = c^2k^2 + \beta k^4A^2\sin^2(kx-\omega t)$. For the softening case ($\beta < 0$), this can be interpreted as a decrease in wavenumber k (increase in wavelength) that is a maximum at the displacement zeros of the wave (where the compressions and rarefactions occur). On this basis, we would expect to eliminate roughly half of the radiation at the fundamental frequency by optimally adjusting the wavelength. That significantly more is eliminated suggests that there is a collective effect in which the different points of a wave influence each other such that a roughly common speed obtains.

Results similar to Fig. 4.8 occur when the sign of the nonlinear coefficient β is positive, where the wavelength must now be decreased to reduce the radiation because the nonlinearity causes points on a wave to move faster. Also, similar results occur for the next excited state that corresponds to three half-wavelengths between the driven sites.

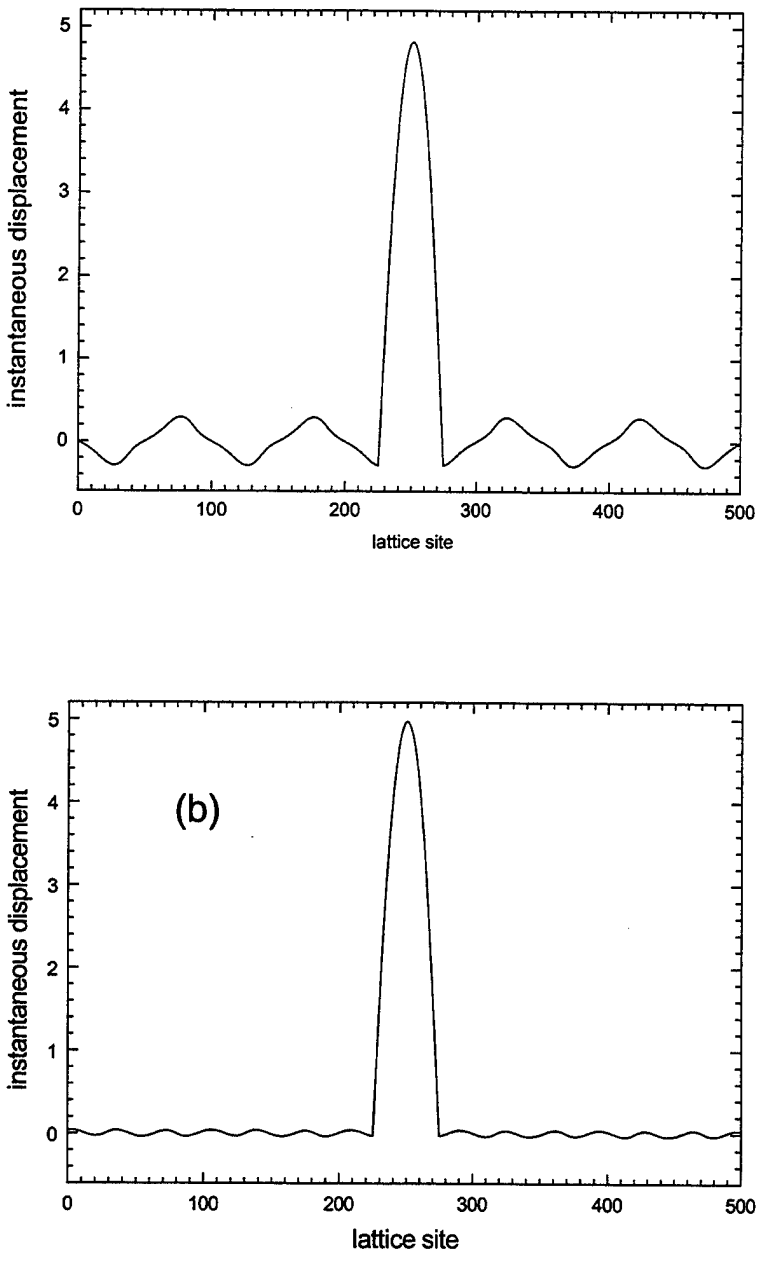

Fig. 4.8 Cubically nonlinear lattice driven at site 225 and 275, where the drive frequency corresponds to (a) one half-wavelength between lattice sites, and to (b) a slightly greater wavelength (the original wavelength increased by 1.6 lattice spacings).

Although the amplitude is now less due to the greater frequency, the nonlinear effects are more pronounced because there is a greater distance between the driven sites compared to the wavelength. For all of our nonlinear simulations, we found that the relative radiation amplitude increases as the drive amplitude is increased, which is expected for nonlinear effects.

In the above explanation of the observations, we tacitly assumed that the counter-traveling nonlinear waves have negligible interaction, which can be shown to be true (Rudenko, 1977). Unidirectional nondispersive waves interact much more strongly. Because our simulations are near the continuum limit, which is nondispersive, we expected the uniformly driven case to yield fundamentally different results than the two-point case above, because unidirectional interaction will then occur. However, we found the results to be very similar when the drive amplitude was 0.05 at each driven site, which yielded roughly the same amplitude of radiation as in the two-point source above. We thus infer that the unidirectional interaction of waves is small in our simulations; the predominant nonlinear effect is the average change in the wave speed due to nonlinearity.

We also compared the relative radiation amplitude for two-point and uniform sources. To make a proper comparison as in Sec. C, we made the frequencies the same by having the two-point drives in antiphase and driving at a frequency corresponding to one wavelength according to the linear dispersion law (4.4). The force for each two-point drive was $F = 0.3$ as above, and so the force for each drive of the uniform source was taken to be $2(0.3)/50 = 0.012$. The standing wave peak amplitude and radiation peak amplitudes were found to be 2.4035 and 0.2801 for the two-point source, and 1.5219 and 0.2801 for the uniform source. The relative radiation amplitudes are thus 0.1165 for the two-point source and 0.0046 for the uniform source. The latter is remarkably reduced by a factor of 25 compared to the former. We can qualitatively understand the difference as follows. The standing wave response is reduced for the uniform source due to the tendency of the individual waves to cancel, so nonlinear effects are reduced. Because nonlinear effects are expected to be proportional to the square of the standing wave amplitude, the radiation will be reduced substantially more, so less relative radiation occurs for the uniform source.

2. Quadratic Nonlinearity

Figure 4.9(a) shows results for a two-point source occupying 50 lattice spacings for a drive amplitude of 0.15 and a quadratic nonlinearity ($\alpha = 1$ and $\beta = 0$). As in Fig. 4.8(a), the drive frequency corresponds to one half-wavelength between the driven points according to the linear dispersion law (3.4), and the time corresponds to a maximum response of the approximate standing wave between the two driven sites. We first note that the lattice has contracted between the two driven sites by roughly 0.3 original lattice spacing. This occurs because the springs harden when they stretch and soften when they compress. Hence, for a standing wave, the springs are now compressed on the average. The opposite occurs for a negative value of α. This phenomenon is responsible for the thermal expansion of solids (Kittel, 1976). In this case, the intermolecular attraction hardens for compression and softens for expansion according to the Leonard-Jones model of the potential, which corresponds to $\alpha < 0$ for a quadratic nonlinearity.

The radiation in Fig. 4.9(a) shows strong fundamental and second harmonic components. Because the distance between the driven sites has decreased, one might think that an increase in the drive frequency (decrease in the wavelength) would result in greater destructive interference. However, from the dispersion law (4.4), the phase velocity of a wave is $\omega/k = (2\omega_o/k)\sin(kr/2)$, which equals $c = \omega_o r$ in the continuum limit. Because the speed per lattice spacing is thus nearly independent of the lattice spacing in our near-continuum case, a wave requires nearly the same time to traverse the distance between the driven sites even though the distance has contracted.

For a positive quadratic nonlinearity, the displacement zeros of a wave travel faster for a compressions and slower for expansions. Hence, there is no average change in the speed to first order, in contrast to the cubically nonlinear case above. We thus expected that altering the drive frequency would not reduce the radiation. Figure 4.9(b) shows the results of our altering the drive frequency to minimize the radiation; specifically, minimizing the fundamental. Surprisingly, increasing the half-wavelength by 0.9 from 50.0 to 50.9 nearly completely eliminates the fundamental. Note that this represents a decrease in frequency, which is the opposite of that required due to the

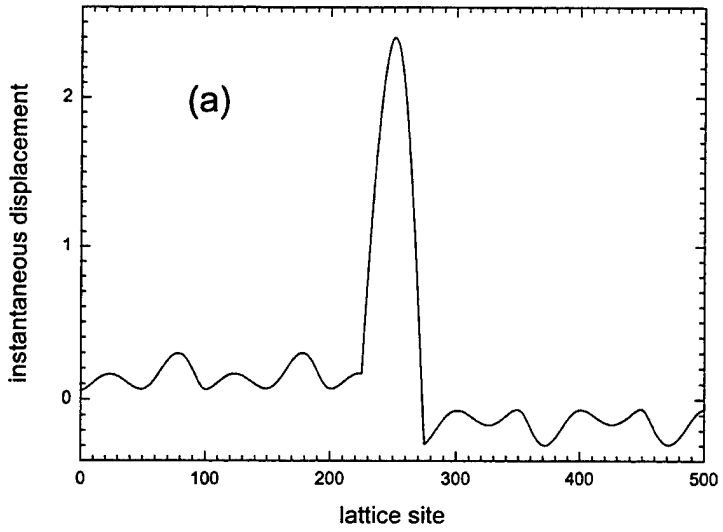

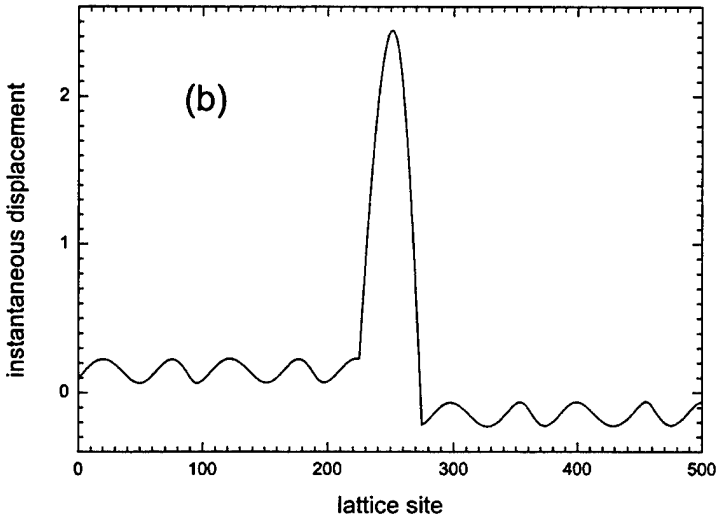

Fig. 4.9 Quadratically nonlinear lattice driven at sites 225 and 275, where the drive frequency corresponds to (a) one half-wavelength between the sites, and to (b) a slightly greater wavelength (the original wavelength increases by 0.9 lattice spacings).

contraction. We suspect that the reason for this shift causing greater destructive interference is that the speed of a wave does change with amplitude, but that this is beyond (i.e., at a higher order than) our qualitative analysis. To appreciate this, note that in the continuum limit the equation of motion for our lattice with the quadratic nonlinearity is $\partial^2 y/\partial t^2 - c^2 \partial^2 y/\partial x^2 = \alpha(\partial y/\partial x)\partial^2 y/\partial x^2$. If we consider the linear wave $y = A\cos(kx-\omega t)$ as an approximate solution, we find $\omega^2 = c^2k^2 + \alpha k^3 A\sin(kx-\omega t)$, which indeed shows no average change in the wavenumber k as a function of position. However, our results suggest that there is a nonzero average at the next order, proportional to $\alpha^2 A^2$.

Results similar to Fig. 4.9 occur when the sign of the nonlinear coefficient α is negative, although there is now expansion between the driven sites. However, we find that the wavelength must still be increased to reduce the radiation, which is consistent with a change in wave speed proportional to α^2 and thus independent of the sign of α. Also, results similar to those for the cubic nonlinearity occur for the next excited state (corresponding to three half-wavelengths between the driven sites) and for the uniformly driven case.

In regard to relative radiation for a lumped (specifically, two-point) source in contrast to a distributed (specifically, uniform) source, due to the contraction of the lattice we define the radiation amplitude as half the difference between the peak-to-peak amplitude. For the proper comparison as in the above case of the cubic nonlinearity, the standing wave peak amplitude and radiation peak amplitudes were found to be 1.2345 and 0.10945 for the two-point source, and 0.76097 and 0.007421 for the uniform source. The relative radiation amplitudes were thus 0.887 for the two-point source and 0.00975 for the uniform source. The latter is remarkably reduced by a factor of 91 compared to the former. Our qualitative understanding of this effect is the same as in the above cubic case.

E. INCLUSION OF NONUNIFORMITY OF MEDIUM

Nonuniformity can be included in a mass-and-spring lattice with an extended drive in a variety of ways: the masses, springs, drive amplitude, or drive phases can vary along the lattice, and the variation may be random or regular. Barring some types of symmetry (Denardo, 1998), all cases are expected to lead to radiation from a source that is nonradiating in the absence of the nonuniformity. We investigate the regularly nonuniform case in which the masses vary linearly with position.

Consider a 501-site lattice in which the mass of each successive site increases by $\Delta m = 0.003$, where the mass of the middle site 250 is 1.0. The masses of sites 0 and 500 are thus 0.25 and 1.75, respectively. For anechoic terminations, these endpoint masses are halved, and numerical dashpots with damping factors given by Eq. (A.7) (see App. A) are added, where $\omega_b^2 = 1/0.25 = 4$ at site 0 and $\omega_b^2 = 1/1.75 = 4/7$ at site 500. As in Sec. B, we consider a two-point source with driven sites 225 and 275. Figure 4.10(a) shows the results for the drive frequency corresponding to a single half-wavelength between the drive points of the uniform lattice with masses equal to 1.0. For such a lattice, no radiation would occur. Figure 4.10(a) shows that the nonuniformity results in substantial radiation.

The results can be understood by examining Fig. 4.10(b), which shows the individual responses of the lattice to each of the two point drives in Fig. 4.10(a), at the same time as that in Fig. 4.10(a). Both the wavelengths and amplitudes of the waves from each driven point continuously change as the waves propagate. The wavelength of each left-traveling wave increases with decreasing lattice site number because the wave speed increases due to the decreasing lattice masses, and because the frequency remains constant. Similarly, the wavelength of each right-traveling wave decreases with distance. However, the change in wavelength is irrelevant here because the waves are affected identically at each point of the lattice, so this does not alter the complete destructive interference. That is, the change in wavelength does not result in radiation from a nonradiating source. This is clearly shown in Fig. 4.10(b) by the fact that the two waves are in exact antiphase outside the driven points.

It is the variation in amplitude that is responsible for the radiation. Figure 4.10(b) shows that the amplitude of each left-traveling wave increases with distance from its source. In addition, the amplitudes are not the same at the two driven sites because the

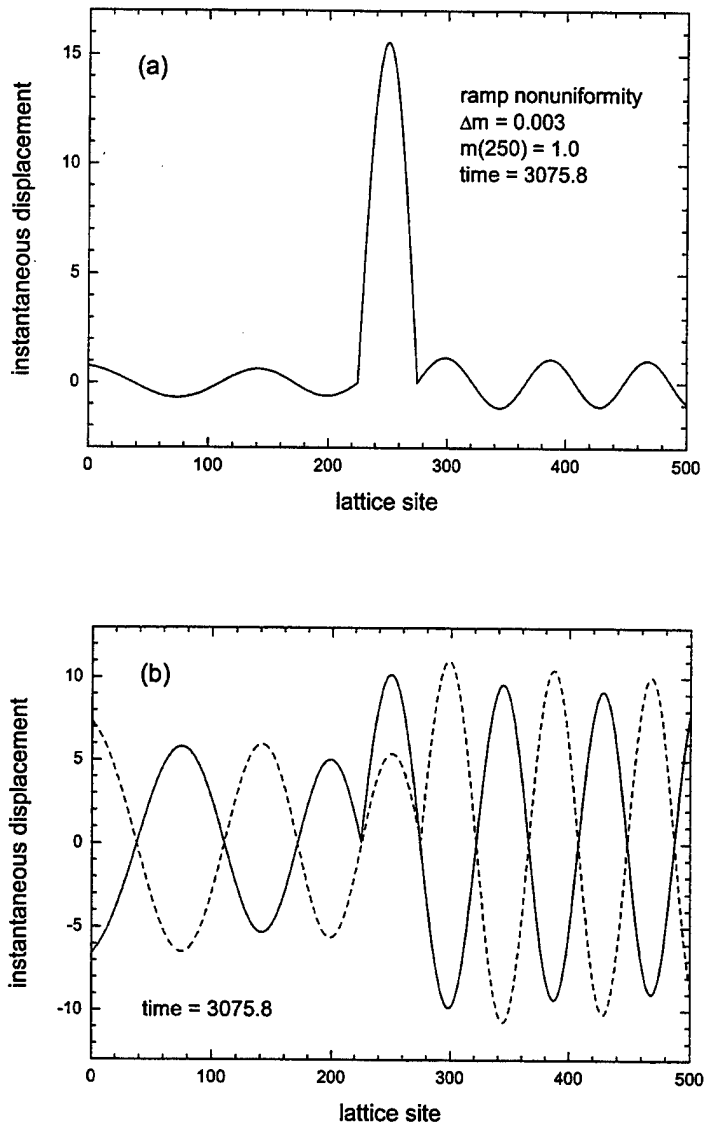

Fig 4.10 Nonuniform Lattice driven at sites 225 and 275 where the mass of the nth site is 1.0+(n-250)Δm, where Δm=0.003. In (a), the drive amplitudes are each equal to exactly 1, and in (b), the left is 1.0775 and the right is exactly 1. The time (3075.8) in each case cooresponds to a maximum response of the approximate standing wave between the drive sites.

input impedances, when each is driven individually, are different. Specifically, the initial amplitude of the left-traveling wave from the drive at site 275 is greater than that from the drive at site 225. That the amplitude increases as a wave propagates to the left can be understood in the continuum limit in the case where the wave changes adiabatically (gradual nonuniformity so that no reflections occur). The average energy per unit length of a traveling wave is twice the average kinetic energy per unit length: $\rho\omega^2A^2/2$, where A is the displacement amplitude, and ρ *is* the mass density. The energy in a wavelength $\lambda = 2\pi c/\omega$ is thus $\pi\rho c\omega A^2$, which remains constant for adiabatic propagation. Substituting $\rho c = (sm)^{1/2}$, we find that the energy per wavelength is proportional to $m^{1/2}A^2$. The mass m of each lattice site decreases as a wave propagates to the left, and so the amplitude A must increase. Similarly, the amplitude of a right-traveling wave must decrease.

In Fig. 4.10(b), the response immediately to the right of each drive point is *greater* than that to the left. This is surprising because it is natural to guess that that the greater masses to the right would cause the response to be less. Parameters for which the response to the right is less than that to the left are readily found. The magnitude and sign of the discontinuity are found to depend in general upon the gradient in the lattice masses, the location in the lattice, and the drive frequency. The cause of this interesting effect remains to be understood, but the discontinuity does not alter the manner in which the amplitudes of the propagating waves change. A related but smaller effect is the variable input impedance referred to above. One might think that the response should be less at site 275 due to the greater lattice masses there than at site 225. However, Fig. 4.10(b) surprisingly shows that the response is *greater*. As in the case of the discontinuity, the magnitude and sign of this effect depend upon the gradient of the lattices masses, the location in the lattice, and the drive frequency.

By our choice of drive frequency, waves traveling in the same direction are in antiphase outside the two-point source. Hence, by scaling the drive amplitude at site 275 so that the amplitude of the left-traveling wave arriving at site 225 has the same amplitude as the left-traveling wave from site 225, we can eliminate the radiation to the left. Numerical simulations indeed show that there is nearly complete destructive interference to the left of the two-point source if the drive amplitude at site 275 is 0.894

of that at site 225. Remarkably, it is found that this also eliminates the radiation to the right. That the radiation can be eliminated in *both* directions is surprising because the lattice is not invariant under spatial inversion. We are thus not guaranteed that the elimination of radiation on one side of the source will also cause the elimination on the other side.

To understand this effect, we consider a two-point source in a regularly nonuniform lattice, and suppose that the drive frequency has been adjusted so that the individual waves are in antiphase immediately outside the two driven sites. The problem is to theoretically determine the relative drive amplitudes such that the radiation is eliminated in both directions outside the source. We ignore for the moment the discontinuity of the response amplitude on either side of a driven point. Let the response amplitude due to a drive at point x_1 be $A_1(x)=h(x)$. The response due to the same drive at point x_2 is then $A_2(x) = \varepsilon\, h(x-d)$, where the distance between the sites is $d = x_2 - x_1$ for $x_2 > x_1$, and where the constant ε accounts for a possible change in input impedance. If the drive amplitude is scaled by a factor, then linearity implies that the response is scaled by the same factor. Let ϕ be a scale factor applied to the drive at x_2. If the waves from the two drive points are in antiphase, the condition for no radiation toward decreasing x outside the two-point source is $A_1(x_1) = \phi A_2(x_1)$, *or* $h(x_1) = \varepsilon\phi\, h(x_1 - d)$. Similarly, the condition for no radiation toward increasing x is $A_1(x_2) = \phi A_2(x_2)$, *or* $h(x_1 + d) = \varepsilon\phi h(x_1)$. Eliminating the product $\varepsilon\phi$ between the two relations for $h(x)$ yields $h^2(x_1) = h(x_1-d)h(x_1 + d)$, which has the general solution $h = h_o e^{\xi x}$, where h_o and ξ are constants.

Hence, nonradiation on both sides of a two-point source is guaranteed only if the amplitude of the wave from a single point varies *exponentially* in space. For our case of a lattice with a linear variation in the masses, the above result $m^{1/2}A^2 =$ constant shows that the amplitude does not vary exponentially but, rather, algebraically as $A(x) = (x + l)^{-1/4}$, where l is a constant. That the radiation is observed to be nearly completely eliminated by adjusting the relative drive amplitude is probably because $A(x)$ does not vary substantially over the length of the lattice, and thus can be fit reasonably well with an exponential.

Results similar to those above occur when the drive frequency of the two-point

source corresponds to three half-wavelengths (rather than one) between the points if the lattice had unit masses. For a uniform source over the 50 sites from 225 to 274, where the drive frequency corresponds to two half-wavelengths over the driven region, there is an unexpectedly small amount of radiation. To quantify this, we calculate the relative radiation amplitude averaged over the two directions, which yields the relative radiation amplitude 0.0096. To compare this to a two-point source of the same frequency, we consider sites 225 and 275 driven in antiphase, so that there are two half-wavelengths between the points if the lattice had unit masses. Simulations in this case yield the relative radiation amplitude 0.057, which is a factor of 6 greater than the corresponding value for the uniform source. This extends the validity of the result for both dissipation and nonlinearity. Compared to lumped point sources, uniform sources tend to yield greater relative destructive interference outside the driven region.

V. CONCLUSIONS AND FUTURE WORK

This thesis represents only an initial investigation of quasi-nonradiating sources in one-dimensional systems. There is a substantial amount of future work that can be done. Using numerical simulations there is an infinite number of possible variations which could be explored. There are also other vibrating wire apparatuses, such as the sonometer, which exhibit different properties than the hot-wire demonstration. In addition, with the successful demonstration of quasi-nonradiating sources in one dimension, it is worthwhile to search for them in higher dimensions.

A. HOT-WIRE DEMONSTRATION

We have successfully demonstrated the first two nonradiating modes of a vibrating wire system for continuous sources of various lengths, as well as for two point driving sources. To our knowledge, our experiment is the first demonstration of the existence of nonradiating sources to be performed. The hot-wire demonstration is well suited for classroom demonstrations.

The hot-wire demonstration also leaves a great deal of questions unanswered that could be explored as future topics of research. Why did the 30 gauge BNC wire work so much better that the 28 gauge? At first we thought that it was only a matter of the cooling properties. The thinner 30 BNC requires less current to glow, and would cool easier. Cooling in a wire increases as the radius decreases. Less current also means the force on the wire is less. But the 30 BNC is less massive so any leakage that did occur would be more pronounced and would produce a larger displacement outside the array. The 30 BNC wire also has a faster wave speed for a given tension. For similar arrays, the 30 BNC would be at higher frequencies, and this should aid in the cooling, producing darker spots. But this works against us as well as for us. It would also be darker in the places we did not want to be dark as a result of faster vibration, should leakage occur.

The 30 gauge BNC has less bending stiffness. In this respect, its behavior while vibrating is more similar to an ideal string than the 28 gauge would be for a given value

of the hanging mass. Bending stiffness would represent a smaller percentage of the total tension [T in Eq. (4.1)] and would perhaps reduce the effects of nonlinear terms in the response of an oscillator. This could be accomplished for the 28 gauge BNC by performing the experiments at a higher tension, but due to time constraints, this was not an avenue we explored. It would be interesting to further investigate why the 30 gauge BNC wire produced a cleaner looking nonradiating wave source than the 28 gauge BNC wire. One way of probing this would be to perform experiments at different tensions.

Unfortunately we did not take measurements of the relative radiation amplitude of the 28 gauge BNC wire systems. We have assumed that this value is indicated by how clean a nonradiating source appears. It is possible that the relative radiation amplitudes would be comparable to those given by the 30 gauge wire. Differences in the cooling properties of the wires may account for the 28 gauge wire not yielding as nice a picture, even though the quality of nonradiation could have been quite good.

It is unknown to us exactly how parameters such as tension and the radius of our vibrating wire system scale in regard to cooling. These would make excellent topics of further study.

B. NUMERICAL SIMULATIONS

By performing numerical simulations of an ideal mass-and-spring lattice, we have confirmed the nonradiating states of two-point and uniform sources at predicted frequencies. The realistic effects of weak dissipation, nonuniformity, and nonlinearity each cause a relatively small amount of radiation to emanate from the source. By adjusting the frequency or the relative drive amplitudes, the radiation can be substantially minimized in some cases. This is most dramatic in the case of a regular nonuniformity, where the radiation is nearly completely eliminated. Another means of reducing the radiation is to distribute rather than concentrate the force. This is most dramatic in the case of nonlinearity, where the relative radiation of a uniform source is one to two orders of magnitude less than the comparable two-point source.

However, the numerical simulations also leave a great deal of room for future

work. With the numerical simulations, we have exclusively dealt with the near-continuum limit of a lattice, and new phenomena may become apparent when the wavelength is not large compared to the lattice spacing. For example, effects of the possible scattering (see below) from nonuniformities may become apparent. We empirically determined the drive parameter values that minimize the radiation. In many cases, these can be predicted from theory, whose validity could then be tested. A greater understanding is required of the apparently general fact that a distributed source yields less relative radiation compared to a concentrated source. It is clear that the greater destructive interference of a distributed source reduces the amplitudes of both the standing wave inside the source and the radiation emanating from the source, but a greater understanding is required for the observation that the *relative* amount of radiation is dramatically reduced.

In the case of nonuniformity due to a gradient of masses (Sec. IV.E), steeper gradients may cause reflections (scattering) from each lattice site, representing a breakdown of adiabatic invariance. The radiation from a source whose amplitudes have been adjusted to yield a nonradiating state for a shallow gradient may be a sensitive measure of the breakdown of adiabatic invariance. It would also be interesting to a consider a *random* nonuniformity. This could be done, for example, for small variations in the masses about a constant value, or for small variations in the drive amplitudes of an otherwise uniform source.

A quantitative understanding is required for the observation that an appropriate adjustment of the drive frequency substantially reduces the radiation in a cubically nonlinear system. The absence of significant collinear interaction of waves in the case of a uniform source for both cubic and quadratic nonlinearities also requires a quantitative understanding. Finally, the apparent higher-order dependence of the speed of waves in a quadratically nonlinear system should be investigated in the context of quasi-nonradiating sources.

C. SONOMETER EXPERIMENT

Another physical system of further research is the sonometer. As explained in App. C, this is a second vibrating wire apparatus that can be used to quantitatively study nonradiating wave sources. The sonometer uses approximately point transducers to measure the displacement of the wire and to drive the wire. It can therefore only be used to simulate a two-point source experiment. A possible configuration is shown in Figure 5.1. A detector between the drivers would measure the standing wave, and a detector outside of the driver would measure the extent to which the quasi-nonradiating wave source leaks. The relative amount of leakage could be measured as a function of the drive level, thus probing nonlinear effects.

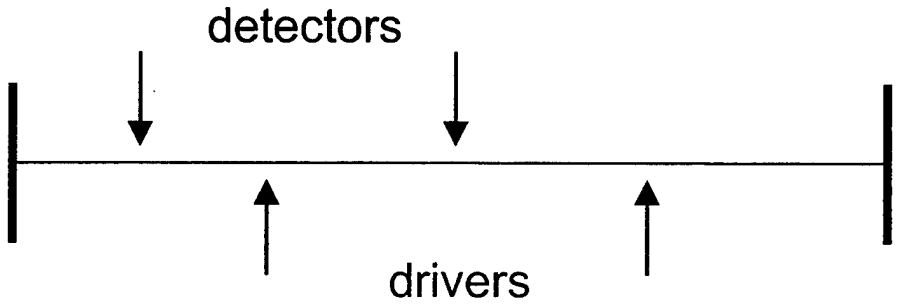

Fig 5.1 A schematic of the proposed sonometer experiment showing the relative positions of the detectors and drivers.

The reason that the sonometer is interesting is that the transducers allow for precise measurement of the displacement of the wire. The nonlinear effects of a vibrating wire can be more thoroughly explored. However, initial measurements (see App. D) show that the sonometer has to be driven into the nonlinear regime in order to produce an amplitude that can be accurately measured.

D. NONRADIATION IN HIGHER DIMENSIONS

In order to be of particular relevance to the military the possibility of nonradiating sources in higher dimensions needs to be explored. As stated in Ch. 1, if nonradiating sources do exist, it may be possible to render a source approximately nonradiating, and reduce the acoustical or electromagnetic signal emitted from a body. A topic for a future thesis may involve a theoretical exploration of how to create a source that does not radiate in two or three dimensions. Numerical simulations to this effect could be feasible, and perhaps the construction of such a source would be possible. While it is my belief that this would involve a great deal more complicated mathematical knowledge, the benefits it could have for the military could justify the effort.

THIS PAGE INTENTIONALLY LEFT BLANK

APPENDIX A. ANECHOIC TERMINATION OF A MASS AND SPRING LATTICE

In this appendix, we investigate a lumped anechoic termination of the mass-and-spring lattice described in Chapter IV. For our numerical simulations, it would be very convenient to be able to terminate the lattice such that there are no reflections when a wave impinges upon either end of the lattice. It is of course possible to design an extended termination consisting of a lattice that gradually damps a wave, thereby yielding only small reflections. However, to minimize computational time, it is desirable to have a termination that consists of "lumped" elements. Our goal here is to derive such an anechoic termination.

A. NEWTON'S LAW DERIVATION OF AN ANECHOIC TERMINATION

In the continuum limit that is described by the standard wave equation, we will show below that an anechoic termination can be achieved for all waves by a mechanical resistance ("dashpot") that is proportional to the velocity. This resistive force is $-R\partial y/\partial t$ evaluated at the dashpot. No reflections occur if the mechanical resistance equals the wave impedance: $R = \rho c$, where the linear density is $\rho = m/a$ in our case. When the impedance is "matched" in this way, the termination is anechoic.

Due to the dispersion in the mass-and-spring lattice, it is natural to suspect that an anechoic termination can only be achieved at a definite frequency. This is satisfactory for our purposes, because our studies of nonradiation are for monofrequency sources. However, it should be noted that such a termination would not be perfect, due to the fact that the source is not operating for an infinite time. That is, because the source starts and stops at some times, the spectrum of the response will have a frequency range in a neighborhood of the frequency of the source.

Because the mechanical resistance in the continuum limit is $R = \rho c$, one might guess that the anechoic termination for the lattice with waves of definite frequency ω has mechanical resistance $R = \rho\omega/k$. As shown below, however, this is incorrect.

To determine an anechoic termination of a mass-and-spring lattice, we consider the generalized termination shown in Fig. A.1.

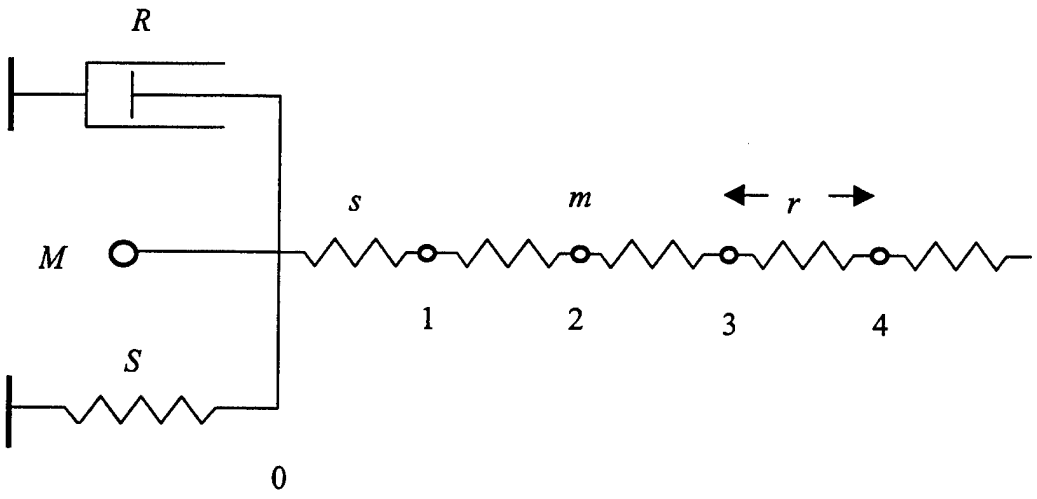

Fig. A.1 Lumped termination of a mass-and-spring lattice. The termination consists of the parallel arrangement of a dashpot, a mass, and a spring.

The equation of motion for the displacement $y_o(t)$ of the termination point is

$$M\frac{\partial^2 y_o}{\partial t^2} = s(y_1 - y_o) - R\frac{\partial y_o}{\partial t} - Sy_o \,. \qquad \text{(A.1)}$$

A simple approach is to demand that no reflections occur at the termination, and to ascertain if there exist values of the termination parameters such that this is possible. Substitution into Eq. (A.1) of the pure left-traveling wave $y_n = A\exp(i\omega t + iknr)$, where $k > 0$ and ω and k are related by the dispersion law (4.4), yields

$$M\omega^2 = s\left(1 - e^{ikr}\right) + i\omega R + S \,. \qquad \text{(A.2)}$$

We first examine this in the continuum limit, which is $kr \ll 1$, and $r \to 0$, $m \to 0$, and $s \to \infty$ such that $\rho = m/r$ and c in Eq. (3.3) remain finite and nonzero. Eq. (A.2) then becomes $M\omega^2 = -iskr + i\omega R + S$. Using the expressions for ρ and c, and the fact that the dispersion law Eq. (3.4) reduces to $\omega = ck$, we find that this is satisfied if $R = \rho c$ and $M\omega^2 = S$. The termination will be anechoic for *all* frequencies if we set $R = \rho c$ *and* $S = M = 0$.

The requirement $M\omega^2 = S$ can be easily understood physically. Given any anechoic termination for waves of definite frequency ω, a particle of mass M and a rigidly anchored spring of spring constant S can always be added to the termination point if $M\omega^2 = S$, because free oscillations of this system have the same frequency as an incoming wave. The amplitude and phase of the mass-spring oscillations can thus be matched to the wave such that there is no effect upon the wave.

We now consider Eq. (A.2) for any allowed frequency $0 < \omega \leq 2\omega_o$ of a propagating wave. Using the identity $1 - \cos(\theta) = 2\sin^2(\theta/2)$, we find that the real part of the equation is

$$M\omega^2 = 2s\sin^2\left(\frac{kr}{2}\right) + S \,. \qquad \text{(A.3)}$$

Use of the dispersion law (3.4) yields

$$\left(M - \frac{m}{2}\right)\omega^2 = S \,. \qquad \text{(A.4)}$$

The simplest way to solve this is by choosing

$$M = \frac{m}{2} \quad \textit{and} \quad S = 0 \,. \qquad \text{(A.5)}$$

As explained above, setting $S = 0$ corresponds to removing a superfluous mass-and-spring combination from the termination, where the spring constant is S and the mass is $M - m/2$ in this case.

The imaginary part of Eq. (A.2) yields

$$R = \frac{s}{\omega}\sin(kr) \; . \tag{A.6}$$

Use of the identities $\sin(\theta) = 2\sin(\theta/2)\cos(\theta/2)$ and $\cos(\theta) = [1 - \sin^2(\theta)]^{1/2}$, as well as the dispersion law (3.4), yield

$$R = \rho c \sqrt{1 - \left(\frac{\omega}{2\omega_o}\right)^2} \; , \tag{A.7}$$

where we have used the fact that $s/\omega_o = m\omega_o = (m/a)\omega_o a = \rho c$. As with the quantity c, the quantity $\rho = m/a$ is defined regardless of whether or not the motion corresponds to the continuum limit. In this limit, note that Eq. (A.7) correctly reduces to $R = \rho c$.

The final result, as displayed in Fig. A.2, is that an anechoic termination for waves of frequency ω on a mass-and-spring lattice is the mass $m/2$ attached to a dashpot of mechanical resistance (A.7).

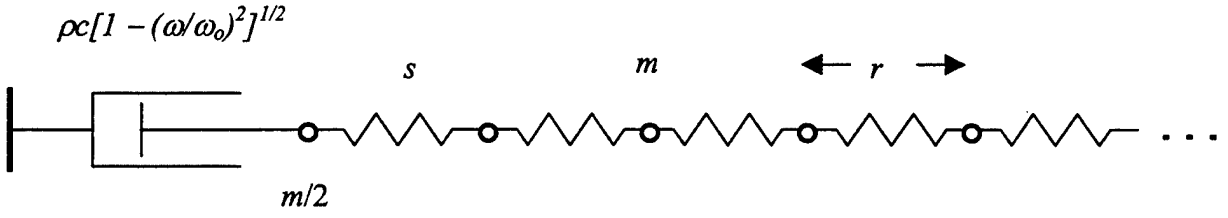

Fig. A.2 Anechoic termination of a mass-and-spring lattice for waves of definite frequency ω. The mechanical resistance of the dashpot is $\rho c[1 - (\omega/\omega_o)^2]^{1/2}$, where $\rho = m/a$ and $c = \omega_o a = a(s/m)^{1/2}$, so $\rho c = (sm)^{1/2}$.

The results Eq. (A.5) and Eq. (A.7) can be physically understood in the case of the maximum frequency $\omega = 2\omega_0$ of a propagating wave, for which $R = 0$. Consider the upper cutoff standing wave mode, in which the masses m are in antiphase. Each mass is subjected to stiffness 4s, where s is the stiffness of each spring, because the center of each spring is a node and two springs act on each mass. If we imagine breaking each mass in half, both the stiffness and the inertia are halved, so the frequency remains the same. Hence, the termination consisting of a mass $m/2$ will not effect the upper cutoff standing wave motion. Because a traveling wave can be considered as a superposition of two standing wave modes that are 90° out-of-phase, the termination will also have no effect upon an upper cutoff traveling wave. That is, the termination will be anechoic. This may appear to be contradiction, because there is no resistance and yet energy appears to be absorbed. However, the group velocity for cutoff modes vanishes, so there is no energy flow in these cases.

B. IMPEDANCE DERIVATION OF AN ANECHOIC TERMINATION

The results Eq. (A.4) and Eq. (A.7) can also be derived with the method of impedance. We imagine driving the endpoint mass of a semi-infinite lattice with a force $F\exp(i\omega t)$, where F is a constant (Fig. A.3). The input impedance depends upon whether a spring or mass is driven or, more generally, at what point along a spring the drive acts, although all of these distinctions vanish in the continuum limit. For our purposes, any driving point can be chosen as long as the lattice is terminated at an appropriate point, as explained below. The results then do not depend upon the choice of driving point.

The equation of motion for the endpoint is $F\exp(i\omega t) + s(y_1 - y_o) = m(d^2y_o/dt^2)$. Substituting the traveling wave solution $y_n = A\exp(i\omega t - iknr)$ into this equation, and solving for the amplitude A, yields $A = (F/s)[1 - \exp(-ikr) - \omega^2/\omega_o^2]^{-1}$, where $\omega_o^2 = s/m$. The input impedance is the force divided by the velocity of the endpoint: $Z = F\exp(i\omega t)/i\omega y_o = F/i\omega A$. Substitution of the expression for A gives

$$Z = \frac{s}{i\omega}\left(1 - e^{-ikr} - \frac{\omega^2}{\omega_o^2}\right). \qquad \text{(A.8)}$$

For a continuum, the wave impedance is defined to be identical to the input impedance for a semi-infinite system. No reflections occur if the impedance of the termination equals the wave impedance. Due to the discreteness of the lattice, this result is valid only if the termination point of the lattice is chosen such that the lattice has an integral number of "unit cells" (i.e., mass-spring combinations) between the driving point and the termination point. Hence, for our choice of driving a mass, the termination must occur at the unloaded end of a spring. We consider the termination shown in Fig. A.1, which meets this requirement. The impedance of the termination corresponds to a series connection of a resistor, inductor, and capacitor, so the impedance of the termination is $Z_{term} = R + i\omega M + S/i\omega$. For no reflections, we set $Z = Z_{term}$. The result is Eq. (A.2) with $-k$ replacing k and $-s$ replacing s, and with $S + m\omega^2$ replacing S. The result Eq. (A.7) for R still holds. The result Eq. (A.4) becomes $(M + m/2)\omega^2 = S + m\omega^2$, which is seen to reduce exactly to Eq. (A.4). Hence, the impedance method yields the identical results as the Newton's second law method in Sec. A.1.

If we had chosen to drive the unloaded end of a spring, rather than a mass m, the input impedance becomes

$$Z = \frac{s}{i\omega}\left(1 - e^{-ikr}\right) \qquad \text{(A.9)}$$

instead of Eq. (A.8). As explained above, we must now add a mass m at the termination point. The result of setting $Z_{term} = Z$ is then Eq. (A.2) with $-k$ replacing k and $-s$ replacing s. The result Eq. (A.7) for R still holds. The result Eq. (A.4) becomes $(M + m/2)\omega^2 = S$. Because there is a mass m at the termination point, in addition to the mass M, the total mass at the termination is $M_{tot} = M + m$. Hence, the result is $(M_{tot} - m/2)\omega^2 = S$, which is identical to Eq. (A.4) with M_{tot} playing the role of M.

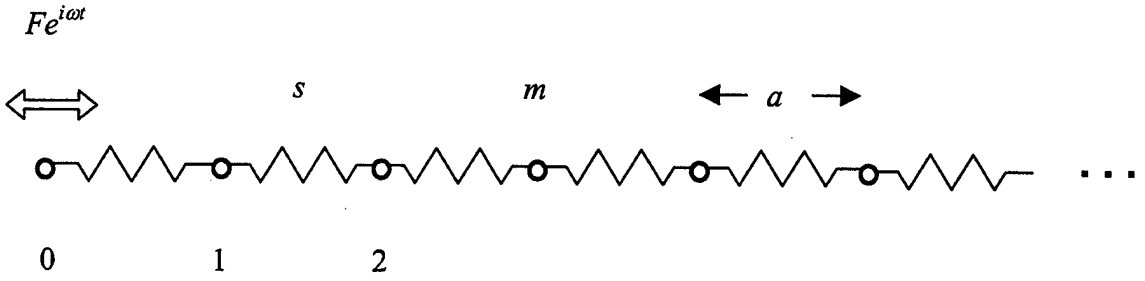

Fig. A.3 Mass-and-spring lattice driven at one end of an unloaded end of a spring.

C. SIMULATION TESTS WITH ANECHOIC TERMINATIONS

The anechoic lattice termination derived in Secs. A.1 and A.2 holds for a pure frequency. In applications, however, a pure frequency is impossible because an infinite time would be required. It is thus of interest to know how well the termination performs for practical situations in which there is a small band of frequencies. We consider two situations: an initial gaussian-modulated wave packet moving toward one end of the lattice, and the center of lattice driven by a modulated amplitude. The first is appropriate as the simplest check of the termination. The second is appropriate for our investigations of nonradiating sources.

We consider an initial gaussian-modulated wave packet moving toward one end of the lattice. For a continuum with a general dispersion relation $\omega = \omega(k)$, such a packet traveling toward decreasing x can be expressed for a small time scale *as* $y(x,t) = A\exp\{-[x-x_o+(d\omega/dk)t]^2/g^2\}\cos[k(x-x_o) + \omega t]$, where the packet has width g and is centered at $x = x_o$ at $t = 0$. The carrier moves with the phase velocity ω/k and the modulation moves with the group velocity $d\omega/dk$. The expression is valid only for a small time scale because we have neglected the fact that the width of the packet increases and the amplitude decreases at a larger time scale. The initial conditions $y(x,0)$ and

dy(x,0)/dt give rise to the above wave. To yield a gaussian-modulated wave packet in a lattice, we thus employ the initial conditions

$$y_n(0) = Ae^{-(n-n_o)^2 r^2/g^2} \cos\left[ka(n-n_o)\right], \tag{A.10}$$

$$\frac{dy_n(0)}{dt} = -Ae^{-(n-n_o)^2 r^2/g^2}\left\{\omega \sin\left[kr(n-n_o)\right] + \frac{2r(n-n_o)}{g^2}\frac{d\omega}{dk}\cos\left[kr(n-n_o)\right]\right\}, \tag{A.11}$$

where ω and k are related by the dispersion relation (3.4) For numerical simulations, we choose all parameters of the lattice to be unity (which incurs no essential loss of generality): $r = m = s = 1$, so $\omega_o = 1$ and propagating frequencies have the range $0 < \omega \leq 2$. We choose the carrier frequency of the packet to be $\omega = 1$, and employ a mechanical resistance based on this value. By the dispersion relation (3.4), the value of the wavenumber is $k = \pi/3$ and the wavelength is $\lambda = 2\pi/k = 6$ lattice spacings. We choose the width to be $g = 3\lambda = 18$ and the amplitude to be $A = 1$. By the uncertainty relation Δk $\Delta x = 1/2$, where $\Delta x = g/2^{1/2}$, the bandwidth of the wave packet centered on $\omega = 1$ is calculated to be $\Delta\omega = (3/2)^{1/2}/2g = 0.034$, which is small.

We employed the Euler-Cromer method with time step 0.001 to simulate motion of a 501-site lattice (n = 0 to n = 500). Figure A.4 shows the evolution for the initial conditions (A.10) and (A.11) with the center of the wave packet initially at the middle site n = 250. For clarity, only line segments between successive data points are shown. (The labels for the points are not shown.) Figure A.4(a) shows the initial displacements, and Fig. A.4(b) shows the displacements at a later time before reflection. Note that there is a slight spreading of the wave packet, which is due to the dispersion of lattice waves. To the right of Fig. 3(b) is a very small-amplitude (roughly 0.0004) packet propagating to the right, which occurs because the initial conditions are exact for a uni-directional packet only for a continuum. Figure A.4(c) shows the displacements after the packet has interacted with the termination. The reflected wave amplitude is only 0.6% of the incident amplitude. Figure A.5 is an expansion of Fig A.4(c). Note that the ordinate has

been expanded by a factor of 100. By contrast, a termination consisting of a dashpot with mechanical resistance $R = \rho c$ connected to a mass m yields 25%.

The relative amplitude of the reflection is expected to decrease as the incident wave approaches a monofrequency wave. To check this, we repeated the above simulation with the same parameters except for the width, which was increased by a factor of 10 to $\gamma = 30\lambda$, and the number of lattice sites, which was increased from 501 to 1001 to accommodate the longer wave packet. In addition, the time step was reduced by a factor of 5. The reflected amplitude was observed to decrease to 0.06% of the incident amplitude. That is, an order of magnitude increase in the width of the wave packet causes an order of magnitude decrease in the amplitude of the reflected wave, which is reasonable. In practice, tests should be performed to ensure that the frequency spread is sufficiently small such that the reflections are negligible for the intended application.

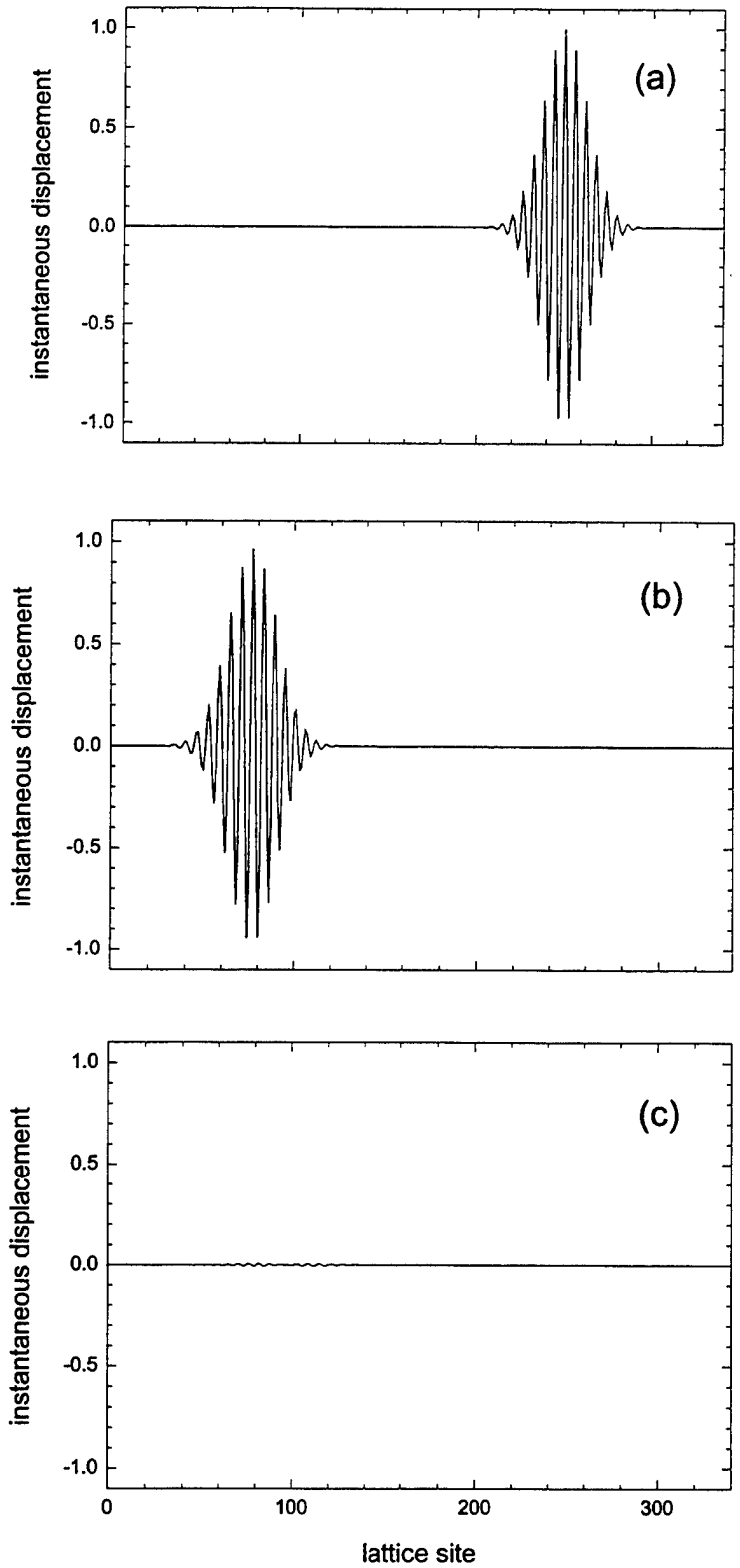

Fig A.4 Gaussian modulated wave packet incident on an anechoic termination at lattice site 0. An expanded version of (c) is shown in the next figure.

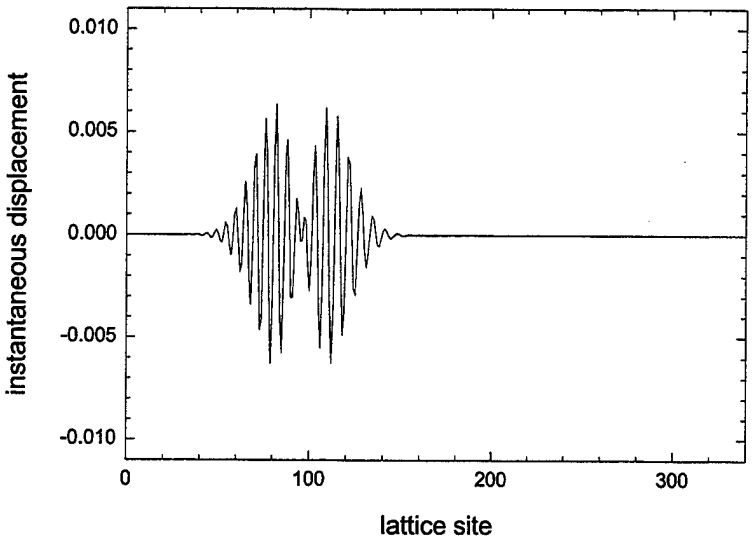

Fig. A.5 Expansion of Fig. A.4(c). The ordinate has been expanded by a factor of 100.

Another test of the anechoic termination is to drive the lattice at an interior site with frequency ω, and observe the reflections from the termination. The simplest drive is a "flat top," which is a sinusoidal force that switches on at some time and switches off at a later time such that the force is continuous. The case we use is shown in Fig. A.6. The frequency is again chosen to be $\omega = 1$, and the number of cycles is chosen to be 10. The center site n = 250 of a 501-site lattice is driven. As in the previous case, the Euler-Cromer method is used. The resultant waveform in Fig. A.7(a), which corresponds to a time before the wave encounters the terminations, has little resemblance to the drive in Fig. A.6. This is due to the dispersion of the lattice and the fact that the drive is abruptly (although continuously) turned on and off. This abruptness causes a band of frequencies to the present, which is evidenced by the significant reflections from the terminations [Fig. A.7(b)].

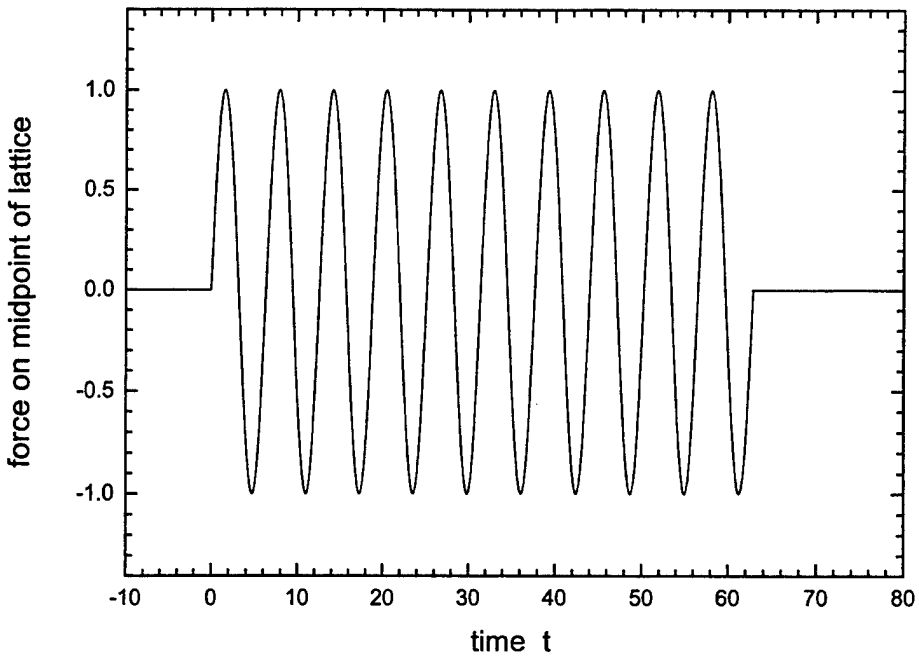

Fig. A.6 External force of a "flat top" drive on the center lattice site vs. time.

Due to the strange appearance of the waveform in Fig. A.7(a) compared to the drive in Fig. A.6, it is natural to suspect that a mistake has been made. As a check, we decreased the time step, and found the same results. Also, we next consider a drive whose amplitude smoothly rises from zero to a constant value, and then smoothly falls to zero. For this case, we find that the waveform closely resembles the drive. When the rise and fall times are decreased, we find that the waveform approaches that in Fig. A.7(a).

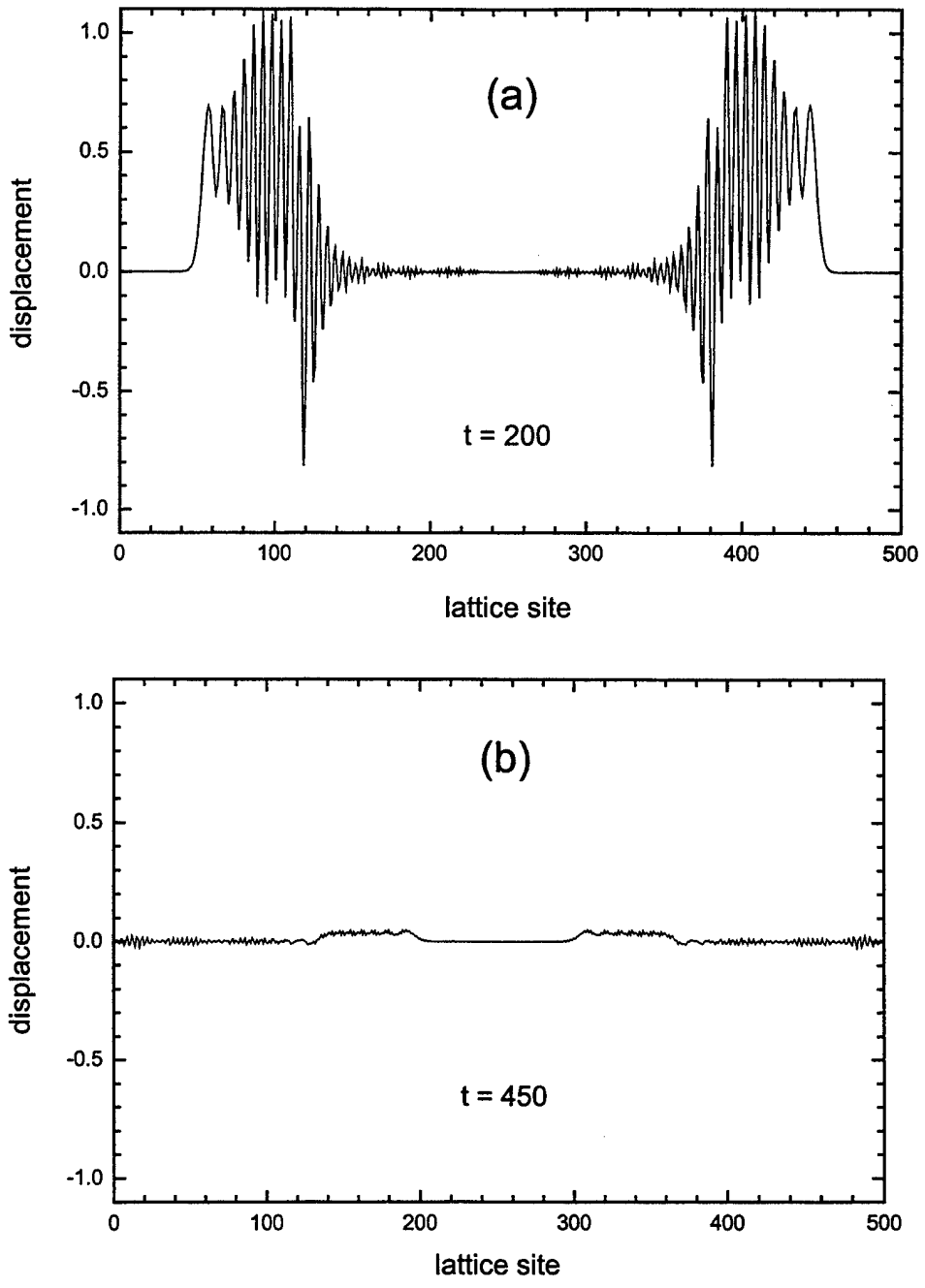

Fig. A.7 Response of the lattice to the flat top drive in Fig. A.3.4 at time (a) t = 200, and (b) t = 450.

To smoothly turn on and off the drive, we consider the force A(t)sin(ωt), where the amplitude is

$$A(t) = F \frac{1 + \tanh\left[(\omega t - \tau_o)/\gamma\right]}{2} \frac{1 - \tanh\left[(\omega t - \tau_1)/\gamma\right]}{2}, \qquad \text{(A.12)}$$

where $\tau_1 > \tau_o$. The second factor is approximately zero for $\omega t < \tau_o - \gamma$ and unity *for* $\omega t > \tau_o + \gamma$, with a smooth exponential transition between. The third factor is approximately unity for $\omega t < \tau_1 - \gamma$ and zero for $\omega t > \tau_1 + \gamma$. Hence, if τ_1 is substantially greater than τ_o, Eq. (A.12) offers a means of smoothly turning on the force to values that approximately equal the constant F, and then smoothly turning off the force.

Figure A.8 shows the force on the center site of a lattice with 501 sites. The values of the parameters in the amplitude expression (A.12) are $F = 1$, $\omega = 1$, $\tau_o = 100$, $\tau_1 = \tau_o + 120$, and $\gamma = 15$. Figure A.9(a) shows the displacement of the lattice sites at time $t = 300$, at which each wave packet is moving toward the nearer termination. The smooth turning on and off of the force has dramatically improved the wave packets compared to Fig. A.7(a). Specifically, the wave packets now bear a very strong resemblance to the drive. Figure A.9(b) and its ordinate expansion Fig. A.8 show the results after the wave packets encounter the terminations. The peak amplitude of the reflected waves are roughly 0.4% of the peak amplitude of the incident waves. In contrast to Figs. A.7(b) and A.8, this substantial reduction is due to the near-monofrequency of the drive as a result of the smooth turning on and off.

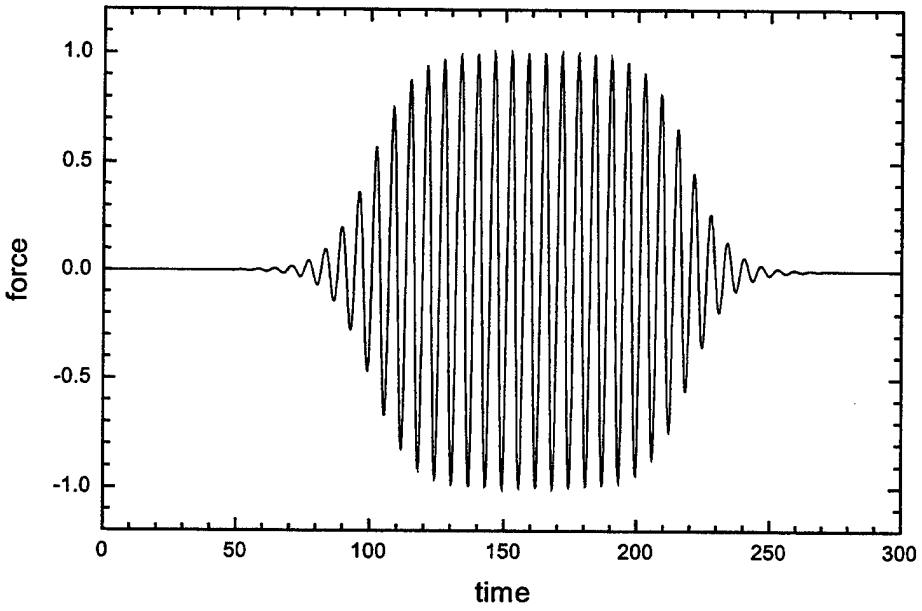

Fig A.8 External force on the center lattice site vs. time. The body is approximately uniform, and the tails are exponential.

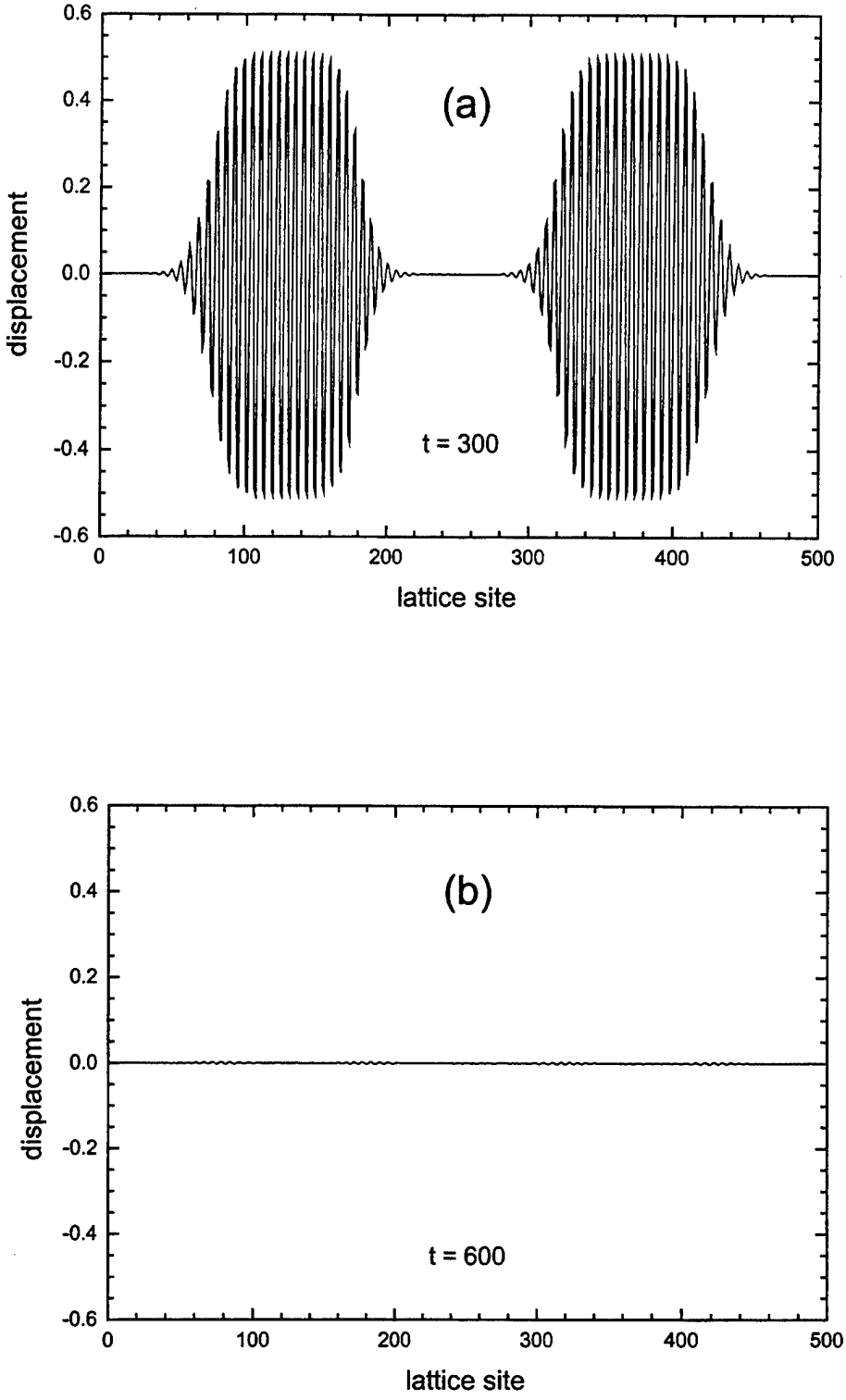

Fig. A.9 Driven lattice wave packets incident upon anechoic terminations t the end of the lattice. An expansion of (b) is shown in the next figure.

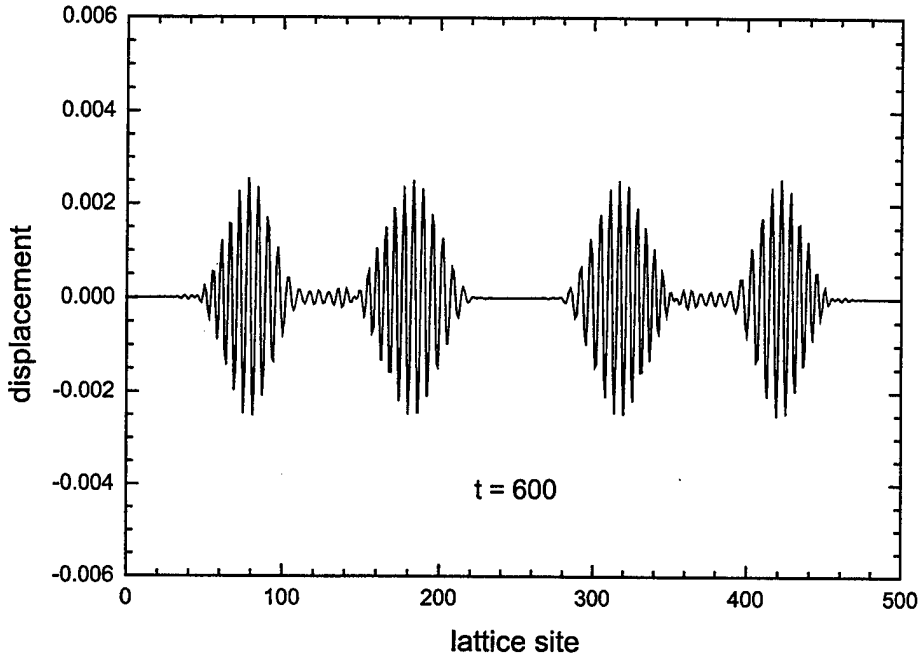

Fig. A.10 Expansion of (b) in Fig. A.9. The ordinate has been expanded by a factor of 100.

THIS PAGE INTENTIONALLY LEFT BLANK

APPENDIX B CODE FOR NUMERICAL SIMULATIONS

Below is a sample of the C++ code used during the many numerical simulations, both for the two-point case and the continuous source. It can easily be adapted to add or remove nonlinear and dissipative terms as the user desires. These samples of code do not include the nonuniformity cases.

A. TWO-POINT SOURCE

```
/*************************************************************************

                                twopoint.cpp

        This program simulates a mass-and-spring lattice with a theoretically
anechoic termination. The Euler-Cromer method (Gupta, 1988) is employed. The lattice
is driven with the same amplitude, frequency and phase at two points whose spacing is
specified. The drive is smoothly turned on. Dissipation and/or nonlinearity may be
present. The lattice spacings, masses, and spring constants are all chosen to be unity.
The terminations consist of a frequency-dependent dashpot and a mass of value 1/2.

Variables:

        y[n] = response at lattice site n, where n = 0, 1, 2, ..., nmax,
                where nmax = total number of lattice points - 1
        v[n] = velocity of response = dy[n]/dt
        w = angular frequency of driven wave = 2sin(k/2);
                0 (continuum limit) < w <= 2 (upper cutoff frequency)
        wavelength = wavelength corresponding to frequency of drive
        k = wavenumber = 2*pi/wavelength
        F = amplitude of force drive
```

```
        R = frequency-dependent mechanical resistance of dashpot;
                0 (upper cutoff mode) <= R < 1 (continuum limit)
        D = damping factor
        N = nonlinear coefficient
        dt = time increment
        tfinal = final time value

**************************************************************************/

#include <stdio.h>
#include <stdlib.h>
#include <math.h>

#define  pi  3.14159265358979323846

double y[1001], v[1001], ynew[1001], vnew[1001];

void main(void)
{
        int n, nmax, site1, site2;
        int tcount, tsteps;

        double t, dt, R, tfinal, arg, D, halfwave, wavelength;
        double w, F, width, shift, amp, drive;
        double right, left, nonlin, N;

        FILE *fout;

        fout = fopen("dataout.dat", "w");


/************  input and calculation of parameter values  *************/

        nmax = 500;

        halfwave = 50.0 + 0.0*2.5;
        wavelength = 2.0*halfwave;
        w = 2.0*sin(pi/wavelength);

        dt = 0.1;
        tfinal = 3074.3;
        tsteps = int(tfinal/dt + 0.0001);
```

```
        width = 20.0;
        shift = 100;

        R = sqrt(1.0 - 0.25*w*w);
        D = 0.01;
        N = 0.0;

        site1 = 225;
        site2 = 275;

        F = 1.0;


/*********************  set initial conditions  *********************/

        for (n = 0; n <= nmax; n++)
  {
                y[n] = 0.0;
                v[n] = 0.0;
        }

/************************  simulate motion  ************************/

        for (tcount = 1; tcount <= tsteps; tcount++)
        {
                t = tcount*dt;

                vnew[0] = v[0] + 2.0*(y[1] - y[0] - R*v[0])*dt;
                ynew[0] = y[0] + vnew[0]*dt;

                for (n = 1; n < nmax; n++)
                {
                        right = y[n+1] - y[n];
                        left = y[n] - y[n-1];
                        nonlin = right*right - left*left;

                        vnew[n] = v[n] + (right - left - D*v[n] + N*nonlin)*dt;
                        ynew[n] = y[n] + vnew[n]*dt;
                }
                arg = w*t - shift;
                amp = 0.5*F*(1.0 + tanh(arg/width));
                drive = amp*sin(w*t);

/*              fprintf(fout, "%f \t %f \n", t, drive);                 */
```

```
/*              vnew[site1] = vnew[site1] + drive*dt;
                ynew[site1] = y[site1] + vnew[site1]*dt;                */

                vnew[site2] = vnew[site2] + drive*dt;
                ynew[site2] = y[site2] + vnew[site2]*dt;

                vnew[nmax] = v[nmax] + 2.0*(y[nmax-1] - y[nmax] - R*v[nmax])*dt;
                ynew[nmax] = y[nmax] + vnew[nmax]*dt;

/*              fprintf(fout, "%f \t %f \n", t, y[250]);        */

                for (n = 0; n <= nmax; n++)
                {
                        y[n] = ynew[n];
                        v[n] = vnew[n];
                }
        }               /*              exit(0);        */

/******************  output initial and final values  ******************/

        for (n = 0; n <= nmax; n++)
        {
                fprintf(fout, "%i \t %f \n", n, y[n]);
        }
        fclose(fout);

        return;
}

/************************  end of main program  ************************/


/*************************  end of program  *************************/
```

B. CONTINUOUS SOURCE

```
/*************************************************************************
```

continuous.cpp

This program simulates a mass-and-spring lattice with a theoretically anechoic termination. The Euler-Cromer method is employed. The lattice is driven with the same amplitude, frequency and phase over a succession of lattice points. The drive is smoothly turned on. Dissipation and/or nonlinearity may be present. The lattice spacings, masses, and spring constants are all chosen to be unity. The terminations consist of a frequency-dependent dashpot and a mass of value 1/2.

Variables:

y[n] = response at lattice site n, where n = 0, 1, 2, ..., nmax,
where nmax = total number of lattice points - 1
v[n] = velocity of response = dy[n]/dt
spacing = number of lattice spacings between the two driven sites
w = angular frequency of driven wave = 2sin(k/2);
0 (continuum limit) < w <= 2 (upper cutoff frequency)
wavelength = wavelength corresponding to frequency of drive
k = wavenumber = 2*pi/wavelength
F = amplitude of force drive
R = frequency-dependent mechanical resistance of dashpot;
0 (upper cutoff mode) <= R < 1 (continuum limit)
D = damping parameter
N = nonlinearity parameter
dt = time increment
tfinal = final time value

**********/

```
#include <stdio.h>
#include <stdlib.h>
#include <math.h>

#define  pi  3.14159265358979323846
```

```
double y[1001], v[1001], ynew[1001], vnew[1001];

void main(void)
{
        int n, nmax, nstart, nfinish;
        int tcount, tsteps;

        double t, dt, R, D, tfinal, arg, wavelength;
        double w, F, width, shift, amp, drive;
        double right, left, nonlin, N;

        FILE *fout;

        fout = fopen("dataout.dat", "w");


/************  input and calculation of parameter values  *************/

        nmax = 500;
        nstart = 225;
        nfinish = 274;

        wavelength = 50 + 0.0*3.5;
        w = 2.0*sin(pi/wavelength);

        dt = 0.1;
        tfinal = 3084.5;
        tsteps = int(tfinal/dt + 0.0001);

        width = 20.0;
        shift = 100;

        R = sqrt(1.0 - 0.25*w*w);
        D = 0.01;
        N = 0.0;

        F = 0.1;


/**********************  set initial conditions  **********************/

        for (n = 0; n <= nmax; n++)
  {
                y[n] = 0.0;
```

```
            v[n] = 0.0;
        }

/************************  simulate motion  ************************/

        for (tcount = 1; tcount <= tsteps; tcount++)
        {
            t = tcount*dt;

            vnew[0] = v[0] + 2.0*(y[1] - y[0] - R*v[0])*dt;
            ynew[0] = y[0] + vnew[0]*dt;

            for (n = 1; n < nmax; n++)
            {
                right = y[n+1] - y[n];
                left = y[n] - y[n-1];
                nonlin = right*right*right - left*left*left;

                vnew[n] = v[n] + (right - left - D*v[n] + N*nonlin)*dt;
                ynew[n] = y[n] + vnew[n]*dt;
            }
            arg = w*t - shift;
            amp = 0.5*F*(1.0 + tanh(arg/width));
            drive = amp*sin(w*t);

/*          fprintf(fout, "%f \t %f \n", t, drive);                 */

            for (n = nstart; n <= nfinish; n++)
            {
                vnew[n] = vnew[n] + drive*dt;
                ynew[n] = y[n] + vnew[n]*dt;
            }
            vnew[nmax] = v[nmax] + 2.0*(y[nmax-1] - y[nmax] - R*v[nmax])*dt;
            ynew[nmax] = y[nmax] + vnew[nmax]*dt;

/*          fprintf(fout, "%f \t %f \n", t, y[250]);        */

            for (n = 0; n <= nmax; n++)
            {
                y[n] = ynew[n];
                v[n] = vnew[n];
            }
        }           /*          exit(0);        */

/*******************  output initial and final values  *******************/
```

```
        for (n = 0; n <= nmax; n++)
        {
                fprintf(fout, "%i \t %f \n", n, y[n]);
        }
        fclose(fout);

        return;
}

/************************  end of main program  ************************/

/*************************  end of program  *************************/
```

APPENDIX C SONOMETER APPARATUS

In addition to the hot-wire demonstration, there was a second vibrating wire apparatus that we intended to use to study nonradiating wave sources.

The sonometer was purchased from Pasco (model WA-9757). This apparatus is designed specifically for vibrating wire experiments with quantitative measurements. A schematic of the setup is shown in Figure C.1.

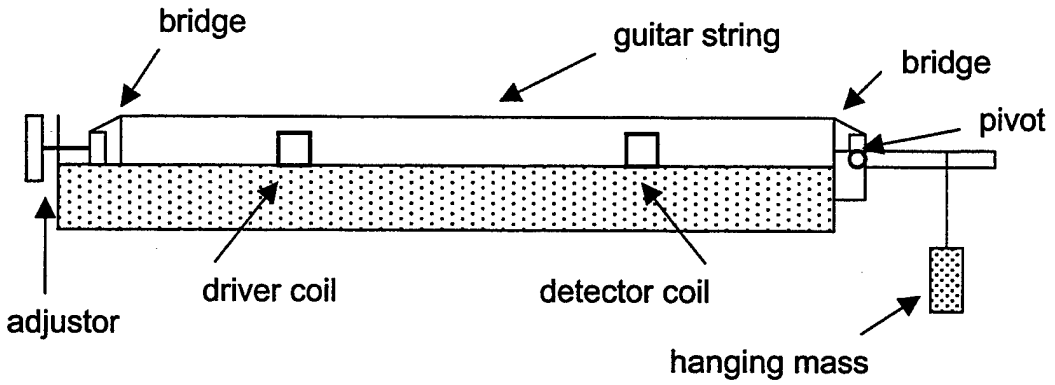

Fig. C.1 Schematic of sonometer setup.

The wire used with this equipment is ordinary steel guitar wire, which is included with the sonometer. The wire is suspended over two bridges, one at each end of the metal bench. The bridges serve to keep the wire at a prescribed height above the divers and detector, and to ensure that the wire is horizontal. The wire is then hooked to a tensioning lever at one end and fixed in place at the other. The tension in the wire is controlled by hanging masses off of the tensioning level at the end of the bench. The value of the tension is determined by the position of the masses along the length of the lever, as well as the value of the mass hung.

Due to the origin of the driving force on the wire, it is only possible to perform nonradiating experiments of the two-point variety and not the continuous field. The drive transducers are only able to drive over a very small region of wire because of their

construction and size.

The first fact that is important to note about the transducers used in the sonometer setup is that the driving transducers and the detecting transducers do not function in the same way. Inside the detector, there is a permanent magnet, but in the drivers there is not. This was easily tested by simply placing the drivers and detectors in close proximity to any steel object (e.g. a file cabinet) and observing whether or not they were attracted to it.

For the drivers, an alternating current was input. Inside is a small solenoid of wire (Fig. C.2). When the current passes through this coil, a magnetic field is setup. This B field induces small magnetic dipoles in the atoms of the steel wire, which are then attracted toward the coil. The end result is that the wire is pulled down toward the driver. When the current sent to the driver passes through a zero, the B field disappears, as do the dipoles and therefore the attractive force. The tension in the wire provides the restoring force, which pulls the wire away from the driver. As the current changes direction, the B field now points the other way, but since the induced dipoles are also reversed, the force is still attractive. It is important to realize that since the wire is attracted to both a North and South pointing B field produced by the coil, the attractive force on the wire will occur at *twice* the frequency of the input current. However, we also observe a smaller response frequency at the same frequency as the drive current.

The detector works in a manner based on similar physical principles as the driver. The permanent magnet induces dipoles in the wire, which do not switch back and forth in time (Fig. C.3). As the wire vibrates, the motion of the dipoles causes a change in flux through the loops of the coil, which induces a voltage in the coil. The voltage in the coil is then seen on the oscilloscope. This is what enables the sonometer setup to be a quantitative experiment. The magnitude of that current is directly related to the amplitude of the wire vibrations, and can be measured with precision.

Based on the description of the transducers above, an accurate recording the amplitude of the wire will become more difficult if the driver and detector are placed in close proximity to each other. This is because the oscillating magnetic field of the driver can be directly detected by the detector. This phenominon is called "cross talk." As the

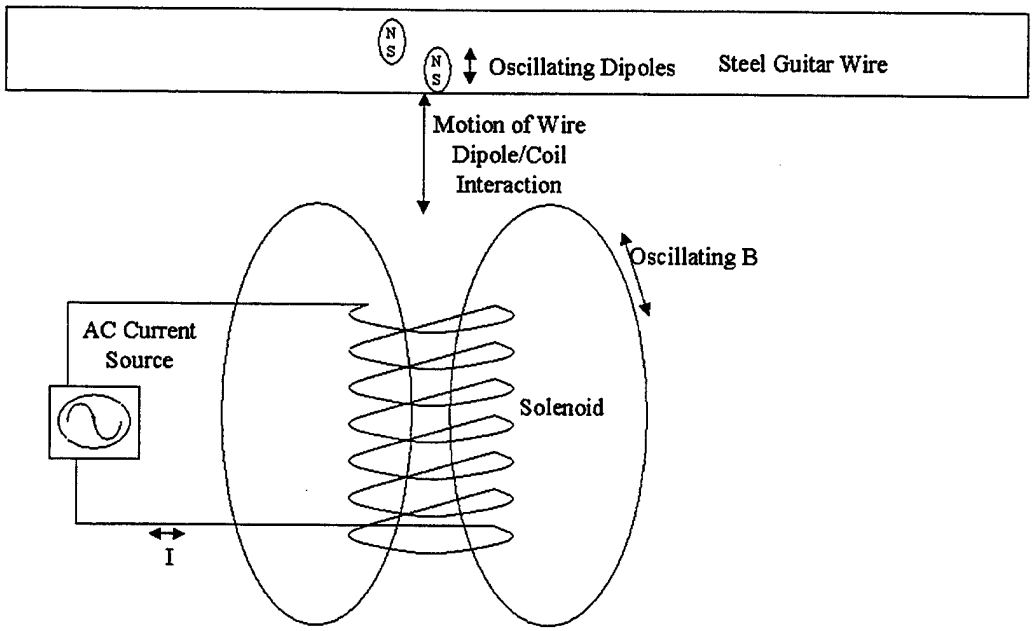

Figure C.2 Driver Schematic

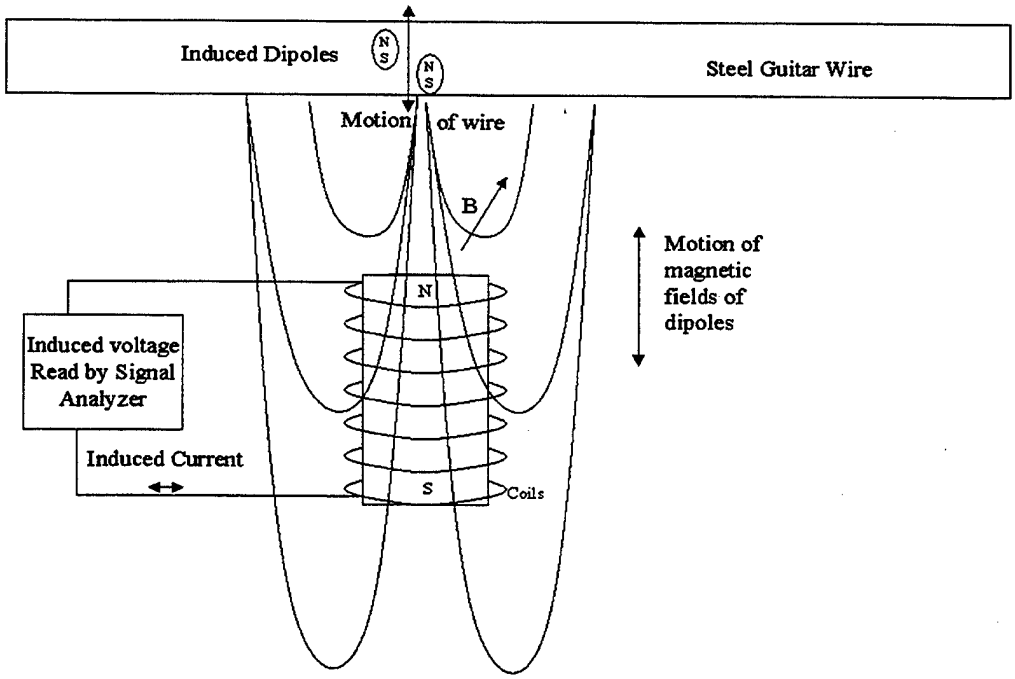

Figure C.3 Detector schematic.

two become closer, this driver-detector interaction begins to dominate and the signal from the wire-detector interaction cannot be seen on the oscilloscope.

The signal analyzer eliminates this problem. Because the field oscillates at the frequency input from the function generator, which is one half of the wire vibration frequency, the detected signal is actually a superposition of two signals, one of which is twice the frequency of the other. The signal analyzer separates these two components, allowing us to see the detected signal at the frequency of vibration, ignoring other detected signals that are at other frequencies. This allows for an accurate measurement of the amplitude of vibration along the entire length of the wire, regardless of the driver detector distance.

We abandoned the sonometer mostly due to time constraints. Initial measurements indicated that the sonometer system is highly nonlinear. Figure C.4 shows a tuning curve taken for the second mode of the sonometer.

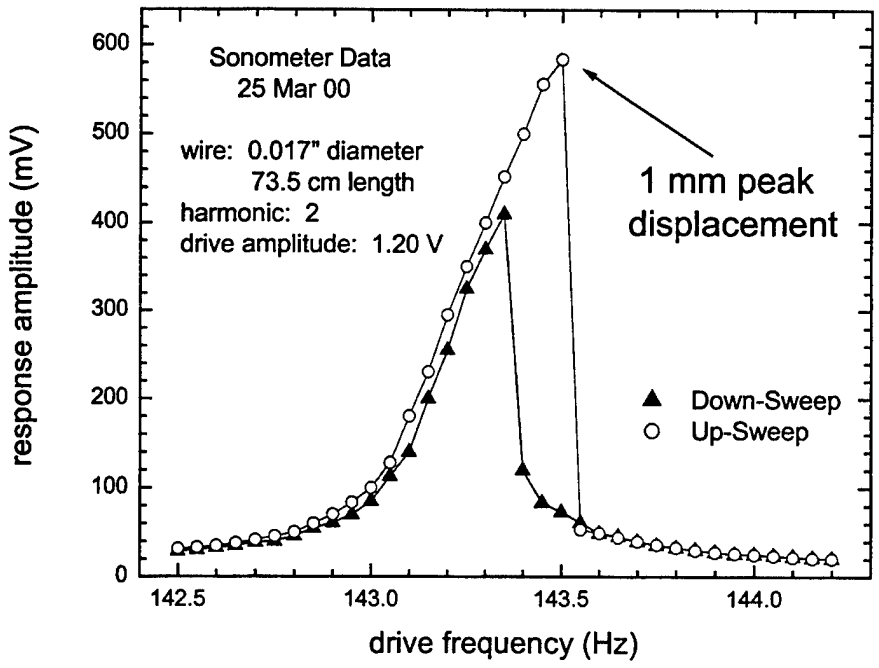

Fig C.4 Response vs. frequency for a nonlinear sonometer with hyseresis.

Notice that during the course of the frequency sweep, not only was a hysteresis discovered, but the frequency of the mode shifted. The points on the down sweep do not match the points on the up sweep.

It is interesting that hysteresis occurs even though the peak amplitude was only roughly 1 mm for a wavelength of 75 cm. This is not the experience for standing waves in the usual case where a string passes over a pulley to a hanging mass. Much greater amplitudes are required for hysteresis to occur. The reason for this may be that the length of the string is not fixed in the usual case, and thus the tension does not increase as quickly with amplitude as in the fixed-length string case of the Pasco sonometer.

We were not able to obtain accurate tuning curves for smaller amplitudes due to large fluctuations of the rms voltage from the pickup transducer. The reason for this behavior is not known. The problem should be solved before proceeding with a nonradiating wave experiment with the sonometer, because what is of interest is to observe the radiation, as the amplitude is increased form linear to nonlinear regimes. We did not have time to pursue this.

THIS PAGE INTENTIONALLY LEFT BLANK

APPENDIX D MAGNET FIELD PROFILES OF INDIVIDUAL MAGNETS

Included in this appendix are the magnetic field profiles of the individual magnets. Since the magnets are not all identical, this information was useful in helping the experimenter select the order of the magnets used in the continuous source experiments, and pairs of magnets in the two-point experiment. It is included here so the reader can see why certain combinations of magnets were chosen. Here one can see the relative strengths of the individual magnets as well as the fringe fields given off by each. Below are graphs indicating the filed strength of the magnet as a function of position along the magnet faces. This is for minimum face separation of the magnets (about 1.3 cm). The magnets are 7.5 cm wide and the left edge of the magnets is position 0. Outside this range corresponds to fringe fields.

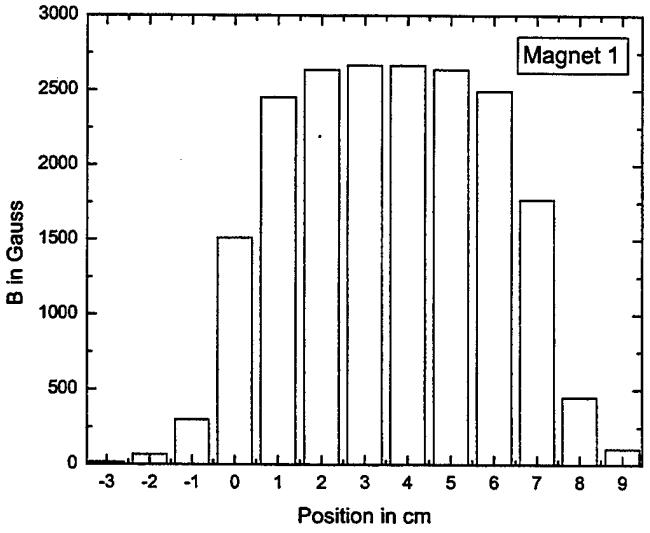

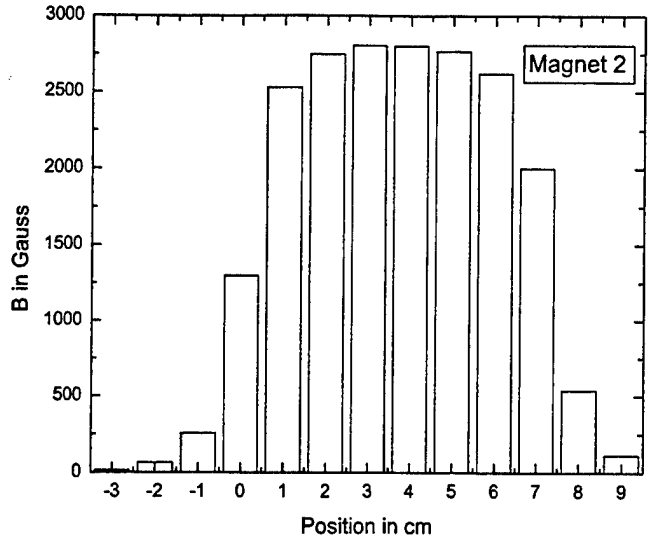
Magnet 2
B in Gauss
Position in cm
3000
2500
2000
1500
1000
500
0
-3 -2 -1 0 1 2 3 4 5 6 7 8 9

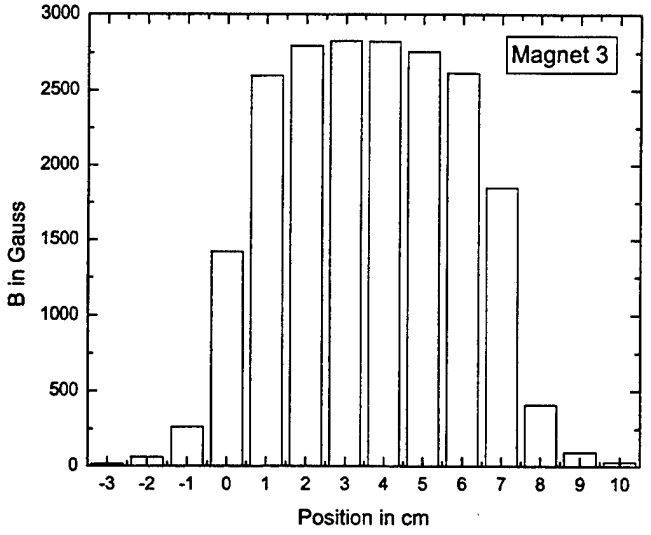
Magnet 3
B in Gauss
Position in cm
3000
2500
2000
1500
1000
500
0
-3 -2 -1 0 1 2 3 4 5 6 7 8 9 10

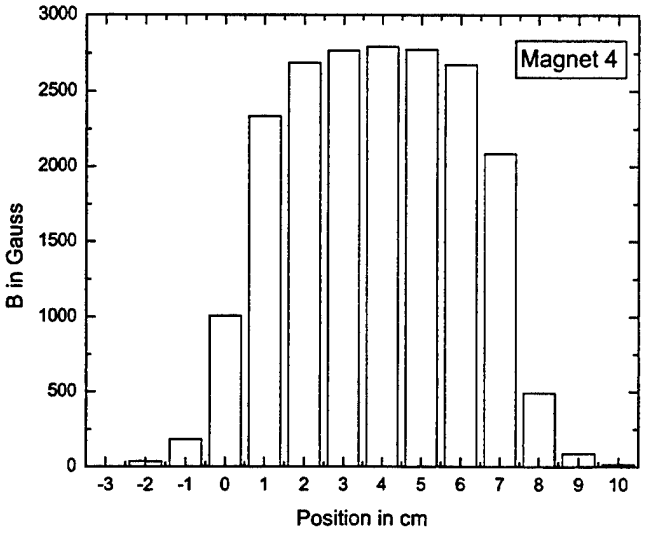
Magnet 4
B in Gauss
Position in cm
3000
2500
2000
1500
1000
500
0
-3 -2 -1 0 1 2 3 4 5 6 7 8 9 10

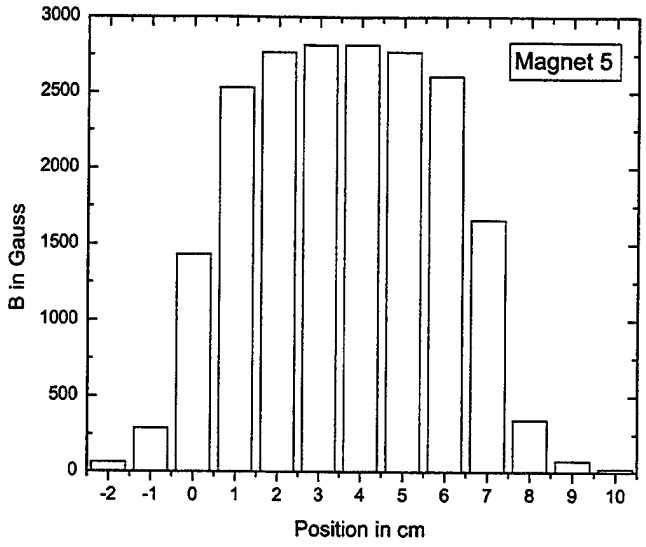
Magnet 5
B in Gauss
Position in cm
3000
2500
2000
1500
1000
500
0
-2 -1 0 1 2 3 4 5 6 7 8 9 10

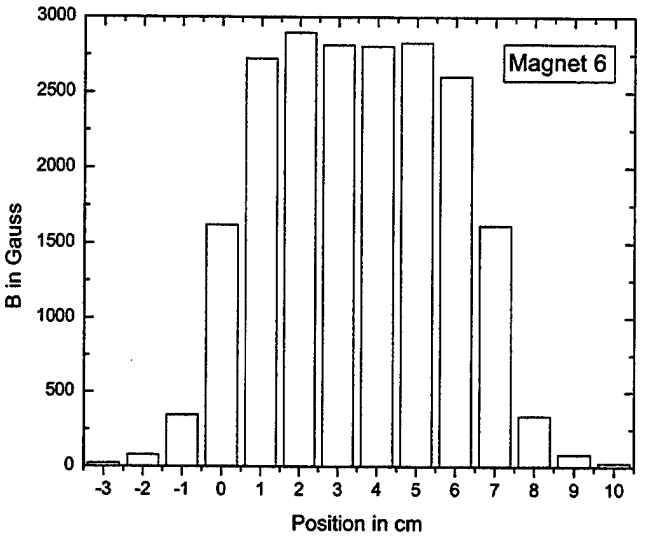
Magnet 6
B in Gauss
Position in cm
3000
2500
2000
1500
1000
500
0
-3 -2 -1 0 1 2 3 4 5 6 7 8 9 10

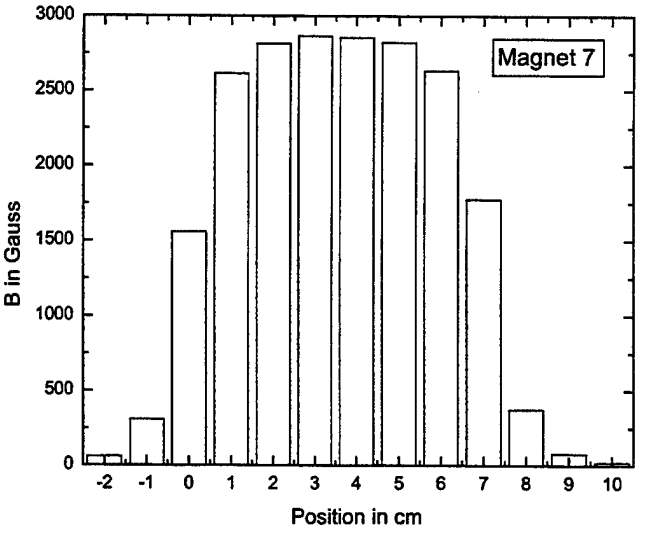
Magnet 7
B in Gauss
Position in cm
3000
2500
2000
1500
1000
500
0
-2 -1 0 1 2 3 4 5 6 7 8 9 10

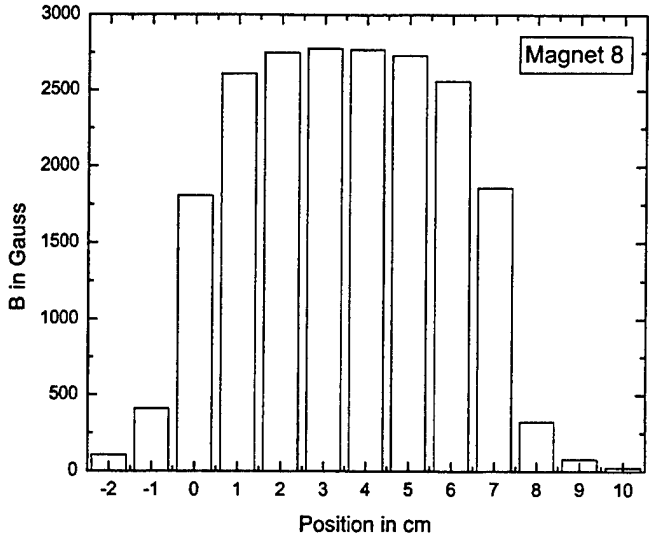
Magnet 8
B in Gauss
3000
2500
2000
1500
1000
500
0
-2 -1 0 1 2 3 4 5 6 7 8 9 10
Position in cm

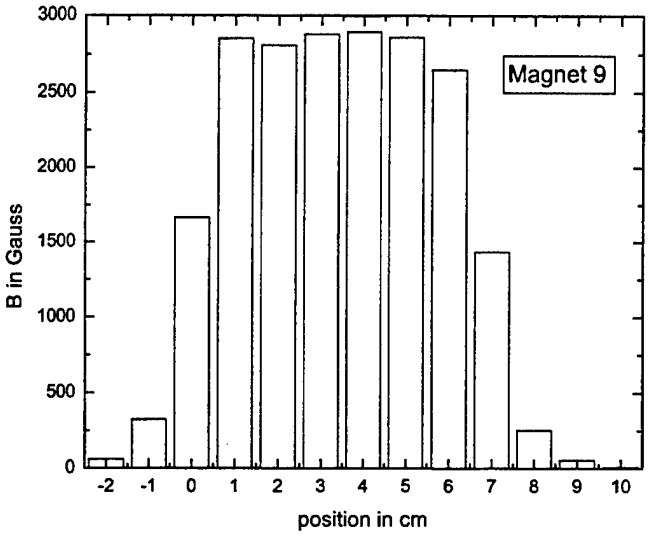
Magnet 9
B in Gauss
3000
2500
2000
1500
1000
500
0
-2 -1 0 1 2 3 4 5 6 7 8 9 10
position in cm

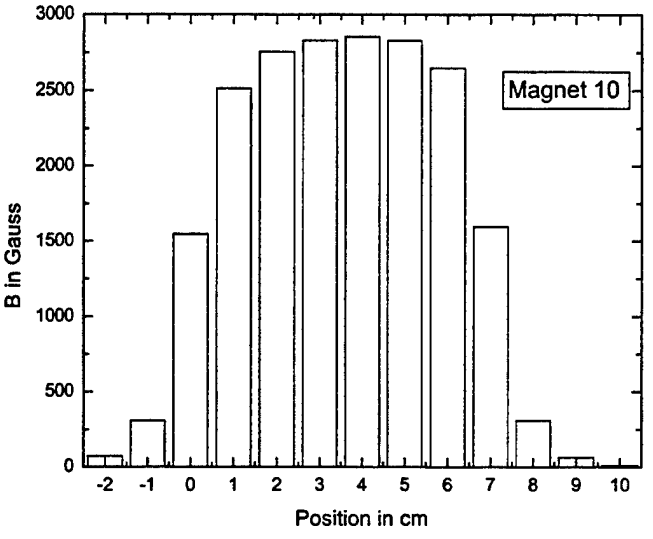
Magnet 10
B in Gauss
3000
2500
2000
1500
1000
500
0
-2 -1 0 1 2 3 4 5 6 7 8 9 10
Position in cm

LIST OF REFERENCES

Arfken, George B. and Weber, Hans J., *Mathematical Methods for Physicists,* 4th ed., Section 7.8, Academic Press, 1995.

Berry, Michael, John T. Foley, Greg Gbur, and Emil Wolf, "Nonpropagating String Excitations," *Am. J. Phys.*, v. 66, pp. 121-123, 1998.

Denardo, Bruce, "A Simple Explanation of Simple Nonradiating Sources in One Dimension," *Am. J. Phys.,* v. 66, 1020-1021, (1998).

Denardo, Bruce, and Steven R. Baker, "Anechoic Termination of a Mass and Spring Lattice," *submitted to Am. J. Phys.,* May 2000.

French, A.P., *Vibrations and Waves,* pp. 259-264, Norton, 1971.

Giordano, Nicholas J., *Computational Physics,* pp. 46-47, 84, 351, Prentice Hall, 1997.

Gupta, Parshotam D., "Coloration on a String Vibrating in a Standing Wave Pattern," *The Physics Teacher.*, v. 32, pp. 371-372, September 1988.

Kittel, Charles, *Introduction to Solid State Physics*, 5th ed., pp. 140-143, Wiley, 1976.

Landau, L.D. and Lifshitz, E.M., *Fluid Mechanics,* pp. 298-304, Pergamon, 1959.

Rudenko, O.V. and Soluyan, S.I., *Theoretical Foundations of Nonlinear Acoustics,* pp. 109-110, Consultants Bureau, 1977.

THIS PAGE INTENTIONALLY LEFT BLANK

INITIAL DISTRIBUTION LIST

1 Defense Technical Information Center 2
8725 John J. Kingman Rd., STE 0944
Ft. Belvoir, Virginia 22060-6218

2. Dudley Knox Library 2
Naval Postgraduate School
411 Dyer Rd.
Monterey, California 93943-5101

3. Professor Bruce Denardo 4
Code Ph/Db
Naval Postgraduate School
Monterey, California 93943-5101

4. Professor Steven R. Baker 1
Code PH/Ba
Naval Postgraduate School
Monterey, California 93943-5101

5. Professor Andres Larraza 1
Code Ph/La
Naval Postgraduate School
Monterey, California 93943-5101

6. Dr. Richard E. Miller 1
1217 Girard Rd.
Pittsburgh, Pennsylvania 15227-1410

7. Engineering and Technology Curriculum. 1
Code 34
Naval Postgraduate School
Monterey, California 93943-5101

8. Physics Department 2
833 Dyer Rd.
Naval Postgraduate School
Monterey, California 93943-5101